Second Order Analyses Methods for Stirling Engine Design

H. Snyman

Thesis presented in partial fulfilment of the requirements for the degree of MScEng in Mechanical Engineering at the University of Stellenbosch.

Thesis Supervisors:

Prof T. M. Harms

Mr J. M. Strauss

01 March 2007

Declaration

I, the undersigned, hereby declare that the work contained in this thesis is my own original work and has not previously in its entirety or in part been submitted at any university for a degree.

Ek, die ondergetekende verklaar hiermee dat die werk gedoen in hierdie tesis my eie oorspronklike werk is wat nog nie voorheen gedeeltelik of volledig by enige universiteit vir 'n graad aangebied is nie.

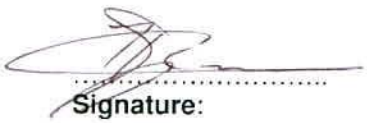

.....
Signature:

7/03/2007.
.....
Date:

Abstract

In the midst of the current non-renewable energy crises specifically with regard to fossil fuel, various research institutions across the world have turned their focus to renewable and sustainable development. Using our available non-renewable resources as efficiently as possible has been a focal point the past decades and will certainly be as long as these resources exist. Various means to utilize the world's abundant and freely available renewable energy has been studied and some even introduced and installed as sustainable energy sources. Electricity generation by means of wind powered turbines, photo-voltaic cells, and tidal and wave energy are but a few examples.

Modern photo-voltaic cells are known to have a solar to electricity conversion efficiency of 12% (Van Heerden, 2003) while wind turbines have an approximate wind to electricity conversion efficiency of 50% (Twele et al., 2002). This low solar to electricity conversion efficiency together with the fact that renewable energy research is a relatively modern development, lead to the investigation into methods capable of higher solar to electricity conversion efficiencies. One such method could be to use the relatively old technology of the Stirling cycle developed in the early 1800's (solar to electricity conversion efficiency in the range of 20-24 % according Van Heerden, 2003). The Stirling cycle provides a method for converting thermal energy to mechanical power which can be used to generate electricity. One of the main advantages of Stirling machines is that they are capable of using any form of heat source ranging from solar to biomass and waste heat.

This document provides a discussion of some of the available methods for the analysis of Stirling machines. The six (6) different methods considered include: the method of Beale, West, mean-pressure-power-formula (MPPF), Schmidt, ideal adiabatic and the simple analysis methods. The first three (3) are known to be good back-of-the-envelope methods specifically for application as synthesis tools during initialisation of design procedures, while the latter three (3) are analysis tools finding application during Stirling engine design and analysis procedures. These analysis methods are based on the work done by Berchowitz and Urieli (1984) and form the centre of this document. Sections to follow provide a discussion of the mathematical model as well as the MATLAB implementation thereof. Experimental tests were conducted on the Heinrici engine to provide verification of the simulated results. Shortcomings of these analyses methods are also discussed in the sections to follow. Recommendations regarding improvements of the simulation program, possible fields of application for Stirling technology, as well as future fields of study are made in the final chapter of this document. A review of relevant literature regarding modern applications of Stirling technology and listings of companies currently manufacturing and developing Stirling machines and findings of research done at various other institutions are provided.

Opsomming

Die tempo van uitputting van die wêreld se nie-hernubare energiebronne die afgelope jare het aanleiding gegee daartoe dat daar toenemend fokus toegespits word op die ontwikkeling van hernubare alternatiewe. Meer doeltreffende benutting van die wêreld se nie-hernubare energie is reeds 'n fokus punt, vir navorsers reg oor die wêreld, vir die afgelope dekades. Die aarde se oorvloedryke hernubare energie bronne word reeds met verskeie metodes ontgin. Die omskakeling van wind-, son- en gety energie na elektrisieteids is net 'n paar voorbeelde.

Die effektiwiteid van sonkrag na elektrisietyds omskakeling van moderne fotovoltaïese selle is in die orde van 12% (Van Heerden, 2003) terwyl die doeltreffendeid van wind energie na elektrisiteit omskakelling in die orde van 50% (Twele et al., 2002) is. Hierdie relatief lae omskelings doeltreffendeid van sonkrag na elektrisietyd, tesame met die feit dat die hernubare industrie nog relatief jonk is, lei tot die soeke na ander meer doeltreffende moontlikhede. Die Stirling siklus is nie 'n moderne beginsel nie, maar die toepassing daarvan veral in die hernubare energie industrie is wel 'n relatiewe nuwe begrip, veral in teme van die omskakeling van sonkrag na elektriese energie (gemiddelde sonkrag na lektriese energie omskakelings doeltreffendeid in die orde van 20-24% is gevind deur Van Heerden, 2003). Die omskakeling van termiese energie na meganiese energie is sekerlik die hoof uitkomste van die Stirling siklus, alhoewel dit ook toepassing vind in die verkoelingsindustrie. Die feit dat die Stirling siklus van enige vorm van termiese energie (bv. son, biomassa, asook hitte geproduseer as byproduk tydens sekere prosesse) gebruik kan maak, is een van die redes wat die tegnologie só aanloklik maak, spesifiek t.o.v. die hernubare energie sektor.

Ses (6) metodes vir die analise van die Stirling siklus word in hierdie dokument bespreek. Dit sluit die volgnde in: Beale-, West-, die gemiddelde-druk-krag-metode (GDKM), Schmidt-, adiabatiese- en die eenvoudige analise metodes. Die eerste drie (3) metodes is handige berekenings metodes tydens die aanvangs en sintesefase van Stirling enjin ontwerp, terwyl die laaste drie (3) meer toegespits is op die volledige ontwerps- en analisefases gedurende die Stirling enjin ontwerps proses. Die drie (3) analise metodes is gebaseer op die werk wat deur Berchowitz en Urieli (1984) gedoen is en maak die kern van die dokument uit. Die wiskundige model, implimentering daarvan in MATLAB, sowel as die eksperimentele verifiëering van die resultate word bespreek. Tekortkominge van die analise metodes word ook aangespreek in elke hoofstuk. Moontlikke verbeterings ten opsigte van die verskeie aannames word in die finale hoofstuk van die dokument aangespreek. Verskeie voorgestelde rigtings vir toekomstige navorsings projekte word ook in die finale hoofstuk van die dokument genoem. 'n Kort oorsig van die relevante literatuur in verband met huidige toepassings van die Stirling tegnologie, asook die name van maatskappye wat tans hierdie tegnologieë ontwikkel en vervaardig, word genoem.

Acknowledgements

I would like to thank the following persons for their assistance and contributions during the course of this study:

Firstly my promoters Prof. Thomas Harms and Mr. Johan Strauss for their assistance, motivation and support during this project. Your passion for research is a great inspiration to your colleagues.

Mr Cobus Zietsman who answered all my questions and helped me acquire and set-up the experimental hardware.

The SMD team especially Anton, Graham and Calvin for their helping hand during the manufacturing of the experimental apparatus. Also special thanks to Peter for his assistance in the store room.

To our loving God for giving me the opportunities and the talents to fulfil my dreams.

To all the guys in M250, thank you for your sense of humour and coffee time stories.

Then last but not least to my family and friends for their motivation and smiles and for always supporting me, with special thanks to Izelle for all her time and effort.

Table of Contents

LIST OF FIGURES

LIST OF TABLES

Nomenclature

A	Area [m^2] or current [A]
cc	Cubic centimetres [cm^3]
C_f	Frictional coefficient
C_{ref}	Reynolds friction coefficient
c_p	Ideal gas specific heat at constant pressure [J/kg.K]
c_v	Ideal gas specific heat at constant volume [J/kg.K]
d or D	Diameter [m]
d_h	hydraulic diameter [m]
F	Force [N] or factor in MPPF equation
freq	Frequency [Hz]
h	Heat transfer coefficient [W/K]
k	Thermal conductivity [W/m.K]
k_p	Swept volume ratio
k_s	Dead space volume ratio
m	Mass or mass flow rate [kg or kg/s]
M	Mass [kg]
MfCK	Mass flow from compression space to cooler [kg/s]
MfKR	Mass flow from cooler to regenerator [kg/s]
MfRH	Mass flow from regenerator to heater [kg/s]
MfHE	Mass flow from heater to expansion space [kg/s]
N_{ST}	Stanton number
N_B	Beale number
Nu	Nusselt number
ω	Omega, angular rotational speed [rad/s]
p	Pressure [bar or Pa]
P	Power [W]
Pr	Prantl number
P_i	Indicated power [W]

P_{shaft}	Shaft power [W]
Q	Heat transfer [J or W]
R	Gas constant [J/kg.K]
Re	Reynolds number
rpm	Revolutions per second
T	Temperature [^{0}C or K] or Torque [Nm]
u	Velocity [m/s]
V	Volume [m^3 or cm^3] or Volt [V]
W	Work [J or W]
W_{net}	Net work [W]

Abbreviations

avg	Average
BDC	Bottom dead centre
CD	Compact disc
CCU	Continuous combustion unit
DC	Direct current
dvar	Derivatives of variable matrix
exh	Exhaust
FPSE	Free-piston Stirling engine
HSE(A)	Heinrici Stirling engine (analysis)
LTD	Low temperature differential value
NTU	Number of transfer units method
MPPF	Mean pressure power formula
max	Maximum value
min	Minimum value
PV	Photo-voltaic or Pressure-volume diagram
SEA	Stirling engine analysis
SE	Stirling engine

sims	Simulations
TDC	Top dead centre
user	User defined value
var	Variable matrix

Greek Symbols

α	phase angle lead of displacer piston over power piston [radians or degrees]
ψ	Angle psi [radians or degrees]
ε	Effectiveness [%] or angle epsilon [radians or degrees]
γ	Ideal gas relation or angle gamma [radians or degrees]
Δ	Angle delta [radians or degrees]
α	Angle alpha [radians or degrees]
φ	Angle phi [radians or degrees] or fin efficiency (Kröger, 1998)
θ	Crank rotational angle [radians or degrees]
ρ	Density [kg/m^3]
μ	Dynamic viscosity [kg/m.s]
τ	Shear stress [N/m^2] or temperature relation for Beale and West methods
η	Efficiency [%]

Subscripts

C	Cold side
c	Compression space
cl	Clearance space in engine
D or d	Displacer piston
f	frictional coefficient or reference to film conditions (film temperature is T_f)
H	Hot side/end
P or p	Power piston
wg	Wetted perimeter

w	Wall
0	Initial or reference value
sw	Swept volume
m or Mean	Mean value
k	Cooler
r	Regenerator
h	Heater
e	Expansion space
ck	Interface between compression space and cooler
kr	Interface between cooler and regenerator
rh	Interface between regenerator and heater
he	Interface between heater and expansion space

1. Introduction and Overview

Depletion of the world's non-renewable energy sources together with recent peaks in oil prices introduces an obvious need to investigate and develop renewable alternatives (like solar, biomass, tidal and wave, and wind energy). Parallel to developing new renewable energy sources is the research involved in using our current energy resources more efficiently. Reducing or reusing waste produced by non-renewable energy systems plays a key role in the latter. The project discussed in this document started out as a feasibility study of a system utilising Stirling engine technology to recover the waste exhaust energy of large internal combustion (IC) engines (for instance locomotives, marine diesels or large road going vehicles). Research and simulation procedures to analyse IC engines is readily available at the University of Stellenbosch due to previous work done by Lotun (2001), amongst others. Stirling engine simulation is however not available and due to the complexity of the Stirling cycle it was decided to amend the objectives of the project. The objective of the work presented in this document is to develop a trustworthy method for Stirling engine analysis in order to enable accurate Stirling engine design. Combining this simulation with work done on IC engines, it would then be possible to design and develop a complete waste heat recovery unit. The Stirling engine simulation can also be used in the development of solar or biomass powered electricity generation units, similar to the solar-dish application discussed by Van Heerden (2003) (refer to Section 3.1.3).

The main purpose of the Stirling engine analysis program presented here is for implementation during the initialisation (Section 5.7), and design phase (Sections 3 and 5.4 to 5.6) of Stirling engine development. The document is divided into three (3) main sections of which the first (Section 3) provides a discussion regarding the literature and derivation of theory around Stirling engine analysis procedures (as presented by Berchowitz and Urieli, 1984). Secondly, the implementation of this theory is discussed (Section 5) and finally an experimental verification of the simulated results is provided (Section 6). Since accurate theory for the analysis of the complex Stirling cycle was the focal point for many scientists (amongst which Berchowitz and Urieli (1984) are considered leaders in this field) over the past decades, it was decided by the authors of this document to study and implement existing simulations rather than to "redesign the wheel". The analysis procedure presented by Berchowitz and Urieli (1984) forms part of a course presented at the Ohio University, Athens, Ohio, and was used as starting point for the Stirling engine simulation presented here.

1.1 Brief Introduction to Stirling Engines

1.1.1 Stirling History

The concept of an "air-engine" was recorded around 1699, approximately when the laws of gases were first set out. In 1816, Reverend Robert Stirling, a minister of the Church of Scotland, invented what he called "A New Type of Hot Air Engine with Economizer" as a safe and economical alternative to steam. In the early days of the industrial revolution, steam engine explosions were a real problem. Metal fatigue was not well understood, and the steam engines of the day would often explode, killing and injuring people nearby. His engines couldn't explode, used less fuel, and put out more power than the steam engines of the day. The engines designed by Robert Stirling and those who followed him were very innovative engines, but there was a problem with the material that was used to build them. In a Stirling engine, the hot side of the engine heats up to the average temperature of the flame used to heat it and remains at that temperature. There is no time for the cylinder head to cool off briefly between power pulses. When Robert Stirling built his first engines, cast iron was the only readily available material, and when the hot side of a cast iron Stirling engine was heated to almost red hot, it would oxidize fairly quickly. The result was that quite often a hole would burn through the hot side causing the engine to lose pressure and cease. As electricity became more widely available in the early 1900s, and as gasoline became readily available as a fuel for automobiles, electric motors and internal combustion engines began to replace Stirling engines. (Hargreaves, 1991)

1.1.2 Past and future of Stirling Engine

Commercial Stirling engines have suffered setbacks regarding development since they were first introduced in the early 1800's. First the lack of proper engineering materials caused it to have a short lifespan (Hargreaves, 1991), thereafter the development of internal combustion and electric motors overshadowed their development in the early 1900's. In the 1930's the Phillips group built up a considerable market for their radio sets in Europe and was looking to exploit further markets which included remote areas like Africa and Asia. Exporting large and expensive batteries raised serious concern, this lead to the research of small power units for their radios. The Phillips group soon became leaders in Stirling development as they invested a considerable amount of time and expertise in the development of small scale power units for their radios. In 1945 negotiations with the US Navy started as they saw direct applications for the external combustion air engines developed by the Phillips group. 1952 was the turning point for Stirling development as the Phillips group as well as its licensee's ceased development. The following reasons were presented for the sudden end to Stirling development: 1) lack of adequate heat transfer at high temperatures, 2) lubrication of pistons, which caused 3) regenerator contamination reducing efficiency and 4) sealing problems. Stirling development once again suffered a

development setback for reasons not completely due to the engine, but also the engineers working on it (Hargreaves, 1991).

The newly developed free piston Stirling engine (FPSE) provided some solution to these problems and in the early nineteen nineties more and more people again began to show interest in the Stirling engine. Hargreaves (1991) states the main reason for this is perhaps the possible involvement of Stirling engines as a solution to global warming. The Stirling engine when applied to the relatively new found global interest in renewable energy could reach its full potential. The increased availability of higher quality engineering materials certainly calls for a revised attempt to utilise this high efficiency energy conversion unit for remote energy applications.

1.1.3 How the Stirling cycle works

The Stirling engines, other than their internal combustion (IC) counterparts, are known as external combustion engines. They convert thermal energy to mechanical energy (or shaft power) and consist of a closed system (thus no valves opening and closing as in IC engines) with three (3) main internal components. These components are the power and displacer pistons, as well as a regenerator. The heater (heat source) and cooler (heat sink) causes the temperature rise and drop when the operating fluid (air, helium etc.) moves through these engine spaces. Expansion and contraction then takes place within these as well as the adjacent engine compartments, this causes the increase and decrease of internal engine pressure which in turn causes piston motion.

Stirling engines are classified as hot-air engines and can also be described as heat pumps operating between a heat sink and a heat source. Since the Stirling engine is ideally reversible, according to the second Carnot principle, it will have the same efficiency as that of any other heat engine operating between the same temperature reservoirs i.e. the maximum efficiency of the Stirling cycle is the same as that of the Carnot cycle which is only a function of the source and sink temperatures. Figure 1 shows a simplified schematic diagram of a heat engine operating between a heat source and heat sink and producing equivalent net work or shaft power output. Figure 1 also shows the implications of the first and second laws of thermodynamics; the latter requires that energy flows from the higher quality source (heater) to the lower quality energy source (cooler). The first law states that energy will be conserved during a process which implies that the shaft output (W_{net}) cannot exceed the amount of energy flowing from source toward sink. Further according to the Kelvin-Planck statement it is impossible for a heat engine to receive heat from a single reservoir and produce net work without rejecting any heat (Çengel and Boles, 2002).

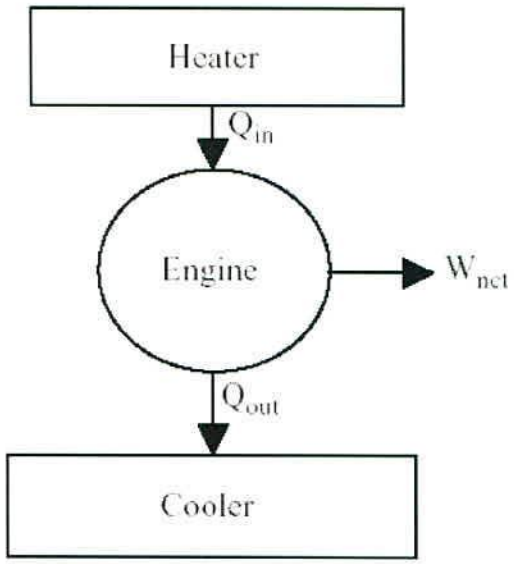

Figure 1: Simplified heat engine diagram (Kontragool, 2005)

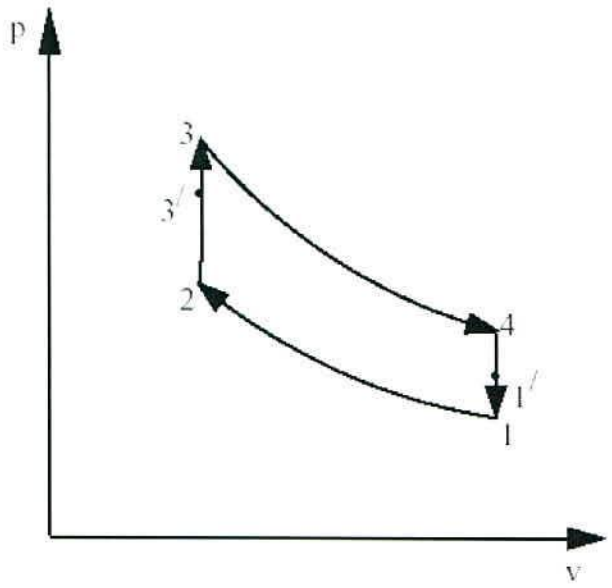

Figure 2: Ideal Stirling cycle PV diagram (Kontragool, 2005)

The ideal Stirling cycle indicated in Figure 2 comprises of the following four (4) idealised processes in the complete cycle: process 1-2 due to compression at constant cooler temperature (T_k), 2-3 due to constant volume heat addition in the heater, 3-4 due to expansion at constant heater temperature (T_h) and 4-1 due to constant volume heat rejection in the cooler. For ideal regeneration, the total heat rejected during process 4-1 is absorbed by a perfect regenerator and released to the working fluid during process 2-3, since in the ideal regeneration has an infinite heat-transfer area and infinite regeneration time.

2. Motivation and Relevance

The per capita consumption of the earth's non-renewable energy sources, which includes gas, petroleum and coal, is related, in one way or the other, to the economical wealth of the society or country involved. Three-quarters of mankind's carbon dioxide production is due to the consumption of non-renewable energy sources (Lotun, 2001). The depletion of these non-renewable energy sources has become a highlighted focus point for scientists throughout the world. Studies to improve the efficiencies of machines (like automobile engines, power generation plants etc.) fuelled by non-renewable energy sources have become a highly specialized field of interest for manufacturers. The consumers demand for "green products" has increased due to global warming and also lead to an increased effort to stop/decrease pollution.

Waste heat recovery systems forms a substantial part of the methods developed to increase the efficiency of various systems. For the past five (5) decades research was focused on large energy system applications and groundbreaking work was done in this field. Lotun (2001) designed and evaluated a small scale waste heat recovery system. He concluded that there is a need for further investigation into waste heat recovery system for application on smaller scale automobile internal combustion (IC) engines. BMW research engineers in Munich, Germany, have combined old and new technology to harness the waste heat energy in the exhaust systems of their cars. The so-called *Turbosteamer* is based on the steam turbine patent and is said to recover 80% of the wasted thermal energy in the exhaust systems of motor vehicles. The *Turbosteamer* generated 10 kW power and 20 Nm torque more, while burning 15% less fuel. BMW said that their long-term plans are to have systems capable of volume production within ten years (*Cape Argus, 10 February 2006*).

Renewable energy in the form of solar electricity generators for remote applications is another possible field of application of Stirling engines. Van Heerden (2003) studied such a solar powered electricity generation system and found that the technology is not mature enough at this point in time mainly due to lack of investment in product development, but that it is capable of delivering an average solar-to-electricity conversion efficiency of 24% which is higher than the current photo-voltaic (PV) systems.

Designing and developing Stirling engines for either the above mentioned applications surely seems relevant to the current progress of research and development, regarding the renewable energy sector in South Africa. Market competitiveness for Stirling engines in the above mentioned fields is a topic being exploited by various research groups, as mentioned by Morrison (1999), and is an indication of the relevance and applicability of the use of this "old technology" to solve modern problems regarding the current rate of fossil fuel depletion.

3. Literature Review

This section is divided into three sub-sections namely: literature found on the internet, published papers and work done at the University of Stellenbosch. All articles mentioned in this document can be found on the compact disc (CD) accompanying this document.

3.1 Internet Searches

3.1.1 Waste Heat Recovery

Hsu et al. (2002) conducted a thermodynamic analysis of the heat transfer aspects of a Stirling engine placed in an incinerator to recover waste heat. Incinerators are used to burn municipal solid waste i.e. it is like a furnace fuelled by solid waste. In earlier years waste heat recovery from incinerators was done by producing steam and using steam turbines to generate electricity. It is however, due to the low steam temperatures achievable i.e. low turbine inlet temperatures, that the efficiency of these turbines is relatively low (10 – 15 %). The authors state that, other than the case for steam turbines, Stirling engines can achieve the same efficiencies with power ranging from tens of watts to several kilowatts. A complete heat transfer model is developed and discussed together with an optimization method for the operating condition for a free-piston Stirling engine with a linear alternator.

Schmid (2004) points out that the possibility of improving the efficiency and fuel consumption of the modern low speed two stroke marine diesel engines is very limited. This is ascribed to the fact that these engines already received highly focussed attention during the past few years. These engines operate with an efficiency of about 50 % which is higher than any other automotive power unit. It is therefore, according to him, more important to focus on the other 50 % or 60 – 70 MW of energy lost through the exhaust. Hereby suggesting that waste heat recovery is still an unexplored field of study, compared to the engine development for these marine engines. A 7 MW output turbo generator proposed by *Peter Brotherhood Ltd.* (supplier of generator-set to author's proposed heat recovery plant) forms part of the total heat recovery plant proposed by the author in this document. The author presents a graphical comparison of the power distribution in the engine (%-wise) with and without the proposed total heat recovery plant.

Koehler et al. (1997) presents a study of the designing, manufacturing and testing of an absorption refrigeration system for heavy duty truck applications utilizing waste heat from the exhaust system. The recoverable energy of the exhaust gases for representative driving conditions (like mountainous, city and flat road driving) is also analysed. The result of these studies showed that the absorption system for truck refrigeration systems is an alternative for operating conditions with long distance driving on flat roads.

3.1.2 Refrigeration and Cooling

Kwon and Berchowitz (2003) from *Global Cooling BV,* studied an alternative cooling technology using a Stirling engine and presented it during an international congress of refrigeration. The difference in approach for a traditional Rankine cooling system and that of the Free Piston Stirling Cooler (FPSC) is pointed out by the authors.

Janssen and Beks (2002) presented a detailed comparison between a Rankine and Stirling based refrigeration system during the 9th International Refrigeration and Air Conditioning Congress. It was found that the comparison of these two refrigeration systems is not a straight-forward task. This is due to the fact that the heat exchanger efficiency differences between both systems needs to be taken into account to be able to determine the exact temperatures of the hot/cold heads of the Stirling cooler and the evaporator/condenser for the Rankine system. It is also mentioned that at low ambient temperatures the Stirling system performed better than the Rankine refrigeration system.

3.1.3 Stirling Technology Reviews

Gale Morrison (1999) discusses the current applications and future possibilities of the Stirling engine in the refrigeration and energy/electricity generation environment. Recent innovative creations and developments done by companies like *Global Cooling BV* (USA), *Sunpower Inc.* (Athens, Ohio), *Biowatt* and *Medis El* (Tel Aviv) utilise Stirling technology. Global Cooling together with *Sunpower Inc.* states that the free-piston Stirling refrigeration system holds various advantages over the conventional Rankine refrigeration system of which lower electricity consumption (up to 30% lower than the Rankine system), no harmful system fluids (fluorocarbons), noise reduction are some. *Biowatt* investigated the use of biomass (like wood pallets, chips, sawdust and other biomass waste) as fuel for the external combustion Stirling engine. Typical applications will be for refrigeration and electricity generation in rural areas and developing counties. *Medis El* worked on a prototype Stirling cycle reciprocating linear compressors that could be utilized for automotive climate control (heating and cooling).

Onovwiona and Ugersal (2004) presented a review of the up-to-date cogeneration technologies available for residential applications. The various technologies discussed include the reciprocating internal combustion, micro-turbine, fuel cell and the Stirling engine based cogeneration systems. The paper also discusses the state of development and the performance, environmental benefits, and costs of these technologies. In addition, a comparative assessment of these technologies in terms of their advantages, disadvantages, costs, efficiency, emissions, durability and availability are outlined. The major advantages of the relatively new developed free-piston Stirling engine are also pointed out. A company called *SOLO* (Technical Documentation: *Solo Stirling 161 CHP Module*. Germany: *SOLO* Stirling Engine.

http://www.stirling-engine.de/engl/index.html) developed and tested a Stirling cogeneration module and output measurements where found to be: electrical power output of 2–9.5 kW and a thermal output of 8–26 kW. While the electrical efficiency is in the 22–24% range, the ability to convert the fuel to domestic usable energy resorts to total system efficiency as high as 92%, depending on the amount of heat utilized. A list of companies involved in development of cogeneration system utilizing free-piston Stirling engines is also provided, with details of the various objectives and applications of each company's product. Conclusions of this article is that these emerging technologies (fuel cells, micro-turbines and Stirling engines) will continue to fight an uphill task against the reciprocating internal combustion engine for small-scale cogeneration application until more data from demonstration projects become available, and they meet or surpass current expectations.

Van Heerden (2003) studied several technologies as a solution to electricity delivery to the remote areas with none or limited access to basic infrastructure. He states that due to the low income of these areas, the demand for electricity is low and together with the remoteness of these areas makes grid extensions marginal. Amongst the 10 technologies considered by the author two of them include the application of Stirling engine, one of which is the solar Stirling dish also studied by Redecker (2004) (refer to section 3.3). The author mentions that the required starting time of such a solar powered Stirling is only 10 seconds from the moment the radiation is focussed on the receiver of the SE to actual electricity generation. Peak cycle efficiency of 29.4% for solar-to-electric conversion was recorded; however the author mentions that the average solar-to-electric conversion efficiency lies more in the range of 20% which still exceeds the normal photo-voltaic conversion efficiencies of 12%. The most significant factors that have an impact on the efficiency of the Stirling dish are the condition of the mirror reflectors and the solar tracking accuracy.

3.2 Published Papers and Books

Reiter (1983) summarized the benefits of waste heat recovery systems in 3 categories; 1) Reduction of energy cost, 2) Reduction of equipment cost and size, 3) Reduction of energy use. He also stated that heat recovery systems are both inflation- and price increase-proof, which is something very few other investments are free of. Reiter provides a systems-approach as well as specific design steps for heat recovery systems. Various heat recovery systems are presented together with methods for choosing the most appropriate system for specific applications. Methods for financial analysis and economical justification are explained. Finally a checklist of steps involved in the design of a complete heat recovery unit is provided.

Pavoni et al. (1975) did a comprehensive and critical study on the state of the art refuse disposal and resource recovery methodology. Chapters of interest in this literature include the method of waste heat

recovery used in incinerators. Incinerators are used to burn solid waste (like domestic waste). The heat produced is then recovered by "add-in" heat recovery units to the main incinerator. In Zurich, Switzerland, the steam generated by these incinerator waste heat recovery plants is provided to nearby hospitals, schools and factories. The authors also stated that the potential for heat recovery in this field are favoured by two main circumstances; 1) Solid waste is "clean" high-energy fuel and 2) The energy content of solid waste has been increasing over the past years and is likely to continue to increase. This indicates yet another possible application for Stirling-powered-electricity-generator waste heat recovery units.

Kolin (2001) presented an in-depth study and comparison between the three different Stirling engine configurations namely alpha, beta and gamma. Their relation on the PV-diagram is used to estimate major differences in efficiency and power output. The following conclusions were made with regard to each individual configuration: 1) *Alpha* – Cannot work without dead-space thus reducing surface area on PV-diagram indicating a reduction in power output. Configurations require high pressure ratios and high temperature differences to operate effectively, at 350 – 100 °C hot and cold side temperature used during tests. Very low efficiencies were measured for this engine configuration. Results were obtained by using the Schmidt analysis and actual work measured. 2) *Beta* – Can touch both the isothermal lines on the PV-diagram (hot & cold temperature lines) thus covering the maximum surface area on the ideal thermodynamic cycle. This indicates that this engine is the most efficient and produces the maximum power output. 3) *Gamma* – Cannot touch both the isothermal lines thus covering the least amount of surface area on the PV diagram i.e. not as efficient as above mentioned two engine configurations. The author states that for discontinuous displacer movement, the beta and gamma engines can fulfil almost 100 % of the ideal cycle.

White et al. (1996) presented a paper on the viability and application of Stirling generators for remote power applications. The authors state that Stirling generators offer higher energy conversion efficiency than its thermoelectric or PV counterparts, but their reliability and life expectancy is considered inferior to these direct conversion systems. The authors are involved in the development of the *RemoteGen* (RG) technologies presented by *Stirling Technology Co.* (STC) in Kennewick, Washington, where they developed the RG range of generators (ranging from power capabilities 10W, 350W and 3kW). These Stirling generators all use the same basic configuration comprising of a free-piston Stirling engine utilizing flexural bearings and clearance seals together with moving-iron linear alternator. The efficiency of the linear alternator is lower than its rotating counterparts due to the fact that its flux cutting speed is not constant as with the rotating alternatives. The authors also stated that there are a substantial amount of remote power systems in the range of 10 – 30 Watt. In the areas where photovoltaic power is not practical, most of these use either radioisotope or propane-fuelled thermoelectric generators. Cost of fuel due to their relatively low efficiency limits their use. The Stirling generators discussed by the authors are

expected to require a quarter to a sixth of the amount of fuel making them a highly desirable alternative. A major mass-market opportunity for residential cogeneration applications is identified but it is stated that this is a highly cost sensitive market. Low production rates limit the viability of these Stirling generators and therefore will only become more readily available (and acceptable) as soon as a large capital investment is made in order to improve production rates thus reducing unit prices.

3.3 Previous Work at University of Stellenbosch

Redecker (2004) conducted a study in utilizing a bidirectional converter for a Stirling energy system (SES). The SES he used was developed by *McDonnel-Douglas* in the mid-1980's and operates on solar energy collected with a parabolic dish. This Dish Stirling Solar Generator set (DSSG-25-MKII) module delivers a gross peak electrical output of 25 kW at V_{LL} = 400 V, 3-phase, 50 Hz. The SES is placed on the focal point of the parabolic dish, solar energy is reflected with mirrors (82 individual mirror facets curved slightly and placed side by side so as to form the overall parabolic dish – 11 meters high and 11 meters wide) forming the surface of the parabolic dish. An Induction Motor (IM) is connected to the Stirling engine and operates as a motor and as a generator depending on the system requirements (as determined by the control unit) i.e. bidirectional. The collector dish tracks the sun in order to obtain optimal solar radiation. The author states that over 92% of the solar radiation reflected by the dish is effectively collected by the thermal receiver. This leads to a 29.5 % solar-to-electric conversion efficiency. The study includes a complete simulation model (focusing more on the electrical aspect than mechanical) together with a practical analysis and a result comparison. It was concluded that the solar dish concept was still in its development stages compared to other technologies like the wind turbine and the PV (photovoltaic) panel concept. Further research was recommended in this field as the solar-to-electric conversion efficiency of the solar dish concept is much higher than that of the other two concepts mentioned.

Lotun (2001) designed and evaluated a small scale waste heat recovery system for road going vehicle (heavy duty trucks) applications. The feasibility of such a unit was investigated; preliminary investigations included an evaluation of the amount of recoverable heat energy available in exhaust gasses of internal combustion engines. Calculations were done on a 6-litre diesel engine and results indicated 77 kW of waste heat could be recovered from the exhaust gases of such an engine. A simple Rankine cycle was then investigated to operate on the recovered energy, optimal Rankine parameter was found to be: 800 kPa at 227.2 °C and a water mass flow rate of 0.0015 kg/s as working fluid. A 10-litre diesel engine (together with the continuous combustion unit) was tested with an exhaust gas flow rate of 0.22kg/s and a heat transfer efficiency in the heat exchanger of 89 %, 18.5 kW of power was extracted at the waste heat recovery unit. This represented 4.9 % of the thermal content of the fuel used. A rate of energy production balance was conducted on this 10-litre internal combustion engine indicating that 37 % of the

available fuel power is used to produce shaft power, 29 % is lost to the coolant while 34 % is lost in the exhaust gases. The author concluded that the proposed small scale waste heat recovery unit was working but that there is still ample room for further optimization of the unit. The author also mentions that there is a need for further investigation into waste heat recovery systems for application on smaller automobile IC engines.

Pieterse (2003) built and tested a model solar powered Stirling engine. The Schmidt and West formulas where used to calculate the indicated engine work together with the Beale formula. The solar collector together with a mathematical model of the solar radiation, heat transfer and the closed loop thermosyphon is discussed. The author concluded that the "self-manufactured" Stirling engine operated well enough (theoretically estimated efficiency of 53.6%) but the solar collector fell short of the required result (heat delivered to hot-end of Stirling engine). A recommendation regarding the solar collector was to use a direct reflecting collector that would reflect the solar energy directly on the hot-end of the Stirling engine i.e. no working fluid is used for the solar collector.

3.4 Summary

Renewable and sustainable energy as well as more efficient devices have become the focus point for many scientists throughout the world. One of the main reasons for this so-called mind-shift in society is the rate at which the earth's fossil fuel supplies are depleting. Recovering waste heat forms the main motivations for the study presented in this document. In Section 3.1.1 some of the literature dealing with waste heat recovery is discussed. Incinerators are used to decompose municipal waste, Hsu et al. (2002) proposed a free pistons Stirling engine (FPSE) electricity generation unit utilising waste heat from incinerators. Schmid (2004) stated that over the years, large displacement marine diesel engines have received highly focussed attention from a design perspective resulting in operating efficiencies up to 50%, he states that this means there is still 60 – 70 MW (50%) of wasted fuel energy to be recovered. Schmid (2004) proposed a 7 MW turbo generator.

An alternative to the Rankine cycle for refrigeration and cooling has been considered by Kwon and Berchowitz (2003), the authors considered a Stirling cooler called a free piston Stirling cooler (FPSC). Morrison (1999) provides a review of current and future applications of Stirling engines in refrigeration and electricity generation. Morrison (1999) states that one of the advantages of the Stirling cooler over the Rankine refrigeration cycle is the lower electricity consumption of the FPSC (30% lower than Rankine cycle). Onivwiona and Ugersal (2004) reviewed the current cogeneration technologies available for residential applications. The authors found that a Stirling cogeneration unit developed by a company called *SOLO* produces electrical output efficiency in the 22 – 24% range, a thermal output of 8 – 26 kW and a total system efficiency of up to 92% depending on the amount of heat utilized.

The viability of Stirling generators for remote applications was studied by White et al. (1996). The authors state that the Stirling generators offer higher energy conversion efficiencies that its thermoelectric or photo-voltaic (PV) counterparts, but their reliability and life expectancy is inferior to these direct conversion systems. White et al. (1996) are involved in the development of a 10W, 350W and 3 kW remote generation units developed by *Stirling Technology Co.* Redecker (2004) studied a solar Stirling dish electricity generation unit, he states that a solar-to-electricity conversion efficiency of 29.5% was possible.

It is clear that global interest and development capital is to some extent focussed on modern Stirling engine applications, specifically in the renewable energy and cooling/refrigeration sectors. Stirling technology is certainly not recently developed but incorrect market orientation lead to its slow development (Hargreaves, 1991). Hargreaves (1991) recommends that instead of competing head to head with modern internal combustion engines, the renewable energy sector could be exploited by the use of Stirling engines. He also mentions that Stirling engines, when considered in renewable energy applications like solar Stirling electricity generators, could provide a substantial alternative to fossil fuels.

4. Stirling Engine Analysis (SEA): Literature

4.1 Introduction

The Stirling Engine Analysis (SEA) program discussed in this document is based on the program and methodology developed by Berchowitz and Urieli (1984). It formed part of a course presented at the Ohio University, Athens Ohio. The section to follow is a brief discussion of the program presented by the authors as well as methodology used for analysis. The program presented by Berchowitz and Urieli (1984) was developed for an alpha type Stirling engine and included different heat exchanger geometries and operating conditions. The analysis discussed in this document (Section 5) is, however, for a beta configuration engine with heat exchangers which are quite different (refer to sections to follow for an in depth discussion for the engine considered in this document) to those presented by Berchowitz and Urieli (1984).

The SEA program presented in this document started out as an analysis of the engine and heat exchanger geometry considered by Berchowitz and Urieli (1984). By developing the SEA program for the same engine configuration as presented by the authors, the first verification phase is achieved i.e. with the same inputs as Berchowitz and Urieli (1984); the same results should be obtained thus verifying that the program/analysis is correct. Refer to Section **Error! Reference source not found.** for comparison of results obtained from program to that presented by Berchowitz and Urieli. Changes were then made to the SEA program in order to incorporate the specific engine configuration considered in this document.

4.2 Schmidt (Ideal Isothermal) Analysis

The Stirling cycle, also known as the Ideal Isothermal or Schmidt cycle is almost the same as the Carnot cycle in that heat is transferred to and from the heat source and sink by means of an isothermal heat addition and rejection process, respectively. The Schmidt cycle only differs from the Carnot cycle in that the two (2) isentropic processes are replaced by the two (2) constant volume regeneration processes of the Stirling cycle (Çengel and Boles, 2002).

The Schmidt analysis requires seven (7) design parameters, namely: mean operating pressure p_{mean}, power and displacement piston swept volumes V_P and V_D respectively, clearance volume V_{cl}, hot and cold side temperature T_H and T_C respectively and phase angle lead α of displacement piston over power piston. It is therefore considered a more complex method than for instance the Beale number method which only requires two (2) design parameters (refer to Section 5.7 for discussion on Beale and other SEA methods). Due to the lack of the Schmidt cycle to predict the real air engine cycle it is used today only as a starting point for the design of Stirling engines.

Assumptions made by Schmidt (West, 1980, Berchowitz and Urieli 1984 and Walker 1980):

- Volumes of the working spaces vary sinusoidal with respect to the crank angle
- Perfect regeneration
- Instantaneous pressure is the same throughout the system
- Isothermal working spaces which implies that the heat exchangers & regenerator are 100% effective
- The engine is considered as a five component mechanism (for the purpose of the program developed in this document). Each component is considered as a homogenous entity
- Expansion space and heater as well as the compression spaces and cooler is isothermal
- There are no temperature gradients in the heat exchangers
- Perfect mixing of the operating fluid in the cylinders
- Total mass of gas in the machine stays constant and consists of the sum of masses within each of the five spaces (described in above point); hence no gas leakage
- Operating fluid follows the ideal gas behaviour
- Steady state conditions prevail

Refer to Figure 3 for a graphical illustration of the isothermal working space assumption. This assumption made it possible for Schmidt to obtain an expression for the working gas pressure as a function of volume variation.

The solution of the Schmidt equation set is presented by Berchowitz and Urieli (1984), "Stirling Cycle Machine analysis" (1984). This book is out of print, however the relevant Appendix that deals with the Schmidt analysis was place on the internet and can be downloaded (http://www.globalcooling.com/pdfs/Schmidt.pdf).

The engine is considered as a five (5) component (or 5 cell) serially connected model, consisting respectively of a compression space c, cooler k, regenerator r, heater h and expansion space. The gas within each cell is represented by its instantaneous mass m, absolute temperature T, volume V and pressure p, with the suffix c, k, r, h, and e identifying the specific cell. Figure 3 below indicates the five (5) engine cells for the simplified alpha type SE. Figure 3 also shows the assumed temperatures (or temperature gradients) in the different cells.

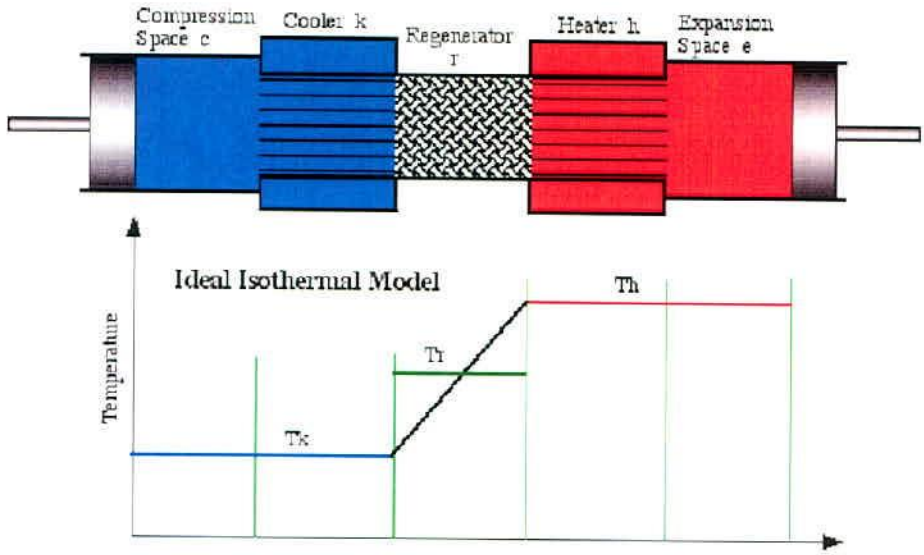

Figure 3: Simplified alpha type SE (Berchowitz and Urieli, 1984)

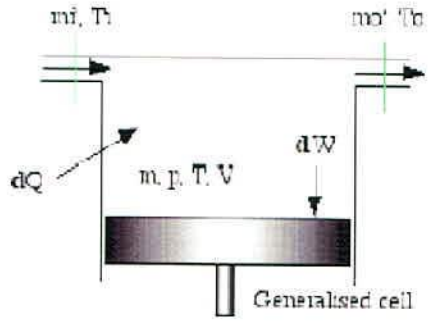

Figure 4: Generalized cell (Berchowitz and Urieli, 1984)

Figure 4 indicates the nomenclature for a generalized cell. For the ideal isothermal model enthalpy is transported into and out of the cell by means of mass flow at certain inlet and outlet temperatures depending on the specific cell involved.

For this generalized cell the energy equation can be stated as;

$$dQ + c_p.(T_i.m_i - T_o.m_o) = dW + c_v.d(m.T) \qquad (4.1)$$

Equation (4.1) is the classical form of the energy equation for non-steady flow problems with the kinetic and potential energy terms neglected.

The starting point for the ideal isothermal analysis is to assume that the total mass of gas in the machine is constant. Hence;

$$M = m_c + m_k + m_r + m_h + m_e \tag{4.2}$$

Substituting the equation of state (also shown in differential form),

$$\begin{aligned} pV &= mRT \\ dp/p + dV/V &= dm/m + dT/T \end{aligned} \tag{4.3}$$

The following relation is found for the total mass of operating gas:

$$M = \frac{p}{R}.\left(V_c/T_c + V_k/T_k + V_r/T_r + V_h/T_h + V_e/T_e\right) \tag{4.4}$$

Berchowitz and Urieli (1984) derived a relation for the assumed linear regenerator temperature (refer to Figure 3) as a function of the log mean difference between heater and cooler temperatures. Regenerator temperature is obtained as follows:

$$T_r = \frac{T_h - T_k}{\ln(T_h/T_k)} \tag{4.5}$$

Thus, given the volume variation (sinusoidal), the equation for pressure as a function of V_e and V_c can be obtained from equation (4.3) and (4.4):

$$p = \frac{MR}{\left(V_c/T_c + V_k/T_k + V_r.\ln(T_h/T_k)/(T_h - T_k) + V_h/T_h + V_e/T_e\right)} \tag{4.6}$$

The total work done and efficiency can then be calculated for a complete cycle:

$$\begin{aligned} W &= W_e + W_c = \oint p.dV_e + \oint p.dV_c = \oint p\left(\frac{dV_e}{d\theta} + \frac{dV_c}{d\theta}\right)d\theta \\ \eta &= W/Q_e \end{aligned} \tag{4.7}$$

Take note that for the isothermal assumption of the Schmidt cycle the efficiency of the engine is ultimately equivalent to the Carnot efficiency (Walker, 1980).

Keeping in mind that for the isothermal model the temperatures of the heater and expansion space as well as the temperature of the cooler and compression space (refer to Figure 3) are respectively constant. Also, with respect to the generalized cell (Figure 4), according to the law of mass conservation the difference between mass inflow (m_i) and mass outflow (m_o) is equal to the mass accumulation (dm) within the cell. The energy equation, equation (4.1) for a specific cell can be simplified to:

$$\begin{aligned} &dQ + c_p.T.dm = dW + c_v.T.dm \quad \text{or} \\ &dQ = dW - R.T.dm \end{aligned} \tag{4.8}$$

With the ideal gas relations:

$$\begin{aligned} &p.V = m.R.T \\ &R = c_p - c_v \\ &\gamma = c_p / c_v \end{aligned} \tag{4.9}$$

The net heat transfer to the working gas over the cycle can then be obtained by integrating dQ over the cycle. According to the assumption of steady state the change of mass in each cell during a cycle is zero, hence:

$$\begin{aligned} &Q_c = W_c \\ &Q_e = W_e \end{aligned} \tag{4.10}$$

The net cyclic heat transfer in the regenerator (Q_r) is equal to zero, this is due to the assumption of perfect regeneration i.e. heat is only transferred to and from the regenerator matrix by the hot and cold gas flowing through the regenerator, thus no heat loss to the environment or regenerator walls. From the geometry of the engine it is clear that $W_k = W_h = W_r = 0$ as there is no work done in the heat exchangers.

The isothermal assumption together with the results of equation (4.10) implies that neither the heater nor cooler contributes any net heat transfer over the cycle i.e. they are not needed for operation and all the required heat transfer takes place over the boundaries of the isothermal working spaces. This is obviously incorrect as the cylinder walls were not designed for heat transfer. A more correct assumption would thus be to have adiabatic simplification for the working spaces but due to the simplicity of this isothermal method it is considered a useful tool during the first phases of Stirling engine design procedures.

The equation set presented by Berchowitz and Urieli (1984) is for an alpha type engine configuration while the engine under consideration in this document is a beta type engine. The thermal analysis is however applicable to any of the three (3) Stirling engine configurations although the volume variations depend on engine configurations as well as drive mechanism. Refer to Appendix A for a summary of the equation set of the Schmidt analysis as presented by Berchowitz and Urieli (1984) for the alpha engine configuration and Appendix C for the derivation of the volume variation for Schmidt analysis based on beta type engine configuration of the Heinrici engine.

4.3 *Ideal Adiabatic Analysis*

As mentioned in Section 4.2 the ideal adiabatic model is superior to the isothermal (Schmidt) model simply because it treats the heater and cooler spaces as adiabatic instead of isothermal. This implies that the net heat transfer over the cycle must be provided by the heat exchangers, which is a more realistic simplification. Energy is only transferred across the interfaces by means of enthalpy transferred to and from the working spaces in terms of mass flow and upstream temperature. Once again the engine is comprised of five components or cells, however the expansion and compression cells are now considered to be adiabatic. Figure 5 illustrates the nomenclature for enthalpy flow through an simplified alpha type engine configuration, where the arrows represent the interfaces between cells. Single suffixes (*c, k, r, h, e*) represents the five (5) engine cells and double suffixes (*ck, kr, rh, he*) represent the four (4) interfaces between cells.

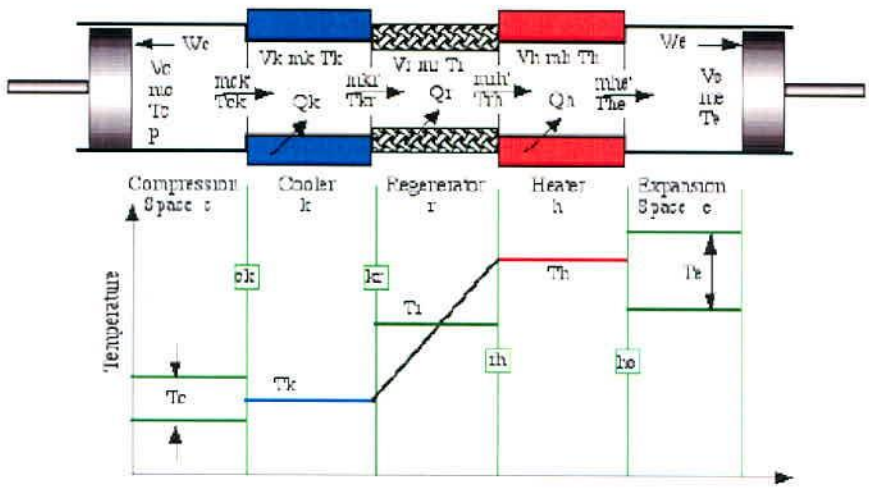

Figure 5: Nomenclature of Simplified alpha type engine (Berchowitz and Urieli, 1984)

Conditional temperatures depending on the direction of mass flow in the engine are the cause of non-linearities within the set of equations developed in this section; this in turn is the reason for using a

numeric approach to solve the equation set instead of using differential or analytical methods. Equation (4.11) states these conditional temperatures:

$$\begin{aligned} &if\ m_{ck} > 0 then T_{ck} = T_c\ else T_{ck} = T_k \\ &if\ m_{he} > 0 then T_{he} = T_h\ else T_{he} = T_e \end{aligned} \tag{4.11}$$

The following assumptions are made for the ideal adiabatic model (Berchowitz and Urieli, 1984):

- Same as for Schmidt analysis stated in previous section, except for adiabatic instead of isothermal assumption
- There is no pressure drop in the engine with regard to resistance to the movement of air over the heat exchangers (i.e. no pumping losses)
- Work is done on the surroundings by means of varying volumes of the respective working spaces V_e and V_c
- Heat is only transferred to/from the working fluid in the allocated heater/cooler spaces
- Heat exchangers are assumed to be isothermal
- Regenerator is externally adiabatic and thus looses no heat to its environment

Relative to the generalized cell shown in Figure 4 the governing equations for the adiabatic model are derived by applying the energy equation (equation (4.1)) and the equation of state (equation (4.3)) to each of the five components. The mass conservation law (continuity equation) is then used to link the resulting equations. Similar to the isothermal model the starting point of the adiabatic model is that the total mass of gas in the engine remains constant. This is summarized by equation (4.2) and is restated below for simplicity:

$$M = m_c + m_k + m_r + m_h + m_e \tag{4.2}$$

The equation for instantaneous engine pressure can be obtained in a similar manner as for the isothermal model; equation (4.6) is restated below for simplicity.

$$p = \frac{MR}{\left(V_c / T_c + V_k / T_k + V_r . \ln(T_h / T_k) / T_h - T_k + V_h / T_h + V_e / T_e\right)} \tag{4.6}$$

By differentiating equation (4.2) the equation for change in mass, yields:

$$dm_c + dm_k + dm_r + dm_h + dm_e = 0 \tag{4.12}$$

Since the temperatures and volumes of the heat exchangers are constant the equation of state given by equation (4.3) is reduced to:

$$dp / p = dm / m \tag{4.13}$$

Reintroducing the equation of state into equation (4.13) a relation for the change in mass for the heat exchanger cells is found:

$$dm = dp.V / R.T \tag{4.14}$$

Substituting equation (4.14) for each of the heat exchanger cells into equation (4.12) yield:

$$dm_c + (dP / R)(V_k / T_k + V_r / T_r + V_h / T_h) + dm_e = 0 \tag{4.15}$$

In order to obtain an explicit relation for the change in internal engine pressure, dm_c and dm_e has to be eliminated from equation (4.15). Consider the adiabatic compression space shown in Figure 6 below:

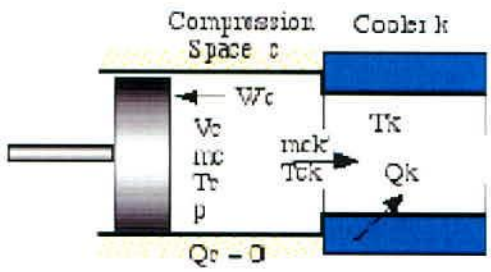

Figure 6: Nomenclature for adiabatic compression space (Berchowitz and Urieli, 1984)

The arrows in Figure 6 indicate the direction of positive mass flow, heat transfer and work done. Applying the energy equation to the adiabatic compression space yields the following relation:

$$-c_p.T_{ck}.m_{ck} = p.dV_c + c_v.d(m_c.T_c) \tag{4.16}$$

Substituting the ideal gas relations (equation (4.9)) into equation (4.16) and simplifying yields the following:

$$dm_c = \left(p.dV_c + V_c.dp/\gamma\right)/R.T_{ck} \tag{4.17}$$

Similarly for the expansion space the change in mass is:

$$dm_e = \left(p.dV_e + V_e.dp/\gamma\right)/R.T_{he} \tag{4.18}$$

Substituting equations (4.17) and (4.18) into equation (4.15) and simplifying yields an explicit relation for the instantaneous internal engine pressure:

$$dp = \frac{-\gamma.p.\left(dV_c/T_{ck} + dV_e/T_{he}\right)}{\left(V_c/T_{ck} + \gamma.\left(V_k/T_k + V_r/T_r + V_h/Th\right) + V_e/T_{he}\right)} \tag{4.19}$$

The change in temperature for expansion and compression space, dT_e and dT_c, is obtained from the differential form of the equation of state (equation (4.3)):

$$\begin{aligned} dT_e &= T_e.\left(dp/p + dV_e/V_e - dm_e/m_e\right) \ \ and \\ dT_c &= T_c.\left(dp/p + dV_c/V_c - dm_c/m_c\right) \end{aligned} \tag{4.20}$$

Applying the energy equation for a generalized cell (equation (4.1)) and substituting the equation of state for a heat exchanger cell, as given in equation (4.14), the following expression is obtained:

$$dQ + \left(c_p.T_i.m_i - c_p.T_o.m_o\right) = c_v.T.dm = c_v.V.dp/R \tag{4.21}$$

Applying equation (4.21) to each of the heat exchanger cells we obtain the change in energy for each cell:

$$\begin{aligned} dQ_k &= c_v.V_k.dp/R - \left(c_p.T_{ck}.m_{ck} - c_p.T_{kr}.m_{kr}\right) \\ dQ_r &= c_v.V_r.dp/R - \left(c_p.T_{kr}.m_{kr} - c_p.T_{rh}.m_{rh}\right) \\ dQ_h &= c_v.V_h.dp/R - \left(c_p.T_{rh}.m_{rh} - c_p.T_{he}.m_{he}\right) \end{aligned} \tag{4.22}$$

Keeping in mind that the heat exchangers are assumed to be isothermal and that the regenerator is ideal we note that: $T_{kr} = T_k$ and $T_{rh} = T_h$. The work done in the compression and expansion cells are given by:

$$\begin{aligned} W &= W_e + W_c \\ dW &= dW_e + dW_c \\ dW_e &= p.dV_e \\ dW_c &= p.dV_c \end{aligned} \tag{4.23}$$

Refer to Appendix B for a summary of the adiabatic equation set as presented by Berchowitz and Urieli (1984) as well as Appendix E for a flow diagram of the adiabatic simulation program (MATLAB).

4.3.1 Method of Solution

The method of solution for the ideal adiabatic analysis begins with the following as user defined inputs:

Table 1: Inputs for adiabatic analysis program

Variable	**Description**
V_k, V_r and V_h	Defined by heat exchanger geometry
R, c_p, c_v and γ	Defined by the choice of operating gas
T_k, T_r, T_h and rpm*	Defined by operating conditions
V_c, V_c, dV_e and dV_c	Analytical function of crank angle θ
p_{mean}	Predefined user input

* Operating frequency (*rpm*) is not a necessary input for the analysis as the analysis considers only a single cycle. The results is however converted using the specified operating frequency to find the overall engine power output in Watts.

With the mean operating pressure of the engine predefined the Schmidt analysis presented in the previous section is then used to evaluate total mass of gas in the engine, where after the adiabatic analysis is done. This method was presented by Berchowitz and Urieli (1984), however for the analysis done on the Heinrici engine considered in this project the method has been altered slightly. It starts out the same but at the end of the simulation the average engine pressure is re-calculated and compared to the original user defined mean operating pressure. The difference is then used to scale the results (including engine pressure) in order to have the beginning and end mean operating pressures the same.

When considering the equation set of which a summary is presented in Appendix B of this document it is found that there are twenty-two (22) variables and sixteen (16) derivatives to be solved for a single cycle. They are:

- T_c, T_e, Q_k, Q_r, Q_h, W_e, W_c – seven (7) derivatives to be integrated
- W, p, V_e, V_c, m_c, m_k, m_r, m_h, m_e – nine (9) analytical variable and derivatives
- T_{ck}, T_{he}, m_{ck}, m_{kr}, m_{rh}, m_{he} – six (6) conditional and mass flow variables

The problem is treated as a quasi steady-flow system, which implies that over each integration interval the four (4) mass flow variables (equation (B.4) in Appendix B) remains constant and there are no acceleration effects. The problem thus becomes a set of seven (7) ordinary differential equations to be solved simultaneously. The approach to solving these differential equations is to formulate it as an initial value problem. With the initial values of the variables know the equations are integrated from that initial state by means of fourth-order Runge-Kutta integration over the complete cycle. The expansion and compression space temperatures are thus initially specified and can be solved through as many cycles as necessary to attain cyclic convergence (for most cases between five (5) and ten (10) cycles/iterations is sufficient).

4.4 Simple Analysis

The simple analysis is based on the adiabatic analysis discussed in the previous section, however some non-ideal effects are considered in the simple analysis that were considered negligible during both the isothermal and adiabatic analyses. These non-ideal effects include non-ideal heat exchangers, non-ideal regeneration and pumping losses. These effects together with the oscillating flow conditions within Stirling engines are extremely difficult to evaluate as available heat exchanger theory is based on documented experimental and empirical studies which were mostly done for steady flow situations. Similar to the adiabatic analysis the Stirling engine is considered as a quasi steady-flow system in that the assumption is made that at any given moment during the cycle the operating fluid behaves as though steady stated conditions prevail. The analysis is called the simple analysis as it is a gross simplification of an extremely complex process. The simple analysis uses the results obtained from the converged adiabatic analysis to introduce or determine the non-ideal effects.

4.4.1 Regenerator effectiveness and thermal efficiency

By definition the regenerator is a cyclic device and in the first cycle, hot gas flows from the heater through the regenerator to the cooler. During this half cycle heat is stored in the regenerator matrix. During the second part of the cycle cool gas flows from the cooler through the regenerator to the heater and by

doing so absorbing the heat, stored during the first part of the cycle, from the regenerator matrix. Theoretically the temperature of the gas leaving the regenerator when flowing from the heater to the cooler should have the same temperature as that of the cooler, similarly when the gas is flowing from the cooler to the heater the gas leaving the regenerator should have the same temperature as the heater. But in reality the regenerator can not be 100% effective. Figure 7 below is a graphical representation of what the regenerator temperature variation is in reality.

The quality of the regenerator is defined on an enthalpy basis in terms of regenerator effectiveness ε, for Stirling engines Berchowitz and Urieli (1984) proposed the regenerator effectiveness to be:

$$\varepsilon \equiv \frac{\left(\begin{array}{l}\text{amount of heat transferred from the}\\ \text{regenerator matrix to the gas in a single blow}\end{array}\right)}{\left(\begin{array}{l}\text{amount of heat transferred from the regenerator}\\ \text{matrix to the gas in a single blow of the ideal adiabatic model}\end{array}\right)} \tag{4.24}$$

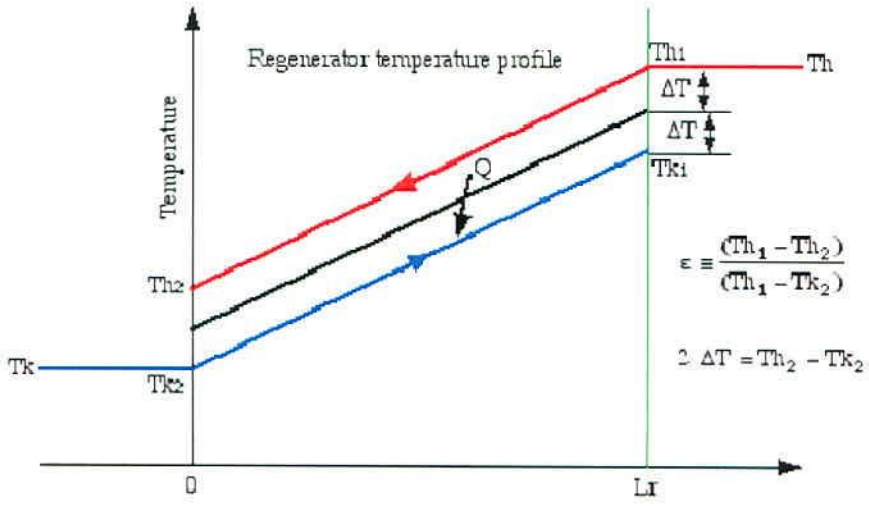

Figure 7: Regenerator effective temperature profile (Berchowitz and Urieli, 1984)

From Figure 7 the regenerator effectiveness can be obtained in terms of the two (2) heater and two (2) cooler temperatures (T_{h1}, T_{h2}, T_{k1} and T_{k2}) as follows (refer to equations (4.29) – (4.31) for further derivations for regenerator effectiveness):

$$\varepsilon \equiv \left(\frac{Th1 - Th2}{Th1 - Tk2}\right) \tag{4.25}$$

Note in Figure 3 how the temperature of the gas drops when flowing from the heater through the regenerator to the cooler and visa versa when flowing in the opposite direction. This implies that the

heater will need to supply more heat to the gas as it enters the heater from the regenerator with a temperature lower than the heater temperature, quantitatively presented as follows:

$$Q_h = Q_{hi} + Q_{ri}(1-\varepsilon) \tag{4.26}$$

Where the suffix "i" represents the heat transfer obtained from the ideal adiabatic analysis.

Similarly the cooler would have to transfer more heat to the environment as the gas entering the cooler from the regenerator would have a temperature higher than the cooler temperature, quantitatively presented as follows:

$$Q_k = Q_{ki} + Q_{ri}(1-\varepsilon) \tag{4.27}$$

The thermal efficiency of the non-ideal engine is then given by:

$$\eta = \frac{\eta_i}{\left[1+\left(\frac{Qri}{Qhi}\right)(1-\varepsilon)\right]} \tag{4.28}$$

Where η_i refers to the efficiency obtained from the ideal adiabatic analysis (refer to Appendix B, equation (B.8)).

Equation (4.25) states the regenerator effectiveness as a function of the two (2) heater and two (2) cooler temperatures (refer to Figure 7). Since these temperatures are not known in reality, regenerator effectiveness is evaluated by means of the number of transfer units (NTU) method. With the analysis based on fluid properties of the operating gas flowing through the heat exchanger instead of actual heat exchanger size, the NTU method is defined in terms of the Stanton number:

$$N_{ST} = h/(\rho u c_p) \tag{4.29}$$

With NTU calculated as follows:

$$NTU = N_{ST}.(A_{wg}/A)/2 \tag{4.30}$$

With the fluid density, ρ [kg/m^3], the gas velocity through the heat exchanger, u [m/s], the total wetted area of the heat exchanger (regenerator in this case), A_{wg} [m^2], the total free flow area of the heat exchanger, A [m^2] and the overall heat transfer coefficient (hot stream/matrix/cold stream), h.

The factor 2 in equation (4.30) stems from the fact that the Stanton number is defined for heat transfer from a gas stream to a matrix only, whereas for the cyclic nature of the regenerator problem described here heat is also transferred from the matrix to the gas stream.

The regenerator effectiveness can then be obtained by the following:

$$\varepsilon = \frac{NTU}{(1 + NTU)} \tag{4.31}$$

4.4.2 Evaluation of Heater and Cooler Effectiveness

The effectiveness of the heater and cooler can be evaluated in much the same way as for the regenerator i.e. by means of the number of transfer units (NTU) the heat exchanger effectiveness then becomes (Refer to the forgoing section for the derivation of the value of NTU):

$$\varepsilon = 1 - e^{-NTU} \tag{4.32}$$

In Figure 8 it can be seen that for the real heater and cooler the mean effective temperatures in the heater and cooler is respectively lower and higher than the respective heat exchanger wall temperatures. This implies that the engine is operating between lower temperature limits than originally specified which effectively reduces the performance of the engine.

The simple analysis for the heater and cooler iteratively determines these lower operating temperature limits by using the convective heat transfer equations. Values for the heater heat transfer (Q_h) and cooler heat transfer (Q_k) is obtained from the adiabatic analysis.

From the basic heat transfer equation:

$$\dot{Q} = h.A_{wg}.(T_w - T) \tag{4.33}$$

Where $\dot{Q}$ is the heat transfer power [W], h is the convective heat transfer coefficient [W/m^2.K], A_{wg} the wetter (wall/gas) area of heat exchanger surface, T_w is the wall temperature [K] and T the gas temperature K}. By applying equation (4.33) to the heater and cooler and reducing the units of $\dot{Q}$ from [W] to [Joule/s] by introducing the cycle frequency, the respective heater and cooler gas temperatures can be found (the units of $\dot{Q}$ is reduced in order to obtain the heat transfer for a single cycle, hence being able to evaluate heater and cooler temperatures during each iterative cyclic analysis):

$$T_k = T_{wk} - freq.Q_k / (h_k . A_{wgk})$$
$$T_h = T_{wh} - freq.Q_h / (h_h . A_{wgh}) \quad (4.34)$$

Where T_{wk} and T_{wh} is the respective cooler and heater wall temperatures, h_k and h_h is the respective cooler and heater convective heat transfer coefficients, A_{wgk} and A_{wgh} is the respective cooler and heater wetted areas while Q_k and Q_h is the respective cooler and heater heat transfer obtained from adiabatic analysis.

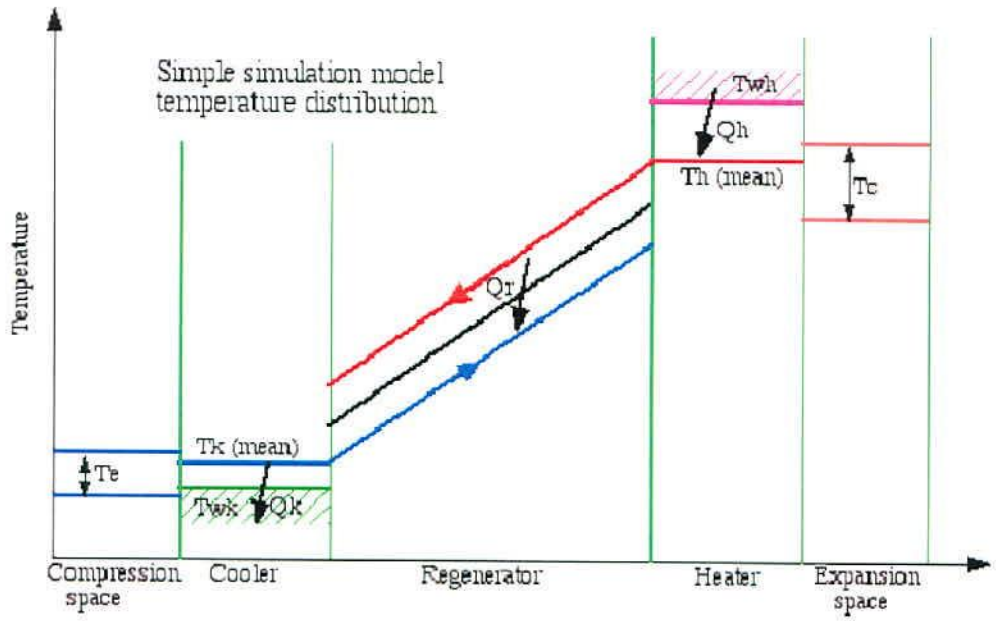

Figure 8: Real SE effective temperature profile (Berchowitz and Urieli, 1984)

The algorithm used for the solution of the heater and cooler gas temperatures requires the iterative invoking of the adiabatic analysis (refer to Figure 17 for simple analysis algorithm). With the heater and cooler heat transfer values (Q_k and Q_h) available after each adiabatic simulation the mass flow rates through the heater and cooler are used to determine the Reynolds numbers and hence the heat transfer coefficients. Substituting these values into equation (4.34) yields the new gas temperatures for the heater and cooler, this process is repeated until the successive values differ with a user defined tolerance i.e. until they are essentially equal.

4.4.3 Evaluation of Pumping Loss

During the isothermal and adiabatic analysis it was assumed that the instantaneous pressure is the same throughout the engine. In the practical engine, however, the fluid friction associated with the flow through

the heat exchangers will in fact result in a pressure drop across the heat exchangers that will in turn reduce the output power of the engine. This is referred to as "pumping loss" and this section attempts to quantify this pumping loss. The pressure drop over the three (3) heat exchangers is evaluated with respect to the compression space and the summation thereof ($\sum\Delta p$) is then used to reduce the total engine work term, *W*.

$$W = \oint p.(dV_e + dV_c) - \oint \sum \Delta p.dV_e = W_i + \Delta W \tag{4.35}$$

Where W_i is the work done per cycle as obtained from the ideal adiabatic analysis and ΔW is pumping loss per cycle converted to work loss. With,

$$\Delta W = \int_0^{2\pi} \left(\sum_{i=1}^{3} \Delta p_i . \frac{dV_e}{d\theta} \right) d\theta \tag{4.36}$$

According to Newton's law of viscosity the shear stress (τ) between adjacent layers of fluid is proportional to the fluid velocity gradient (*du/dz*), with the dynamic viscosity (μ) [kg/m.s] a measure of internal fluid friction, the shear stress between particles is:

$$\tau = -\mu . \frac{du}{dz} \tag{4.37}$$

Viscosity is however dependant on temperature. Temperature dependency is obtained from the following equation (Berchowitz and Urieli, 1984):

$$\mu = \mu_0 . \left(\frac{T_0 + T_{SU}}{T + T_{SU}} \right) \left(\frac{T}{T_0} \right)^{3/2} \tag{4.38}$$

Where T_0 = 273 K and T_{SU} is the Sutherland constant defined by the choice of operating fluid.

The frictional drag force can then be obtained as follows:

$$F = \tau . A_{wg} \tag{4.39}$$

With the wetted area $A_{wg} = 4.V/d_h$, and d_h being the hydraulic diameter of the flow passage. By defining a coefficient of friction (C_f) and substituting for τ in equation (4.39) the frictional drag force is obtained as follows:

$$C_f \equiv \frac{\tau}{0.5.\rho.u^2}$$
$$F = 2.C_f.\rho.u^2.V / d_h \qquad (4.40)$$

With u the bulk fluid velocity and ρ the fluid density.

Noting that the frictional drag force (F) is equal and opposite to the pressure drop force ($\Delta p.A$) equation (4.41) is obtained, this however violates the conservation of mass principle when the direction of flow is reversed. By introducing the Reynolds friction coefficient (C_{ref}) as the product of the Reynolds number ($Re = \rho.u.d_h/\mu$) and the coefficient of friction (equation (4.40)) the pumping loss pressure drop (Δp) can be obtained independent of the direction of flow:

$$\Delta p = \frac{-2.C_{ref}.\mu.u.V}{d_h^2.A} \qquad (4.41)$$

Berchowitz and Urieli (1984) states that due to the highly oscillating nature of flow within Stirling engines it is reasonable to assume that the flow would always be turbulent. Organ (1997) mentions that this is still a mere assumption in order to be able to analyse the actually ill understood situations within Stirling engines. Organ stated: "*The general case of cyclically reversing, compressible flow with friction, heat transfer and pressure swing is not understood. Regenerator and Stirling engine design thus remains dependant on the use of steady flow correlations and subject to the arbitrary rationalizations involved in applying these.*"

5. Heinrici Stirling Engine Analysis (HSEA)

5.1 Introduction

The methodology presented in the previous section of this document is based on work done by Berchowitz and Urieli (1984). This section is a discussion of how this SEA program was implemented to analyse the Heinrici Stirling Engine (HSE) used for experimental verification of simulated results. The code presented by Berchowitz and Urieli (1984) was for an alpha type engine configuration while the Heinrici engine is of the beta type with topology as described in Section 5.3. Segments of the computer code are shown in this section to improve understanding as well as to illustrate the implementation of the methodology discussed in Section 4 of this document. A layout of the computer code is also presented and discussed together with algorithms to indicate iterative procedures.

In the previous section, Figure 5 states the nomenclature of the simplified five (5) cell, alpha configuration engine considered by Berchowitz and Urieli (1984). The Heinrici engine used for experimental testing is however a much less complex engine, Figure 10 and Section 5.3 presents the engines topology. The Heinrici engine has no regenerator matrix (like foil or metal gauze) with the ability to store heat during the cycle. It also has no internal heat exchanger surface (like slots of tubes) but depends only on the hot and cold-end cylinder walls for heat addition and heat rejection. The annulus formed between the hot-end sleeve wall and the displacer piston (refer to Figure 10) is defined as the regenerator. The thin wall of the displacer piston can be considered to have some regenerative effect during the cycle but for the sake of the analyses methods described in this document the regenerator is considered as non-existing with a porosity of 100%. The regenerator is, however given a physical volume in order to relate to the five (5) volume methodology presented by Berchowitz and Urieli (1984) and discussed in Section 5.3. Refer to Appendix G for photographs of the Heinrici engine as well as Section 6.2.1 for further information regarding the particular engine.

5.2 MATLAB Program Layout and Discussion

A layout of the main Stirling Engine Analysis (SEA) program is presented here. The program consists of five (5) different methods (B - F in Figure 9) of analysis for Stirling engines. Refer to Section 5.7.2 for discussion of the *Beal* and *West* methods shown respectively by E and F. Section 5.4 contains the discussion of the *Isothermal/Schmidt* (D) method while Sections 5.5 and 5.6 discuss the ideal *adiabatic* (B) and *simple* (C) methods, respectively. The *Define* block (A) in Figure 9 contains the input variables and user defined operating conditions.

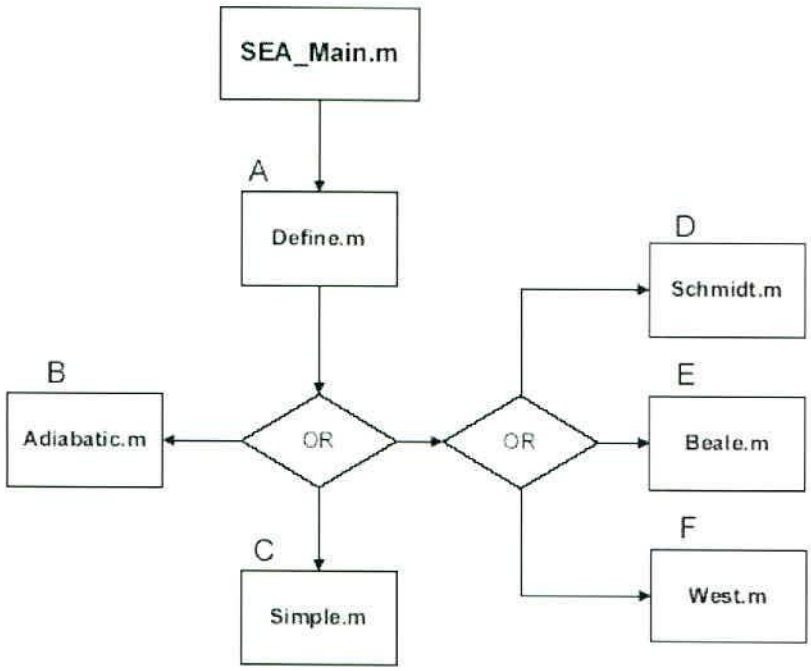

Figure 9: Layout of main SEA computer code

Refer to Appendix D, E and F for the complete layout of the main computer code indicating sub-functions invoked by each method (A to F) shown in Figure 9. Appendices D, E and F also give an indication of the order of invoking and/or dependencies between sub-functions. Each block in Figure 9 represents a different MATLAB m-file; these m-files execute the following tasks:

SEA_Main.m: This is the main Stirling analysis file from which one or more of the other (A – F) m-files are invoked. *Sea_Main.m* starts out by opening *Define.m* in order to define operating conditions for the analysis. It then presents the user with a choice of five (5) methods to be used to analyse the particular Stirling engine under consideration. *SEA_Main.m* is thus the user interface of the Stirling analysis program.

A) *Define.m*: Global variables are listed here; these variables are then recalled and recalculated in the various sub-functions invoked during a cycle. Operating conditions for the analysis are also defined here. User defined inputs include:

- Upper (T_h) and lower (T_k) temperature limits (refer to *operat.m*)
- Engine rotating speed (rpm) (refer to *operat.m*)
- Geometry of heat exchanger and regenerator (refer to *heatexch_geo.m* and *regen_geo.m*)
- Choice of operating fluid (Helium, Air, Hydrogen) (refer to *gas.m*)
- Engine drive mechanism (Yoke drive, Heinrici drive) (refer to *engine.m*)

B) *Adiabatic.m*: This m-file invokes the necessary sub-function to do the adiabatic analysis. The Schmidt analysis is used as a starting point to the adiabatic analysis and is thus the first sub-function to be invoked. Outputs include:

- Mass of operating fluid [kg]
- Cyclic thermal efficiency [%]
- Power gained at heater and lost and cooler [W]
- Work/power output of engine [W]

C) *Simple.m*: This m-file invokes the necessary sub-function to do the simple analysis. The adiabatic analysis is used as a starting point for the simple analysis and is thus the first sub-function to be invoked (*adiabatic.m*). Real effects like non-ideal heat exchangers (*hotsim.m* and *kolsim.m*), non-ideal regenerators (*regensim.m*) and pumping loss (*worksim.m*) are considered. Outputs include

- Cyclic thermal efficiency [%]
- Mass of operating fluid in engine [kg]
- Thermal power gained at heater and lost at cooler [W]
- Work/power output of engine [W]
- Regenerator net enthalpy loss [W] (*regensm.m*)
- Regenerator wall heat loss [W] (*regensm.m*)
- Pumping loss [W] (*worksim.m*)
- Actual power generated by engine [W] (*worksim.m*)
- Actual power gained at heater [W] (*worksim.m*)
- Actual efficiency [%] (*worksim.m*)

D) *Schmidt.m*: Ideal isothermal analysis is bases on work done Berchowitz and Urieli (1984). Refer to Section 4.2 for the listed seven (7) design parameters required for operation of this method. Outputs include:

- Total internal mass of gas [gram]
- Cyclic thermal efficiency [%]
- Engine power output [W]
- Cyclic work done [J]
- Heat energy gained at heater [W]

- Heat energy dissipated at cooler [W]

E) *Beal_MPPF.m*: Kontagool et al. (2005) presented the methods of Beal and Mean Pressure Power Formula (MPPF). Outputs include:

- Beale estimated engine power output [W]
- MPPF estimated engine power output [W]

F) *West.m*: Kontragool et al. (2005) presented the method of West. The West method is similar to the method of Schmidt. This method only returns the following outputs:

- Indicated engine work [W]

5.3 Heinrici Engine Topology

The methodology developed by Berchowitz and Urieli (1984) utilises a five (5) volume approach similar to that indicated for the simplified engine in Figure 3. The Heinrici engine considered here however does not have a regenerator or specific internal heater and cooler heat exchangers as is the case for the simplified model. For this reason the internal volumes of the Heinrici engine is defined in such a way that it satisfies the five (5) volume approach. Figure 10 indicates the five (5) volumes within the Heinrici engine and provides the point of departure for the discussion to follow in the sections below.

NOTE: From Figure 10 it is clear that for the Heinrici engine, the volume of the cooler (V_k) is not constant and depends on the crank angle (theta) or position of the power piston. This was the case for the alpha type engine configuration considered by Berchowitz and Urieli (1984). Refer to Section 5.6.2 for further discussion on the assumption of constant cooler volume for the Heinrici engine.

The nomenclature of the expansion space shown in Figure 11 for the beta type Heinrici engine configuration is similar to that of the alpha type engine configuration considered in the literature and shown in Figure 6. Note that Figure 6 shows the compression space while Figure 11 shows the expansion space. For the Heinrici engine the expansion space are considered in order to indicate to the reader that although the function and geometry is not the same, the same methodology applies to both these spaces (refer to Figure 3).

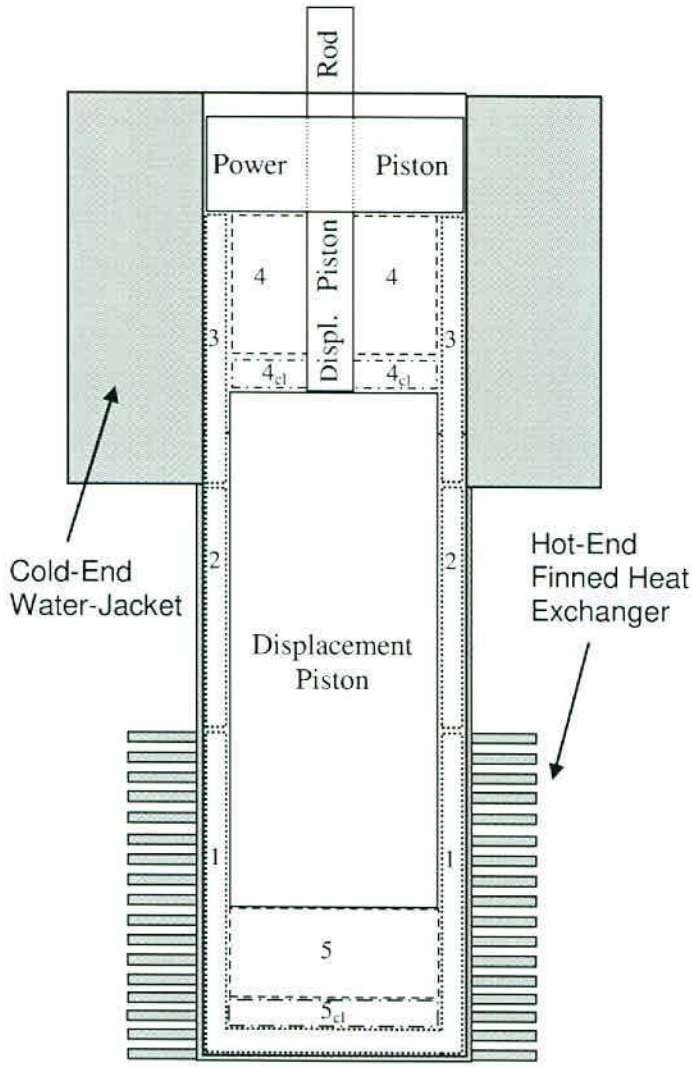

1) Heater volume (V_h)
2) Regenerator volume (V_r)
3) Cooler volume (V_k)
4) Compression space volume (V_c)
4_{cl}) Compression space clearance volume (V_{clc})
5) Expansion space volume (V_e)
5_{cl}) Expansion space clearance volume(V_{cle})

Figure 10: Heinrici engine volume definitions for simulation purposes

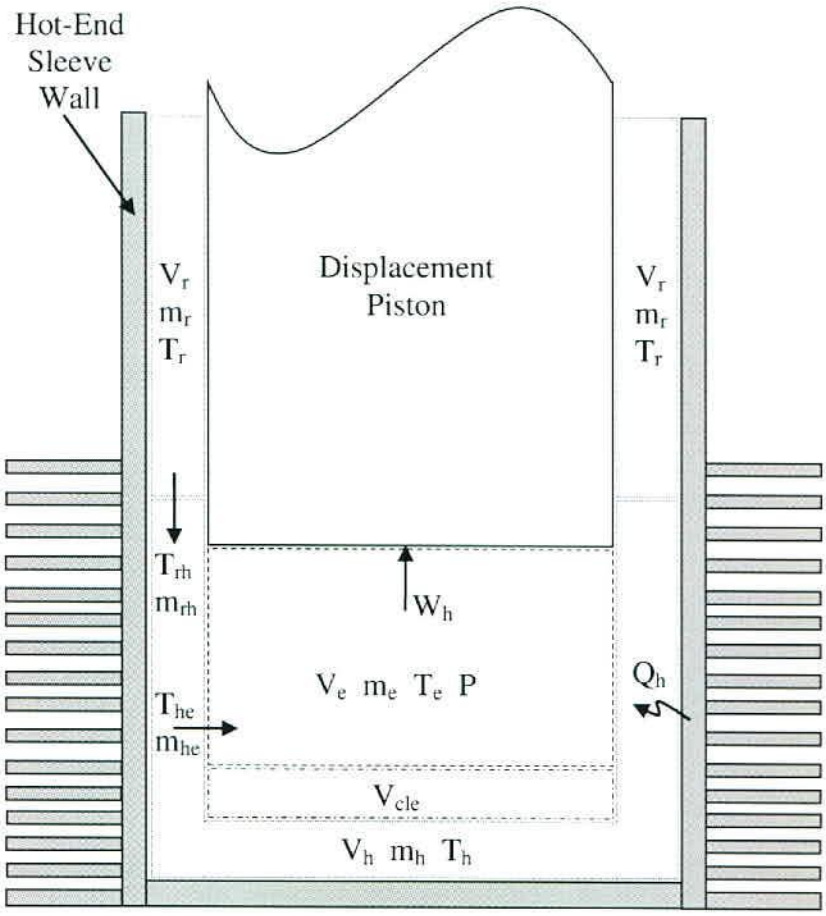

Figure 11: Nomenclature of expansion space of HSE for adiabatic model

5.4 Schmidt (Ideal Isothermal) Analysis

The Schmidt analysis referred to in the computer program presented in this document is based on the equation set described by Berchowitz and Urieli (1984) for the ideal isothermal model with sinusoidal volume variation (refer to Section 4.2). Care should however be taken with regard to the specific engine configuration and relevant volume variation equations. The equation set presented by the authors is for an alpha type engine configuration while the engine under consideration in this document is a beta type engine of which the topology is described in Section 5.3. Refer to Appendix A for a summary of the equation set of the Schmidt analysis as well as Appendix C for the derivation of the volume variation for Schmidt analysis based on Beta type or Heinrici engine configuration.

Note that for the alpha configuration engine considered in literature, the void volumes of the heater (V_h) and cooler (V_k) are constant. For the beta configuration (Heinrici) engine this is however not the case as the heater void volume (V_h) is constant but the void volume of the cooler (V_k) depends on the position of

the power piston i.e. V_k depends on crank angle theta. The varying cooler void volume is accommodated by taking the average volume (and heat transfer area) over the cycle, and using that as a constant for further calculations. The constant cooler length is calculated by averaging the length of the cooler (as a function of crank angle) over a single cycle. Cooler volume is determined by multiplying the cooler annulus area (refer to Figure 10) by the length of the cooler (L_k).

5.4.1 Results from Schmidt analysis

The measured data from experimental tests is used as user defined operating conditions for the Schmidt analysis performed on the Heinrici Stirling Engine (HSE). These operating conditions are listed in Table 2 below:

Table 2: Operating Conditions for HSE

Description/Variable	**Value**	**Unit**
Mean operating pressure (p_{mean})	1.148	bar
Cold side wall temperature (T_k)	46	^{0}C
Hot side wall temperature (T_h)	448	^{0}C
Operating frequency (*rpm*)	73.3	rpm

Figure 12 shows the simulated change in pressure and volume for the total working space (also know as the pressure–volume or PV diagram) for the Schmidt model. The area of the total work diagram is said to be the principle design criterion; the bigger the area the better the engine (Walker, 1980). Maximising this working area and engine efficiency is one of the main purposes of the Stirling engine designer. Choice of operating fluid, heat exchanger and engine geometry and drive mechanism are only some of the variables affecting the above mentioned criterion for a well designed engine.

In reality Pressure-Volume diagrams does not exist for Stirling engines since there will be different pressure values along the internal gas circuit of the engine. It is also important to note that it would be more informative to have a Pressure-Volume diagram for each of the two working spaces within the engine when comparing different the Schmidt, adiabatic and simple analyses methods to each other. Due to the complexity of the pressure measurement equipment required at the hot end of the machine it was decided to only compare measurements and theory at the cold end (placed beneath the power piston).

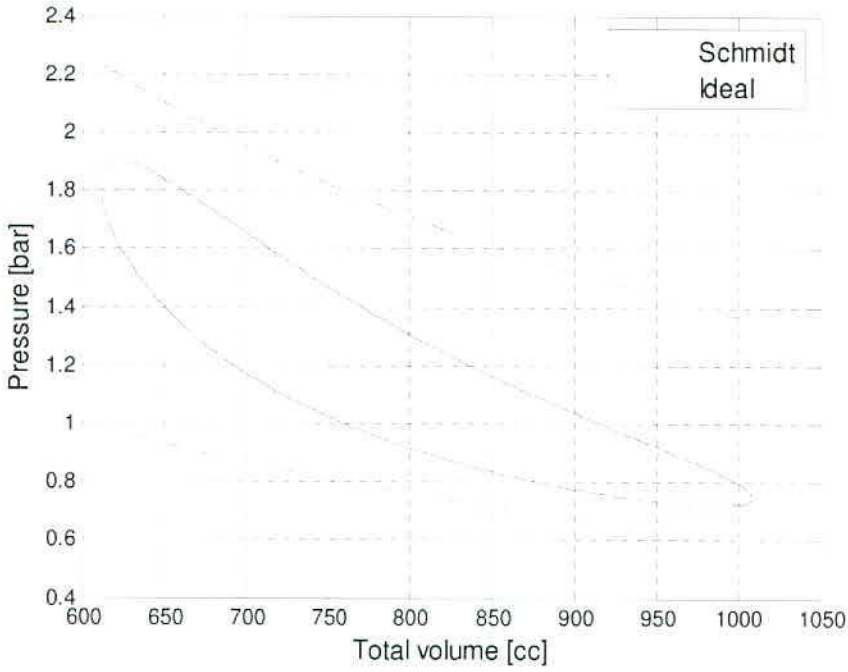

Figure 12: P-V diagram: Schmidt analysis

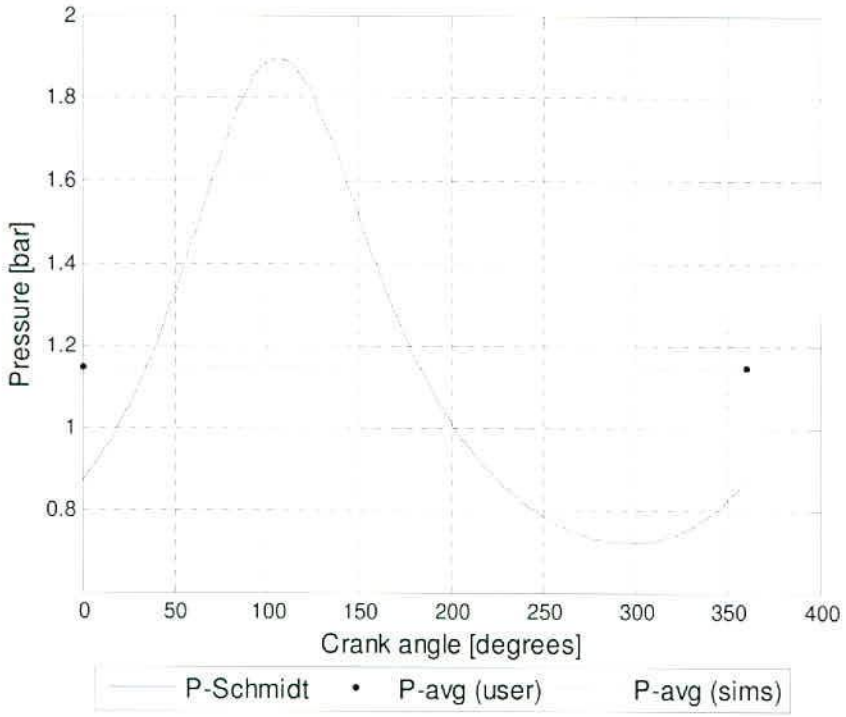

Figure 13: Engine internal pressure variation from Schmidt analysis

Note the difference in area enclosed between the two (2) lines illustrating the upper and lower limits of the ideal PV diagram and the area enclosed by the Schmidt PV diagram in Figure 12. As mentioned earlier the Schmidt analysis does not incorporate non-ideal effects and lacks the ability to (accurately) predict the internal engine pressure and temperature fluctuations. This is a possible reason for the dramatic difference between the PV diagrams of the adiabatic, simple (discussed in sections to follow) and isothermal analysis. Since the Schmidt analysis is the most idealized of the three (3) methods it is expected that it should be the closest to the ideal scenario, this is however not the case. Further discussion on this regard can be found in sections to follow

The ideal PV diagram's upper and lower limits are determined using the equation of state for an ideal gas (equation (4.3)) with the total mass of gas as obtained from the Schmidt analysis (refer to Appendix A for a summary of the Schmidt analysis equation set). Upper and lower limits are determined by setting the total engine volume at the user defined hot-side (T_h) and cold-side temperatures (T_k), respectively.

The ideal Stirling cycle indicated in Figure 12 comprises of the following four (4) idealised steps in the complete cycle: 1) the lower limit is due to compression at constant cooler temperature (T_k), 2) left or minimum volume limit is due to constant volume heat addition in the heater, 3) the upper limit is due to expansion at constant heater temperature (T_h), 4) right or maximum volume limit is due to constant volume heat rejection in the cooler.

Figure 13 shows the change in internal engine pressure as a function of crank angle position. Note that the average value of the simulated pressure (legend in Figure 13: "P-avg(sims)") is the same as the user defined input average pressure. During iterative simulation procedures the average engine pressure changes from that specified by the user. At the end of the simulation the average simulated engine pressure is compared to the initial user defined values, the difference is then used to obtain an updating factor or pressure correction factor (refer to Table 3). Values for compression and expansion space work done as well as mass of gas in engine are then updated by this factor.

Table 3 below contains the numeric results obtained from the Schmidt analysis of Heinrici Stirling Engine (HSE) with operating conditions and geometry as stipulated in Table 2 and Appendix H respectively. Note that the power output is the total predicted power output of the engine, and not only the cyclic power output i.e. the cyclic work in Joule is multiplied by the operating frequency to obtain the total power output of the engine.

Table 3: Numeric results from Schmidt simulation of HSE

Description	Value	Unit
Pressure Correction Factor	0.426*	-
Mass of gas	0.6605	g
Thermal efficiency	55.76	%
Power output of thermodynamic cycle	21.81	W

*The pressure correction factor for the Schmidt analysis forms the initial correction factor and is therefore a higher amount than that of the adiabatic or simple analyses.

5.5 *Ideal Adiabatic Analysis*

The implementation of the adiabatic simulation for the Heinrici engine has the same inputs as stipulated in Table 1 with the engine's topology described in Section 5.3. The method of solution for the equation set described in Section 4.3.1 (and summarised in Appendix B) is implemented in MATLAB by creating two (2) matrices, one containing the variables (22 variables in a matrix called "var") and the other the sixteen (16) derivatives (16 derivatives in a matrix called "dvar"). The first seven (7) derivatives (refer to Section 4.3) are integrated at each degree of rotation of the crank system i.e. for 360 degrees or one cycle. Thus is done by using fourth order Runge-Kutta integration. These seven variables are: Compression (T_C) and Expansion (T_E) space temperatures, heat transferred to cooler (Q_K), heat transferred from heater (Q_H), cyclic heat transferred to/from regenerator (Q_R) and work done by the compression (W_C) and expansion (W_E) spaces. Every 10^{th} value in this integration cycle is then saved to create a matrix of size 22x37.

The Schmidt analysis is used to initialise the adiabatic analysis procedure i.e. the mass of gas in the engine is obtained by doing the Schmidt analysis. Since the main adiabatic analysis program (*adiabatic.m*) is only invoked once the Schmidt analysis only return the initial values once, this is however not the case for the Simple analysis (refer to 5.6 for discussion). Each row in the "var" matrix has an assigned index number indicating the definition of the variable, for example *var(TC) = var(1) = compression space temperature*. The indices are assigned and implemented as follows in MATLAB code:

```
%Define vars
TC = 1;        %compr temp (K)
TE = 2;        %exp temp (K)
QK = 3;        %heat trans to cooler (J)
QR = 4;        %heat trans to regen (J)
QH = 5;        %heat trans to heater (J)
WC = 6;        %work done by comr space (J)
WE = 7;        %work done by exp space (J)
W = 8;        %total work done (WE+WC) (J)
P = 9;        %pressure (J)
VC = 10;        %compr space vol (m3)
VE = 11;        %exp space vol (m3)
MC = 12;        %gas mass in comr space (kg)
MK = 13;        %gas mass in cooler (kg)
MR = 14;        %gas mass in regen (kg)
MH = 15;        %gas mass in heater (kg)
ME = 16;        %gas mass on exp space (kg)
TCK = 17;        %temp from compr space -> cooler (K)
THE = 18;        %temp from heater -> exp space (K)
MfCK = 19;        %gas mass flow from compr space -> cooler (kg/rad)
MfKR = 20;        %gas mass flow from cooler -> regenerator (kg/rad)
MfRH = 21;        %gas mass flow from regen -> heater (kg/rad)
MfHE = 22;        %gas mass flow from heater -> exp space (kg/rad)
```

During each cyclic integration two columns are created, one containing the current (crank position, theta) values ranging from *y(TC)* to *y(MfHE)* for the twenty-two (22) variables mentioned above and the other containing the values of the 16 derivative variables ranging from *dy(TC)* to *dy(ME)*. Cyclic integration is implemented as follows in *adiabatic.m*:

```
while terr>eps & it<maxit
    it = it + 1;
    if it == maxit, break, end    %stop within max # of iters
    for I = 1:1:360
        %do 4th order Runge-Kutta integration
        [theta,y,dy] = rk4('dadiab',n,theta,dtheta,y);
    end
    %calculate change in temperature
    terr = abs(tc0 - y(TC)) + abs(te0 - y(TE));
end
```

The variable columns (y values) are then saved in the 22x37 matrix as follows (keep in mind that the first column of the 22 variable matrix has all zero values, except for user defined inputs summarised in Table 1, in order to initiate integration):

```
for i = 2:1:37
    for j = 1:1:10
        [theta,y,dy] = rk4('dadiab',n,theta,dtheta,y);
    end
    %writes y & dy values to var & dvar matrices
    [var,dvar] = filmatrix(i,y,dy,var,dvar);
End
```

Where *n* is equal to seven (7) and depicts the first seven integrated variables (*y(TC)* to *y(WE)*) in the "var" matrix . The "dadiab" function calls the *dadiab.m* file where the sixteen (16) derivatives are analytically calculated for the current crank position i.e. for each theta (θ) value. The *dadiab.m* function calls *volume.m* which returns the current volume and volume derivatives. Refer to Appendix C for

derivation of volume variation and volume derivative for the Heinrici engine and Appendix E for a layout of the adiabatic program.

These derivatives are then used for the fourth order Runge-Kutta integration procedure. The sixteen (16) derivatives obtained analytically in *dadiab.m* are implemented as follows:

```
[y(VC),y(VE),dy(VC),dy(VE)] = volume(theta);

%pressure & Pressure derivatives
voidv = vk/tk + vr/tr + vh/th;
y(P) = mgas*rgas/(y(VC)/y(TC) + voidv + y(VE)/y(TE));
top = -y(P)*(dy(VC)/y(TCK) + dy(VE)/y(THE));
bot = (y(VC)/(y(TCK)*gama) + voidv + y(VE)/(y(THE)*gama));
dy(P) = top/bot;

%mass accumulation & derivatives
y(MC) = y(P)*y(VC)/(rgas*y(TC));
y(MK) = y(P)*vk/(rgas*tk);
y(MR) = y(P)*vr/(rgas*tr);
y(MH) = y(P)*vh/(rgas*th);
y(ME) = y(P)*y(VE)/(rgas*y(TE));
dy(MC) = (y(P)*dy(VC) + y(VC)*dy(P)/gama)/(rgas*y(TCK));
dy(ME) = (y(P)*dy(VE) + y(VE)*dy(P)/gama)/(rgas*y(THE));
dpop = dy(P)/y(P);
dy(MK) = y(MK)*dpop;
dy(MR) = y(MR)*dpop;
dy(MH) = y(MH)*dpop;

%mass flow between different sctions of engine (kg/rad)
y(MfCK) = -dy(MC);     %gas mass flow from compr space -> cooler
y(MfKR) = y(MfCK) - dy(MK);    %gas mass flow from cooler -> regenerator
y(MfHE) = dy(ME);      %gas mass flow from heater -> exp space
y(MfRH) = y(MfHE) + dy(MH);     %gas mass flow from regen -> heater

%temperature conditions depending on direction of air flow in SE
y(TCK) = tk;
if y(MfCK) > 0     %air flowing from compr space to cooler
    y(TCK) = y(TC);
end
y(THE) = y(TE);
if y(MfHE) > 0     %air flowing from  heater to expansion space
    y(THE) = th;
end

%7 derivatives as integrated by rk4 (n=7, dvars)
%temperatures of working space
yVC = y(VC);
yMC = y(MC);

%change in working space temps
dy(TC) = y(TC)*(dpop + dy(VC)/y(VC) - dy(MC)/y(MC));%differential form of Ideal
gas eq
dy(TE) = y(TE)*(dpop + dy(VE)/y(VE) - dy(ME)/y(ME));

%Energy derivatives
dy(QK) = vk*dy(P)*cv/rgas - cp*(y(TCK)*y(MfCK) - tk*y(MfKR));
dy(QR) = vr*dy(P)*cv/rgas - cp*(tk*y(MfKR) - th*y(MfRH));
dy(QH) = vh*dy(P)*cv/rgas - cp*(th*y(MfRH) - y(THE)*y(MfHE));
dy(WC) = y(P)*dy(VC);
dy(WE) = y(P)*dy(VE);

%net work done
dy(W) = dy(WC) + dy(WE);
y(W) = y(WC) + y(WE);
```

At the end of the adiabatic analysis the average simulated engine pressure is calculated and compared to the initial user defined mean engine pressure. The difference is then used to scale the relevant predicted engine performance values. The code below shows the calculation of the scale factor as well as the variable to be corrected:

```
avgP = sum(var(P,:)) / length(var(P,:));
corr_fact = (pmean - avgP) / avgP    ;

var(QK,:) = var(QK,:)*(1 + corr_fact); %heat trans to cooler (J)
var(QR,:) = var(QR,:)*(1 + corr_fact); %heat trans to regen (J)
var(QH,:) = var(QH,:)*(1 + corr_fact); %heat trans to heater (J)
var(WC,:) = var(WC,:)*(1 + corr_fact); %work done by comr space (J)
var(WE,:) = var(WE,:)*(1 + corr_fact); %work done by exp space (J)
var(W,:) = var(W,:)*(1 + corr_fact); %total work done (WE+WC) (J)
var(P,:) = var(P,:)*(1 + corr_fact); %pressure (J)
var(MC,:) = var(MC,:)*(1 + corr_fact); %gas mass in comr space (kg)
var(MK,:) = var(MK,:)*(1 + corr_fact); %gas mass in cooler (kg)
var(MR,:) = var(MR,:)*(1 + corr_fact); %gas mass in regen (kg)
var(MH,:) = var(MH,:)*(1 + corr_fact); %gas mass in heater (kg)
var(ME,:) = var(ME,:)*(1 + corr_fact); %gas mass on exp space (kg)
%gas mass flow from compr space -> cooler (kg/rad)
var(MfCK,:) = var(MfCK,:)*(1+corr_fact);
%gas mass flow from cooler -> regenerator (kg/rad)
var(MfKR,:) = var(MfKR,:)*(1+corr_fact);
%gas mass flow from regen -> heater (kg/rad)
var(MfRH,:) = var(MfRH,:)*(1+corr_fact);
%gas mass flow from heater -> exp space (kg/rad)
var(MfHE,:) = var(MfHE,:)*(1+corr_fact);

dvar(QK,:) = dvar(QK,:)*(1 + corr_fact); %heat trans to cooler (J)
dvar(QR,:) = dvar(QR,:)*(1 + corr_fact); %heat trans to regen (J)
dvar(QH,:) = dvar(QH,:)*(1 + corr_fact); %heat trans to heater (J)
dvar(WC,:) = dvar(WC,:)*(1 + corr_fact);%work done by comr space (J)
dvar(WE,:) = dvar(WE,:)*(1 + corr_fact); %work done by exp space (J)
dvar(W,:) = dvar(W,:)*(1 + corr_fact); %total work done (WE+WC) (J)
dvar(P,:) = dvar(P,:)*(1 + corr_fact); %pressure (J)
dvar(MC,:) = dvar(MC,:)*(1 + corr_fact);%gas mass in comr space (kg)
dvar(MK,:) = dvar(MK,:)*(1 + corr_fact);   %gas mass in cooler (kg)
dvar(MR,:) = dvar(MR,:)*(1 + corr_fact);   %gas mass in regen (kg)
dvar(MH,:) = dvar(MH,:)*(1 + corr_fact);   %gas mass in heater (kg)
dvar(ME,:) = dvar(ME,:)*(1 + corr_fact); %gas mass on exp space (kg)
```

The results obtained from the above described implementation are then graphically presented over the full cycle. Refer to Section 5.5.1.

5.5.1 Result from Adiabatic Simulation of the Heinrici Engine

The adiabatic analysis performed on the Heinrici Stirling Engine (HSE) was done under the same user defined operating conditions stated in Table 2. Refer to Appendix H for indication of engine layout and dimensions as well as Appendix G for photographs of the HSE.

Figure 14 shows the internal pressure variation of the engine as a function of the crank position. The pressure variation obtained from the Schmidt analysis is also shown to indicate differences. Note that although the maximum and minimum pressures predicted by the adiabatic analysis are higher and lower respectively, than that predicted by the Schmidt analysis, the pressure variations of the two methods are in phase i.e. peaks and troughs are at the same crank position. Note that the predicted pressure ratio

(±3.2 according to the adiabatic simulation) is higher than that of modern Stirling engines which falls within a range of ±1.3 - 1.8 (Personal communication with Dr. K. Mahkamov, Durham University, UK, 2006). This can be attributed to the heat exchangers design of the engine (or lack thereof). Dead space caused by void volumes in the heat exchangers and flow passages of adjacent engine cells decrease the pressure ratio; due to the absence of proper heat exchangers in the Heinrici engine dead volumes are reduced which in turn increases the pressure ratio of the engine.

Figure 15 shows the temperature variations of the expansion and compression spaces of the HSE. The dramatic temperature fluctuations can be ascribed to the highly ineffective (non-existent) regenerator of the Heinrici engine. By absorbing heat during the first half of the cycle and then adding the stored heat to the cooler gas passing through the regenerator during the next half of the cycle the regenerator serves as a temperature buffer. This temperature buffer assists in reducing the temperature fluctuations within the expansion and compression spaces of the engine which in turn reduce the cyclic heat load on the heater and cooler heat exchangers.

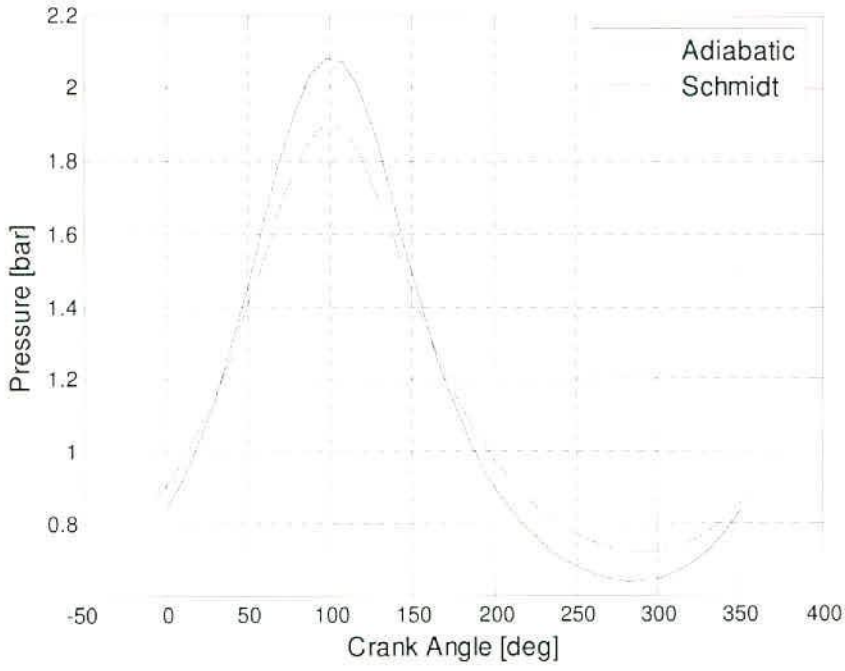

Figure 14: Engine internal pressure variation from adiabatic analysis

certainly fulfils most of these requirements with the exception of energy conservation of the cylinder walls. As mentioned in the previous section of this document the simple analysis is based on the ideal adiabatic analysis, except for the addition of some non-ideal effects like pumping loss and heater/cooler wall heat transfer effects. Other than in the case of the adiabatic and Schmidt methods the heater and cooler heat exchangers are considered non-ideal in the sense that there exist temperature gradients between the walls (user defined input source and sink temperatures) and the gas within the respective heat exchangers. Reader (1983) mentions that the mere use of an adiabatic path instead of an isothermal path is not particularly informative, especially for low compression ratios as is the case with the Heinrici engine. Substitution of the isothermal model with an adiabatic model, coupled with a further heat transfer process as considered in the simple analysis is a more comprehensive approach. The simple analysis also incorporates pumping losses and non-ideal regeneration. Figure 17 below indicates the algorithm for the simple analysis.

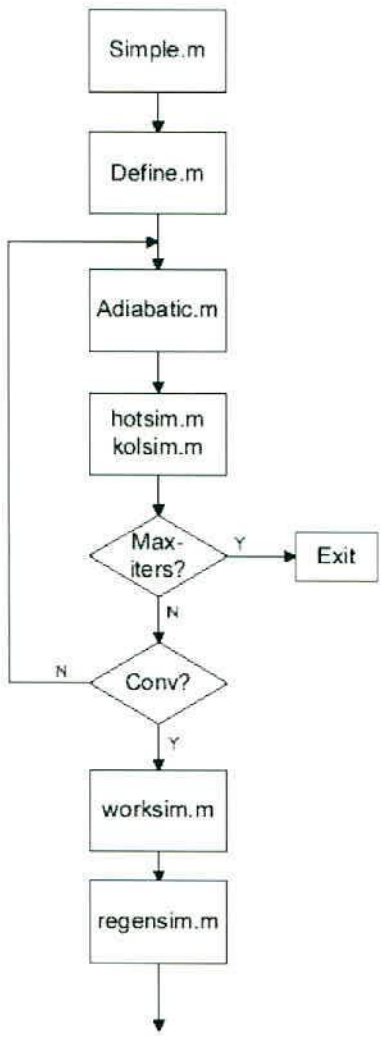

Figure 17: Simple analysis algorithm

Since the adiabatic analysis is invoked iteratively by the simple analysis the Schmidt analysis will also be invoked more than once. The Schmidt analysis only provides the initialisation phase for the adiabatic analysis and therefore it is decoupled from the adiabatic analysis as soon as the first iteration of the simple analysis is completed.

The iteration loop for the non-ideal effects considered by the simple analysis is implemented in the *Simple.m* file using the following MATLAB code:

```
while terr > eps & conv == 0
    it = it + 1; %Iteration counter
    [var,dvar] = adiabatic;%Do ideal Adiab analysis with new temps
    tgh = hotsim(var,twh); %obtain new heater gas temp
    tgk = kolsim(var,twk);        %obtain new cooler gas temp
    terr = abs(th - tgh) + abs(tk - tgk); %calc temp change
    th = tgh;                  %update heater temperature
    tk = tgk;                  %update cooler temperature
    tr = (th - tk)/log(th/tk);    %obtain new regenerator temp

    if it == maxit, conv = 1;end %test for max # of iterations
    if terr <=  eps, conv = 1;end       %test for convergence
end
```

The functions "hotsim" and "kolsim" ("k" because cooler variables have subscript "k") are sub functions used to evaluate heat transfer in the heater and cooler, respectively. The following MATLAB code is implemented in *hotsim.m* to evaluate the heat transfer performance of heater:

```
%Calc Reynolds numbers over cycle
for i = 1:1:col
    %Evaluate mass flow rate through heater
    gah(i) = (var(MfRH,i) + var(MfHE,i))*omega/2;     %[kg/s]
    gh = gah(i)/ah;                  %obtain mass flux [kg/m^2.s]
    %obtain Re at current crank angle conditions
    [mu,kgas,re(i)] = reynum(th,gh,dh);  %returns Re at theta
end
%obtain maximum & avg Re
sumRe = 0; remax = re(1);
for i = 1:1: length(re));
    sumRe = sumRe+re(i);
    if re(i) > remax
        remax = re(i);
    end
end
Reavg = sumRe/(length(re) - 1);  %calc avg Re
%Obtain heat transfer coef & friction factor
[ht,fr] = pipefr(dh,mu,Reavg);    %Update heater gas temperature
tgh = twh - var(QH,37)*freq/(ht*awh);  %heater gas temperature [K]
```

Similarly the heat transfer performance of the cooler is evaluated using the following implemented code in *kolsim.m*:

```
%Calc Reynolds numbers over cycle
for i = 1:1:col
    %Evaluate mass flow rate through cooler
    gak(i) = (var(MfCK,i) + var(MfKR,i))*omega/2; %[kg/s]
    gk = gak(i)/ak; %obtain mass flux [kg/m2.s]
    %obtain Re at current crank angle conditions
    [mu,kgas,re(i)] = reynum(tk,gk,dk);
end
%obtain maximum & avg Reynolds numbers
sumRe = 0;remax = re(1);
for i = 1:1:length(re));
```

```
        sumRe = sumRe + re(i);
        if re(i) > remax
            remax = re(i);
        end
    end
    Reavg = sumRe/length(re) - 1);
    %obtain heat transfer coef & friction factor
    [ht,fr] = pipefr(dk,mu,Reavg);
    %Update cooler gas temperature
    tgk = twk - var(QK,37)*freq/(ht*awk);  %cooler gas temperature [K]
```

The following equation is used to evaluate the thermal conductivity of the operating fluid.

$$k = c_p.\mu / Pr \tag{5.1}$$

The Reynolds number for each incremental crank position is obtained as follows:

$$Re = |\dot{m}|.d_h / \mu \tag{5.2}$$

Where d_h [m] is the hydraulic diameter of the specific engine cell or heat exchanger flow passage and $\dot{m}$ [kg/s] is the mass flow rate through the cell. The absolute value of the mass flow rate is used to eliminate the applied nomenclature presented in Figure 3 for the positive direction of flow.

Regenerator performance and effectiveness is evaluated in the MATLAB m-file called *regensim.m*. The following code indicates the implementation of the regenerator evaluation in *regensim.m*:

```
NTU = st*awr/(2*ar); %number of transfer units
Reff = NTU/(1+NTU); %evaluate regenerator effectiveness
%calc regenerator net enthalpy loss (qrloss)
for i=1:1:37;
    qreg(i) = var(QR,i);
end
%Obtain effective regenerator net enthaly loss
qr_min=min(qreg);
qr_max=max(qreg);
qrloss = (1-Reff)*(qr_max-qr_min);
```

With *NTU* obtained from equation (4.29).

Enthalpy loss (*qrloss*), as well as the heat leakage through the wall (thermal conductance through regenerator wall) of the regenerator is added to the heat load on the heater. The actual heat power to be supplied by the heater is then calculated using the following MATLAB implementation in *SEA_main.m* (including non-ideal effects section):

```
qrloss=regensim(var); %net enthalpy loss of regenerator [J]
qwrl=cqwr*(twh-twk)/freq; % wall heat loss of regenerator [J]
%cqwr is the user defined regenerator housing thermal conductance value [W/K]
```

Pumping loss is evaluated in the MATLAB m-file called *worksim.m*. Pumping loss is calculated separately for each engine cell over a complete cycle and summed to obtain the overall engine pumping loss. The pressure drop caused by the pumping loss through the engine is then converted to a work loss value

(Joule). The actual work produced by the engine is obtained by subtracting the work loss from the indicated work obtained by the adiabatic analysis.

Below follows the implementation of the actual work done and actual thermal efficiency calculated for the Heinrici engine, as done in *SEA_main.m*:

```
 dwork = worksim(var,dvar); %obtain pumping work loss [J]
 actWpower = var(W,col)*freq - dwork*freq;%calc act work power [W]
%calc actual heat power required from heater
 actQhpower = var(QH,col)*freq + qrloss*freq + qwrl*freq; %[W]
%calc actual engine thermal efficiency
 actEff = actWpower/actQhpower;
```

Refer to the compact disc (CD) accompanying this document for further discussion of the implementation of the simulations in MATLAB code, the CD contains the complete MATLAB program with comments included in code.

5.6.1 Results from Simple Simulation of Heinrici Engine

Table 5 stipulated the numeric results obtained by the simple analysis of the Heinrici engine. Non-ideal heat exchangers and regeneration as well as pumping losses caused by fluid friction are considered. The first section of Table 5 presents the temperature gradients within the heater and cooler heat exchangers while the second section presents the engine's performance before consideration of frictional losses. Specifications of non-ideal regeneration as well as actual engine performance, after work loss due to friction, are presented in the final two sections of the table. Note that the power output is the total predicted power output of the engine and not only the cyclic power delivered i.e. the cyclic power in Joule is multiplied by the operating frequency to obtain the total power output of the engine. This applies to all power [Watt] relevant (heat or output power) values displayed in the table below. Also note that the power produced is only a function of the thermodynamic cycle and not of the engines drive mechanism. The pressure correction factor in Table 5 becomes negative and the corrected average pressure of the engine becomes closer to that obtained by the Schmidt analysis.

Table 5: Numeric results from Simple analysis of HSE

Description	Value	Unit
Temperature effects of non-ideal heat exchangers		
Hot side wall temperature (T_h-wall)	448	^{0}C
Hot side gas temperature (T_h-gas)	428.9	^{0}C
Cold side wall temperature (T_k-wall)	46	^{0}C
Cold side gas temperature (T_k-gas)	63.7	^{0}C
Engine performance results		
Pressure Correction Factor	-0.0012*	-
Gas mass	0.6606	g
Thermal efficiency of thermodynamic cycle	38.43	%
Power output of thermodynamic cycle	14.25	W
Heat power added by heater (Q_h)	37.1	W
Heat power rejected by cooler (Q_k)	-22.82	W
Results of non-ideal regenerator		
Regenerator effectiveness	74.59	%
Regenerator wall conductance	0.7859	W/K
Regenerator net enthalpy loss	47.53	W
Regenerator wall heat loss	315.96	W
Results from fluid frictional losses		

Pumping loss	0.2031	W
Actual power of thermodynamic cycle	14.0475	W
Actual heat power required	400.57	W
Actual efficiency	3.51	%

* This is the final correction factor during the iterative solution procedure of the simple analysis, the adiabatic analysis in invoked iteratively creating a vector of correction factors with values from each iteration.

When considering the PV diagram for the simple analysis presented in Figure 18 below it is clear that the consideration of the non-ideal heat exchangers caused a larger deviation from the ideal PV diagram than that of the adiabatic analysis. Reader (1983) states that this phenomenon occurs due to the fact that the cylinder walls do not provide a sufficient heat transfer medium to ensure constant gas temperatures within the cylinders, thus causing deviation form the isothermal conditions, hence the consideration of the non-ideal heat exchangers. Reader (1983) also mentions that the deviation is more pronounced on the hot-side of the engine than on the cold-side, as illustrated by Figure 18. Comparing these results to that of the Schmidt analysis it becomes clear that the PV diagram of the Schmidt analysis deviates even more from ideal scenario than that of the adiabatic or simple models. A possible explanation for this could be that the Schmidt model used here is based on years of experimental work done by the authors on engines operating at higher revolutions. However, the Schmidt analysis provides a more accurate approximation of the internal gas mass than would be achievable from normal ideal gas relations. It is therefore only used as input value for the adiabatic and simple models instead of being a concurrent analysis tool on its own – as was the case in the past. The area included within the PV diagram represents the engine power developed. It is not very obvious in Figure 18 that there is a significant difference in area, but upon comparison of the results obtained for the adiabatic and simple analyses (Table 4 and Table 5) it is clear that the work predicted by the simple analysis (14.05 W) is less than that of the adiabatic analysis (16.18 W). This is expected as the simple analysis gives a better approximation of the practical conditions existing within Stirling engines.

Figure 19 shows the cyclic pressure variation in the Heinrici engine. It is assumed that the internal pressure of the engine is constant at any given instant. This implies that the pressures in the five (5) cells of the engine are the same. The pressure variation of the Schmidt analysis is also shown in Figure 19 for comparison to the results of the simple analysis. Note the difference in relative magnitude as well as the phase similarity between the two curves. The difference in magnitude can be ascribed to the increased temperature fluctuation predicted by the simple analysis (this is not the case in the Schmidt analysis), which causes the increase in pressure.

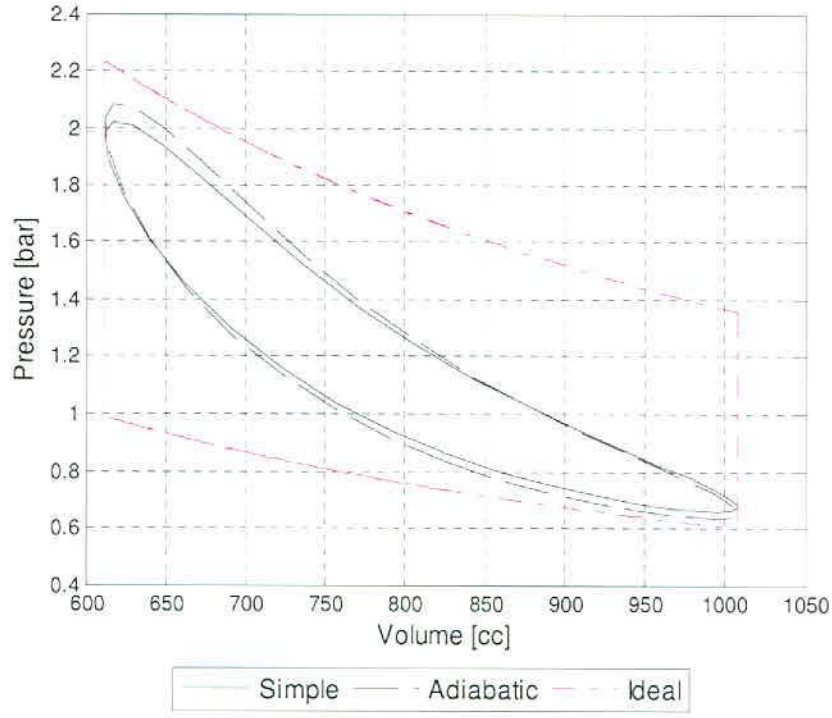

Figure 18: P-V Diagram: Simple analysis

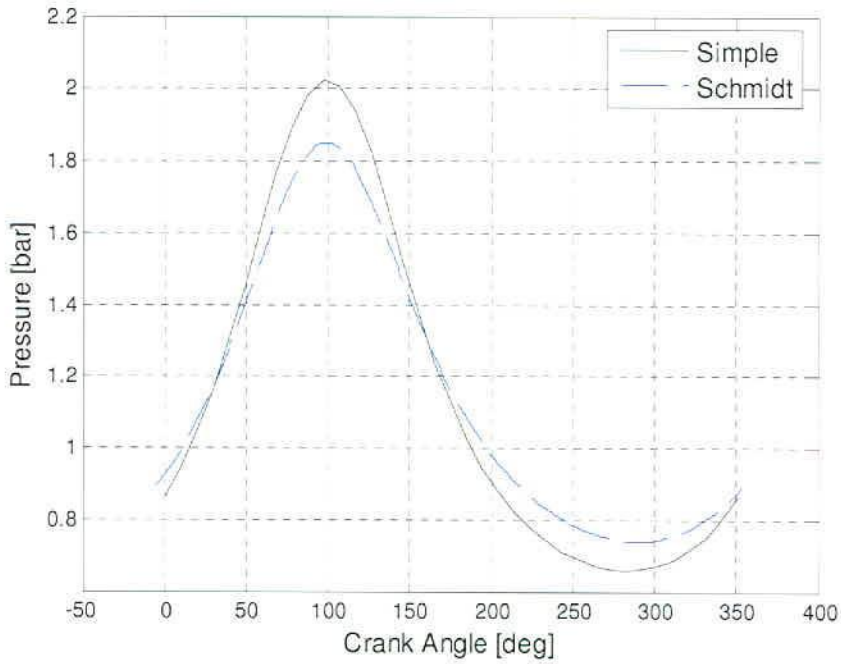

Figure 19: Pressure variation: Simple analysis

Figure 20 below shows the cyclic energy flow in the three heat exchangers of the engine as well as the total work done per cycle. Values for the heat rejected by the cooler (Q_k) and heat added by the heater (Q_h) as well as total work done (W) are indicated. These numeric results can be found in Table 5. Note the difference in magnitude of energy flow between the regenerator and that of the heater and cooler. Also note that the total cyclic energy flow through the regenerator sums to zero (0). The energy flow in the regenerator is in the order of five (5) times more than that of the heater and six (6) times more than that of the cooler i.e. the heat transfer capacities of the heater and cooler is respectively five (5) and six (6) time less than that of the regenerator. In Table 6 below the maximum and minimum values of the energy flow within the three heat exchangers are stipulated. This result is in accordance with the recommendation by Reader (1983) who stated that the regenerator must be able to deal with four (4) to five (5) times the heat load of the heater. Reader mentions that, should the design fail to meet this requirement an extra heat load will be placed on the other heat exchangers which will reduce the internal operating temperature difference and thus reduce engine power.

Figure 21 indicates the instantaneous mass flow rates in each engine cell. Keep in mind that the quasi steady-flow assumption implies that at any given moment the engine pressure is constant throughout the engine. The question regarding where the mass flow comes from arises. The instantaneous mass in each engine cell is calculated using the equation of state, similarly the mass accumulation within each cell is obtained from equations (4.12), (4-16) and (4-17). The mass flow rate within each cell is then obtained as a function of the direction of flow and depends on the mass flow rate of the adjacent engine cells. Refer to Appendix B for a summary of the adiabatic equation set, under the "equations for masses" section.

Table 6: Maximum and minimum thermal load on the 3 heat exchangers

Heat Exchanger	**Maximum [W]**	**Minimum [W]**
Heater cyclic energy flow (Q_h)	31.2	-6.1
Cooler cyclic energy flow (Q_k)	0	-23.1
Regenerator cyclic energy flow (Q_r)	145.8	-7.4

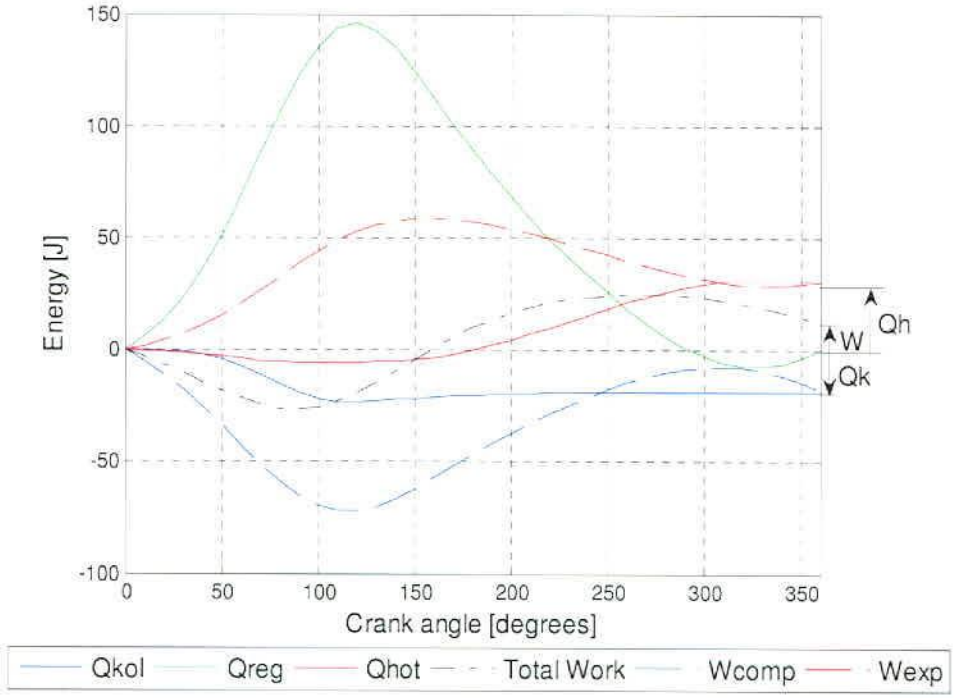

Figure 20: Cyclic energy flow within each engine cell

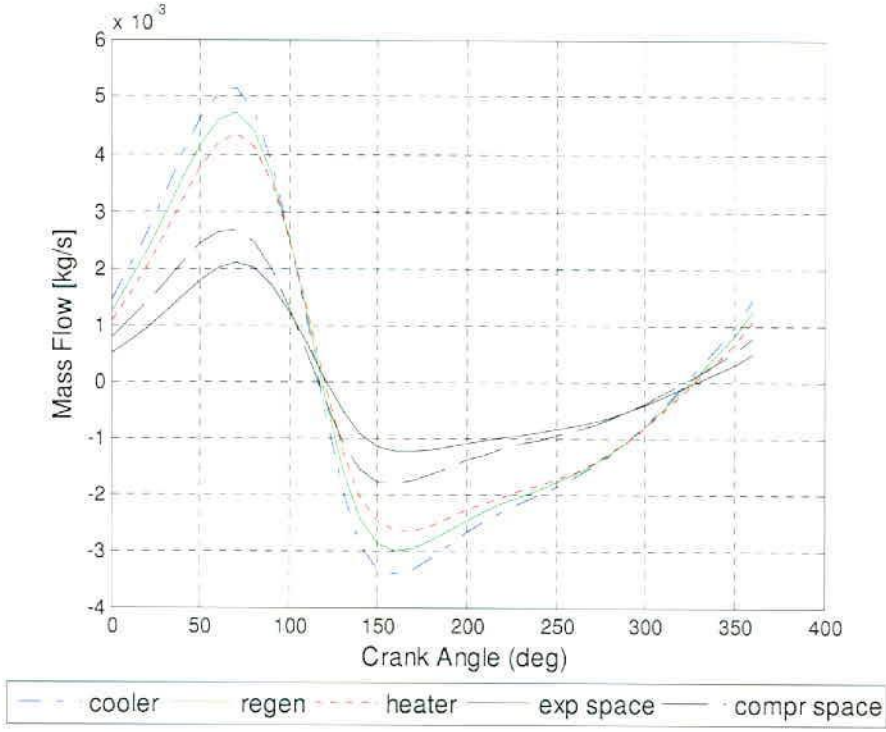

Figure 21: Mass flow rate within each cell

Figure 22 indicates the instantaneous mass of gas in each cell of the engine. The pressure variation is also shown to indicate the interaction between mass and pressure within the heater, cooler and regenerator cells. The pressure curve is however, scaled in order to be able to present it on the same axis as that of mass (refer to the legend on Figure 20 for an indication of scaling used for each graph). Note that the graph representing the instantaneous mass of gas in the compression space is almost a direct mirror image of that of the expansion space. This indicates that most of the gas is within the compression space when compression occurs (heat rejection). Similarly for the expansion space most of the gas is within the expansion space when expansion occurs. Increase in pressure is caused by expansion (heat addition) which occurs as soon as the majority of the operating fluid is contained within the expansion space and is heated. Hence the similarity between the trends of the pressure and expansion space mass curves. This is easily explained when considering the equation of state for an ideal gas; increase in mass and temperature at the same volume constitutes an increase in pressure.

NOTE: In Figure 22 the graphs for the expansion space, compression space, and engine pressure and sum of masses is scaled in order to improve the graphical representation of the instantaneous masses in the individual engine cells.

NOTE: The graph for the sum of mass (refer to legend in Figure 22) is included to improve the trustworthiness of the results. It indicates that the sum of the mass of gas in individual cells of the engine at any given moment is constant, thus satisfying the mass conservation law.

Figure 23 below shows the pressure drop across the three heat exchangers. Note the phase similarity of the pressure drop between the heat exchangers. Also note the relative magnitude between the pressure drop over the regenerator and that over the heater and cooler. The regenerator is clearly the obstruction in the flow field causing the highest resistance to mass flow i.e. the regenerator governs the pumping loss in the engine. The regenerator of the Heinrici engine is almost non-existing (as mentioned earlier on), it has no regenerative matrix (hence a very low heat storing capacity). This is however, one of the reasons for the relatively low pressure drop over the regenerator. Pressure drop over the regenerator of the D-90 Ross-Yoke engine is up to 3000 Pascal due to the presence of the regenerator matrix, keep in mind that the operating conditions of the two engines are different as the Ross-Yoke engine operates at a mean pressure of 200 kPa and a frequency of 3000 rpm (refer to Table 2 and Table 14).

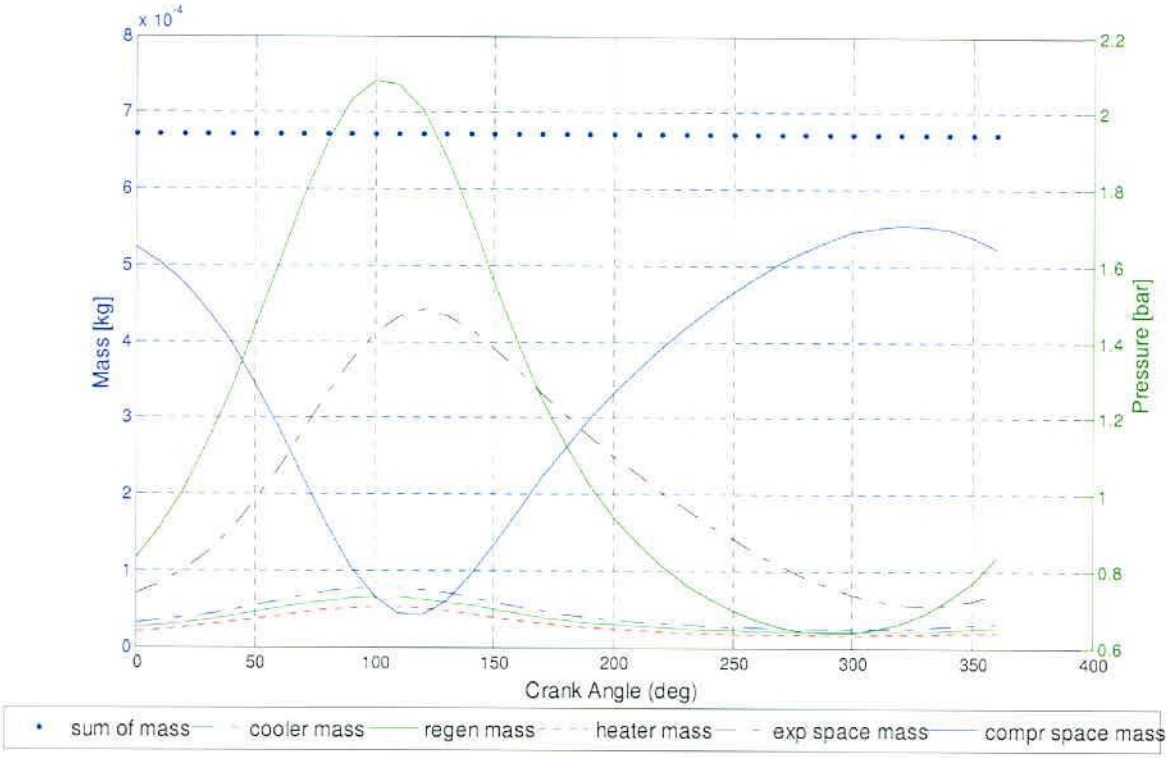

Figure 22: Instantaneous mass of gas in each engine cell

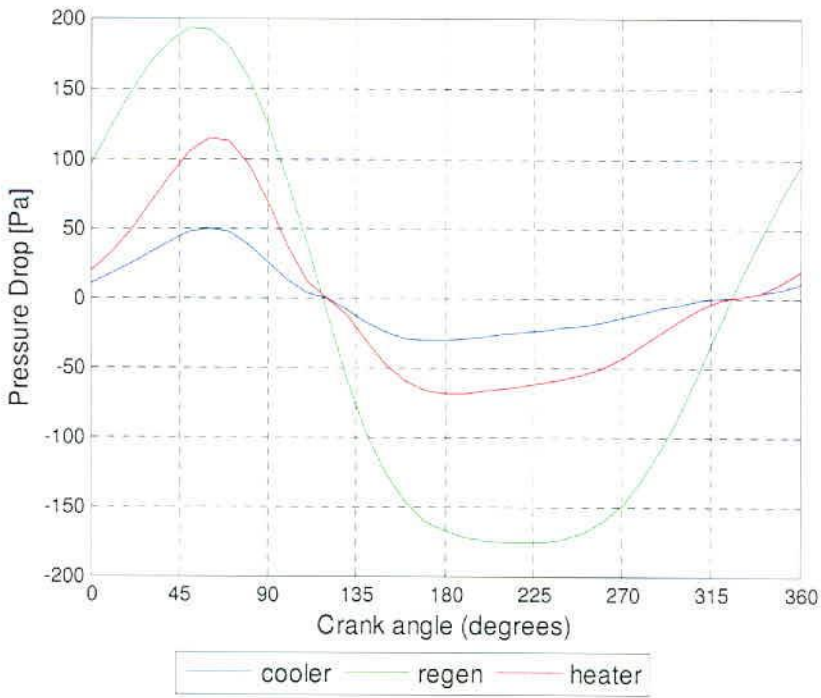

Figure 23: Cyclic pressure drop over each engine cell

Note that the pressure drop in each engine cell is not calculated as part of the simulation procedure, it is only calculated afterwards i.e. when the pumping loss of the engine is evaluated after convergence of the simulation procedure, the pressure drop is calculated. The internal pressure drop of the engine is calculated in order to evaluate the pumping loss of the engine.

Figure 24 below shows the temperature fluctuations of the expansion and compression spaces as well as the constant regenerator temperature as obtained from the simple analysis of the Heinrici Stirling engine. The simple analysis incorporates the effect of non-ideal heat exchangers thus introducing a temperature gradient between the wall and the gas within the heater and cooler heat exchangers. Note that the non-ideal heat exchanger simulation indicates that the hot side gas temperature is lower than the user defined hot side wall temperature. Similarly the cold side gas temperature is higher than the user defined wall temperature. This is in fact the case in actual Stirling engines and implies that the engine actually operates between lower temperature limits, thus producing less power than predicted by the adiabatic and/or isothermal models. Constant user defined wall temperatures are also indicated in Figure 24 (legend: *Th-wall* & *Tk-wall*), these are the same temperature as the hot (T_h) and cold (T_k) side temperatures used for the adiabatic analysis. The gas temperatures are also indicated (legend: *Tk-gas* and *Th-gas*).

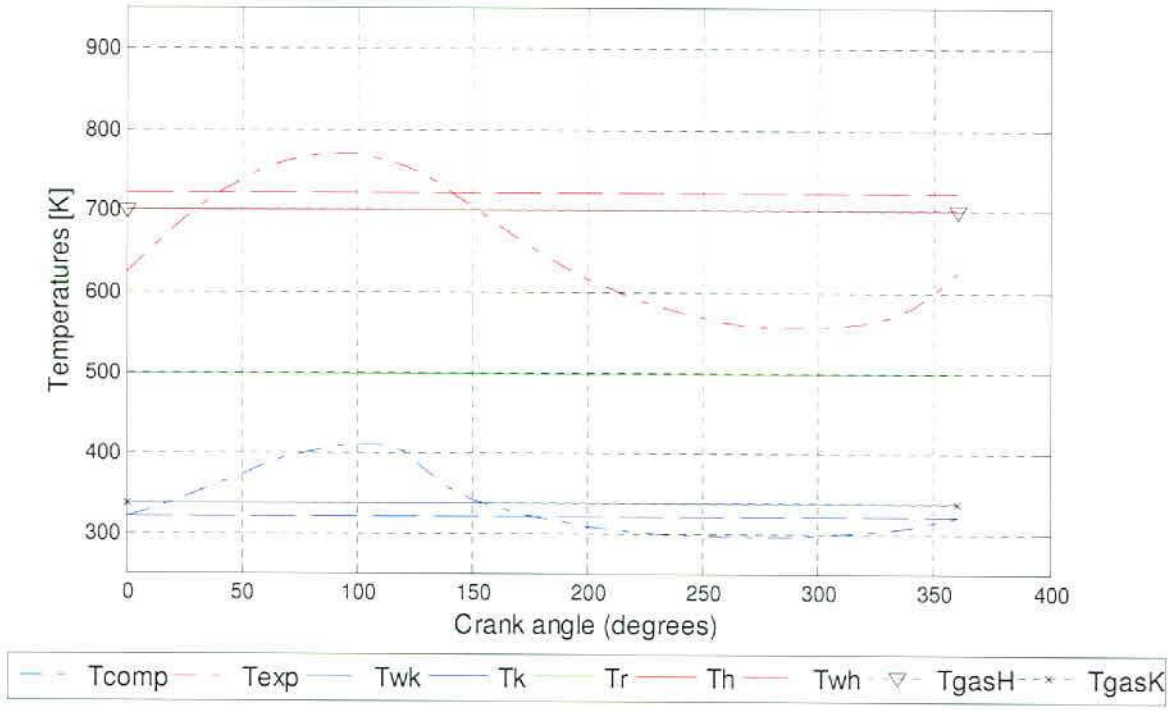

Figure 24: Temperature fluctuation: Simple analysis

5.6.2 Constant Cooler Volume approximation for Heinrici Engine

As mentioned earlier, the cooler volume of the Heinrici engine is assumed to be constant. Upon consideration of the volume definitions presented by Figure 10 it becomes clear that the length (and volume) of the cooler is dependant on the position on the power piston which is a function of the crank position i.e. the cooler volume is a function of the crank position. The section aims to discuss the effect of this assumption on the predicted performance of the Heinrici engine.

Investigation on the effect of this assumption on the predicted engine performance was done by keeping the cooler volume constant at seven (7) different values. The first four (4) values are determined by multiplying a factor of 1, ¾, ½ and ¼ with the maximum length of the cooler. The 5th value is determined by taking the average value of the cooler length, as a function of crank angle, over a single cycle. The final two values are set as the maximum and minimum values of the cooler length. These values are obtained by having the power piston at top dead centre (TDC) and bottom dead centre (BDC). Cooler volume is then obtained by multiplying the cooler length by the annulus area of the cooler (refer to Figure 10). Table 7 stipulates the results of the effect of the change in cooler length on the engine efficiency, total mass of gas as well as predicted power output of the Heinrici Stirling engine (HSE). The mass of gas decreases as the cooler length decreases but this is expected as the total engine volume is decreased and thus, according to the equation of state at constant temperature and pressure, the mass has to decrease.

Table 7: Effect of constant cooler length

Fraction of Maximum Length	**1/4**	**1/2**	**min**	**3/4**	**1/1**	**avg**	**max**
L_k **[m]**	0.0224	0.0449	0.0635	0.0673	0.089	0.1112	0.1533
Mass of gas [mg]	0.5468	0.5959	0.6161	0.6195	0.6363	0.6497	0.673
Efficiency [%]	24.779	33.35	35.743	36.08	37.52	38.43	39.64
Power of thermodynamic cycle [W]	8.73	12.46	13.45	13.57	14.04	14.25	14.36

Figure 25 and Figure 26 indicate the effect of cooler length on the predicted HSE power and efficiency. The constant cooler length was assumed to be equal to the average length of the cooler over a single

cycle. This value is indicated in the two figures below as the second to highest value for L_k. The change in engine power for a change in cooler length between 0.09 m and 0.15 m is minimal. The assumption of a constant cooler length within this range is thus feasible.

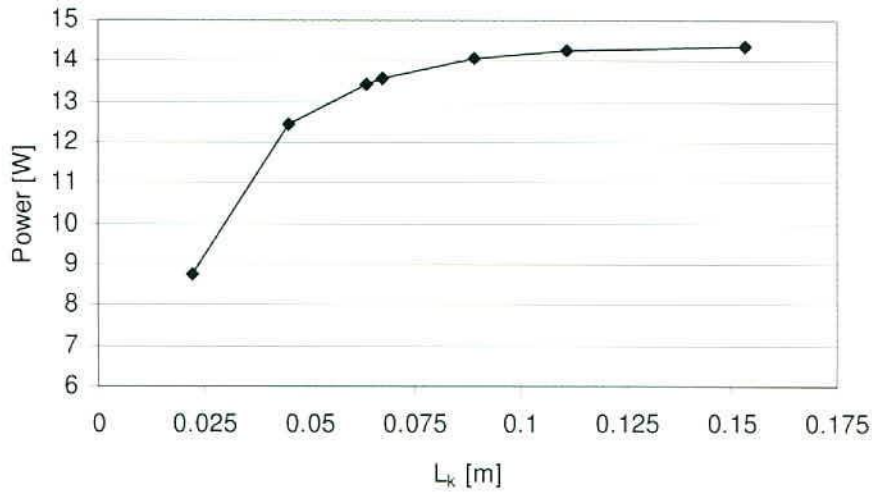

Figure 25: Effect of cooler length on predicted HSE power

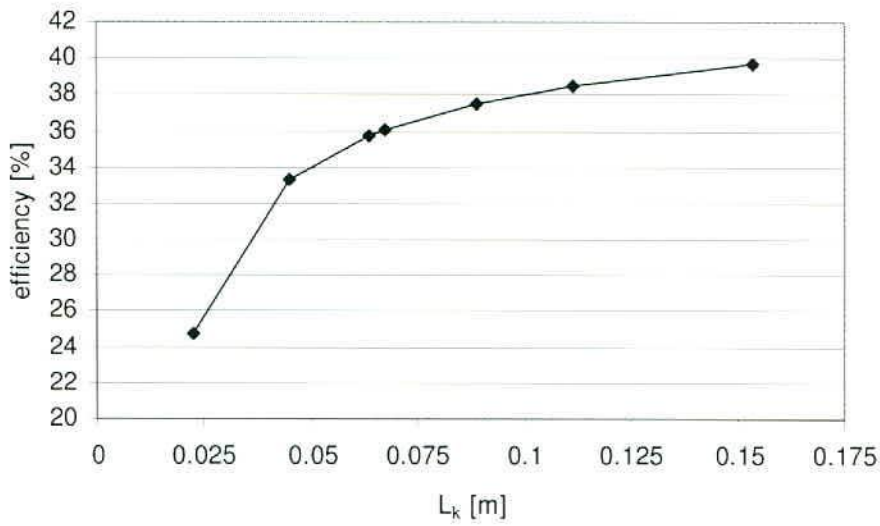

Figure 26: Effect of cooler length on HSE efficiency

The variation in engines efficiency for this range of cooler lengths is more than that of the power curve, although the difference is only 2.1 %. The change in cooler length thus has a more dramatic effect on the predicted engine efficiency but is not enough to prove the assumption as non-feasible. With regards to

the simplicity introduced by this assumption for the analytical simulation of the HSE, this increased effect on the efficiency is insufficient reason to prove the assumption infeasible.

5.7 Other SEA Methods

This section presents three (3) Stirling engine analyses methods less complex than those presented in the previous sections of this documents. These are well known back-of-the-envelope analyses methods for Stirling engines and play an important role during the initialisation phases of Stirling engine design procedures. The simulation program presented in this document includes these programs, however these methods form part the initialisation phase during design procedures and do thus not fall within the scope of this study. The three methods presented in the forgoing sections are useful tools in Stirling engine design and/or analysis while the methods presented here are applicable to system synthesis (Reader, 1983).

5.7.1 West Method

West proposed a method to determine the indicated work, indicated power and shaft power similar to that of the Schmidt method discussed above (Kontragool, 2004). Both these methods require the same seven (7) design parameters (refer to Section 5.4) and therefore have the same degree of complexity. The term design parameters refer to the physical engine configuration parameters. The West method, however, also requires an "*Experience factor*", which is not classified as a design parameter and therefore has no effect on the level of complexity of the method. The equation proposed by West for the indicated net work is as follows:

$$W_{West} = p_m V_p \pi \sin(\alpha) \left(\frac{1-\tau}{1+\tau}\right)\left(\frac{1}{2+k_P+2k_S}\right) \tag{5.3}$$

Where k_P is the swept volume ratio (V_P/V_D), k_S is the dead space volume ratio (V_D/V_{cl}) and α is the phase angle lead of the displacer piston over the power piston.

The indicated power and shaft power is as follows:

$$\begin{aligned} P_i &= W_{net} \cdot f \\ P_{shaft} &= (Experiencefactor).P_i \end{aligned} \tag{5.4}$$

Kontragool (2004) suggests that the shaft power be obtained by reducing the shaft power obtained by the Schmidt analysis by an "*Experience factor*" of 35%, while Reader (1983) suggests an *Experience factor* of 30-50% should be used for well-designed engines.

5.7.2 Beale Method

William Beale, a professor of Mechanical Engineering at Ohio University in Athens, Ohio, invented the first free-piston-Stirling-engine (FPSE) in 1964. He is also founder of a company called *Sunpower Inc.* incorporated in 1974, one of the leaders in Stirling engine technology today. Over the years *Sunpower* developed a range of highly efficient, low mass, reliable, state-of-the-art FPSE as well as other products like cryo-coolers and linear compressors. One of the simplified Stirling engine analysis methods was named after him as he developed the Beale power equation from which the concept of the Beale number originated; equation (5.5) below describes this method.

Beale noted that an empirical relation exists that could be used to approximate the power output of several observed Stirling engines. The Beale method only requires a few design parameters and is very convenient in the preliminary design phase as well as for back-of-envelope calculations. The following equation is known as the Beale formula (Walker, 1980) and can be used for all engine configurations and sizes:

$$P = N_B \cdot p_m \cdot V_p \cdot f \tag{5.5}$$

Where P is the engine output power [W], p_m is the mean engine pressure [bar], V_p is the displacement volume of the power piston [cm^3], f is the cycle frequency [Hz] and N_B is the Beale Constant.

From the Beale equation it can be shown that when the Beale number (N_B) is the subject of the equation we are left with a dimensionless group on the right hand side of the equation. The Beale number is a dimensionless parameter based on experimental data and is a function of the source and sink temperatures. Kontragool (2004) presents various methods for the calculation of the Beale number, he states that these methods become unusable for low temperature differential Stirling engines (LTD SE) i.e. heater temperatures below 475 K (202 ^{0}C). The reason for this temperature limitation can be seen in Figure 26 below. The Beale number approaches zero as the source temperature decrease and will reach approximately zero at a source temperature of 475 K.

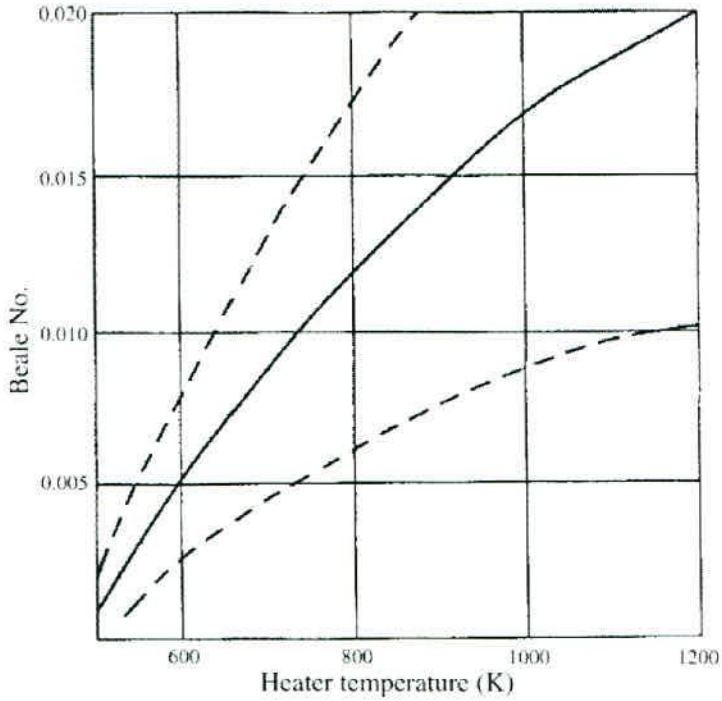

Figure 27: Beale number as a function of source temperature (Kontragool, 2004)

The solid line in the Figure 27 indicates the relationship between Beale number and source temperature. The upper dashed line represents high efficiency, well designed engines with low sink temperature while the lower dashed line represents moderate efficiency, less well designed engines with higher sink temperatures.

The relation for the Beale number used in the Stirling engine analysis (SEA) program presented by this document is the following:

$$N_B = 0.034 - 0.054\tau \tag{5.6}$$

Where $\tau = T_c/T_h$. This relation, presented by Kontragool (2004), for the Beale number was used as it provides a linear relation for the Beale number as a function of source and sink temperatures. The Beale number for the lower temperature limit can thus easily be determined and used as a limiting value in the program. Kontragool (2004) also states that the accuracy of the Beale number is critical to the accuracy of the Beale formula.

Reader (1983) states that by means of the Beale number the performance of one engine can be compared to another. He mentions that the purpose of the Beale equation is to synthesise rather than

analyse a system i.e. given a required engine power output the approximated engine operating parameters can be evaluated.

5.7.3 Mean Pressure Power Formula

Kontragool (2004) presented a Mean Pressure Power Formula (MPPF) as a variation of the Beale equation. The MPPF only differs from the Beale equation stated in the previous section, in that another factor *F* is introduced.

$$P = F.p_m V_p f.\frac{1-\tau}{1+\tau} \tag{5.7}$$

This factor *F* is said to be equal to two (2) for the ideal Stirling cycle. However, the ideal Stirling cycle does not take into account the effects of frictional, mechanical etc. losses. Therefore it is recommended that F should be between 0.25 and 0.35 for practical applications. The combination of the factor F and the Beale number then becomes:

$$N_B = F.\frac{1-\tau}{1+\tau} \tag{5.8}$$

The second term in the above equation is a variation of the Beale number presented in the previous section by equation (5.6). Once again τ is the ratio of heat sink to source temperatures.

Similar to the Beale method only a few design variables are required to be able to use the MPPF, making it a useful tool during initialization phases of Stirling engine design.

5.8 Summary

The methodology of Berchowitz and Urieli (1983) presented in Section 4 of this document is implemented in MATLAB. Sections of the code are included and discussed in this section in order to improve understanding of the code developed to simulate Stirling engines. A layout of the MATLAB program is presented in Figure 9 and discussed in Section 5.2. This layout can also be found in Appendix D together with an illustration of the interdependence of the sub-functions.

The Heinrici engine is simulated using the Schmidt, Adiabatic and Simple analyses methods described in Section 4 of this document. Less complex methods like that of West, Beale and the Mean Pressure Power Formula (MPPF) are also used to check the effectiveness and/or trustworthiness of these

methods on low revving (typically 360 rpm) Stirling engines operating at medium temperature differences (typically 400 ^{0}C). Refer to Section 6 for a discussion on the experimental tests done on the Heinrici engine as well as Appendix G and H which include pictures and layout drawings of the engine configuration.

Table 8 below compares the results obtained from the 3 methods used to analyse the Heinrici Stirling engine (HSE). Note that for the Simple analysis in Table 8 the results only incorporates the non-ideal heater and cooler heat exchangers effects while the value shown in brackets includes the effects of pumping loss and non-ideal regeneration.

Table 8: Comparison of HSEA results from 6 methods

Analysis Method	**Gas Mass [g]**	**Power [W]**	**Efficiency [%]**
Schmidt	0.66054	21.81	55.76
Adiabatic	0.672	16.2	42.1
Simple	0.6606	14.21 (14)	38.4 (3.51)

The assumption of constant cooler length for the Heinrici engine is discussed in Section 5.6.2. It was found that the increased complexity, with regard to heat transfer effects, of the simulations (Schmidt, adiabatic and Simple) upon introduction of a crank angle dependant cooler length is not viable in terms of accuracy gained in results. This was tested by varying the length of the cooler from minimum to maximum cooler length and obtaining the effect on engine power and efficiency.

6. Experimental Analysis

6.1 Introduction

Sections 4 and 5 of this document discuss the methodology and implementation of the Stirling engine analysis (SEA) program. In Section 4, results for the simulation of the Heinrici Stirling engine (HSE) are presented. These results were verified by means of experimental tests done on the HSE.

This section serves as the main verification of the results obtained from simulations. A description of the measurement equipment and test procedure is presented in conjunction with the experimental results obtained. The experimental results are then compared to the simulated results for the engine in order to test the validity of the simulation procedures.

6.2 Apparatus

A discussion of the various measurement equipment used during experimental testing of the Heinrici engine is provided in the section to follow. A description is also provided for the HSE, as well as for the continuous combustion unit (CCU).

The HSE has a build-in water jacket that provides the sink (cooler) temperature while the source (heater) temperature is provided by the exhaust gasses of the CCU. The finned heat exchanger (hot-end) section of the HSE is placed in the exhaust system of the CCU in such a way that the exhaust gas is forced through the un-finned (or free flow) area of the heat exchanger by mean of guide vanes (refer to Appendix G, Figure 45, for a photograph of the guide vanes). The reason for using this approach instead of less complicated options like simply using a Bunsen-burner is to enable closer approximation of the waste heat recovery process as found in internal combustion engines, as well as to provide a uniform heat source for the heater instead of a "point source" as would be the case with a Bunsen-burner.

A direct current (DC) motor, used as a DC generator, is connected to the output shaft of the HSE in order to measure the actual power output of the HSE. The DC motor is also used to run the HSE engine (turn the HSE at the same rpm as operational rpm developed by HSE during tests) in order to measure the frictional, pumping and other losses within the Heinrici engine. This is done by connecting the DC motor to the output shaft of the HSE at stand still conditions i.e. at constant overall temperature (room temperature) conditions for the HSE engine. Refer to Section 6.4 for a further discussion on quantification of losses of HSE.

6.2.1 Heinrici Stirling Engine (HSE)

Hargreaves (1991) states that various engineers were building Stirling machines up until 1900, of which Heinrici in Germany was one. He mentions that Heinrici however continued to make their simple, inefficient but reliable small Stirling engine up to the mid 1930's. The Stirling engine used during experimental verification of simulated results was one of the variations of the Stirling engines developed by Heinrici (or Heinrici Stirling engine (HSE) as referred to in this document). It is a beta type engine configuration with a fly-wheel crank drive-mechanism; Figure 28 shows a transparent side view of the HSE. The smaller red piston in Figure 28 is called the power piston while the larger grey piston is referred to as the displacer piston. The thicker blue section just below the fly-wheel is the water jacket and forms the heat sink for the engine while the fins at the bottom of the picture forms the hot-end heat exchanger and is thus the heat source for the engine.

The hot end of the Heinrici engine was mounted in the exhaust system of the CCU in order to recover waste exhaust energy as to illustrate the ability of a SE to operate on a low quality heat source. A finned hot-end heat exchanger screws into the bottom of the water jacket section of the HSE, this hot-end absorbs the thermal energy available in the exhaust gasses. Refer to Appendices G and H for further photos of the hot-end as well as layout drawings thereof.

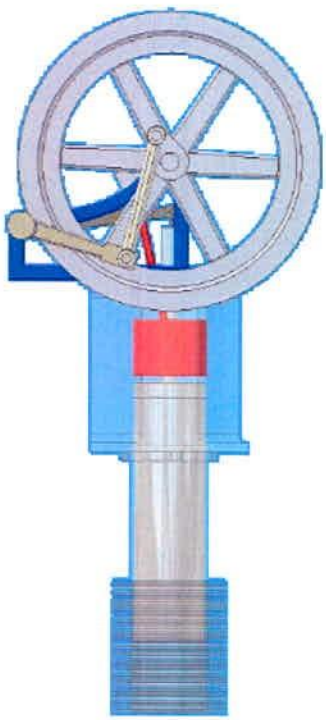

Figure 28: HSE transparent side view

Figure 29: HSE Finned hot-end

6.2.2 Continuous Combustion Unit (CCU)

The Hilton Combustion Demonstration Unit was built approximately in 1970 by P.A. Hilton Ltd, England, UK. It offers a wide range of application, from simple demonstrations for boiler operators to research and development projects. One of the main uses of this unit is to provide heat exchanger projects with sufficient energy in form of hot exhaust gases, when engine exhaust gas or solar energy is not available. It also finds use during experimental illustrations for undergraduate and post graduate studies. Re-commissioning of the continuous combustion unit (CCU) at the University of Stellenbosch was done by A. Schwack and T. M. Harms (2000). A commissioning report as well as instructions for start-up and shutdown procedures of the CCU can be found on the compact disc (CD) accompanying this document.

Figure 30 shows the CCU with the combustion chamber on the left hand side of the picture while Figure 31 shows the control unit or users interface of the CCU with the fuel and air mass flow rate manometers shown on the right hand side of the picture.

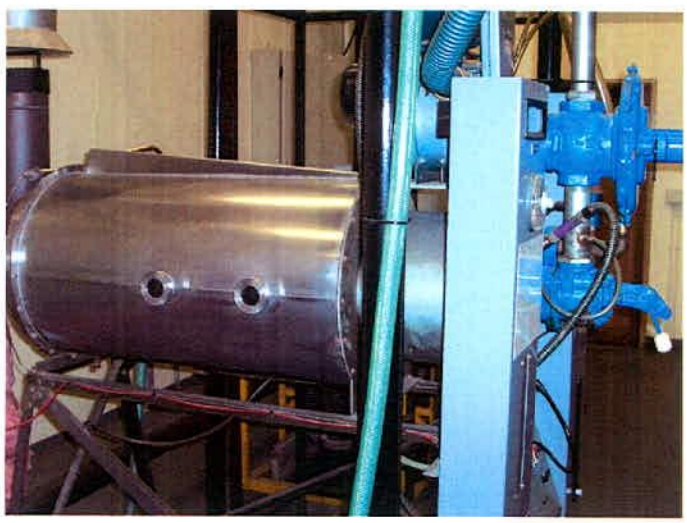

Figure 30: Continuous Combustion Unit (CCU)

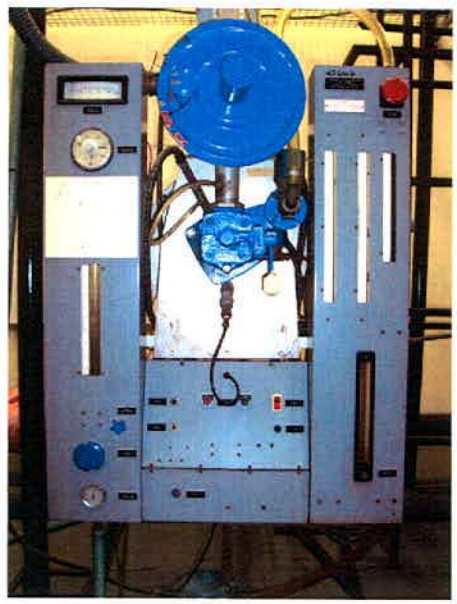

Figure 31: CCU control unit

6.2.3 Measurement Equipment

Table 9 below lists the measurement equipment used during the experimental testing of the Heinrici engine while Table 10 provides a description of the placement of the measurement equipment on the HSE.

Table 9: List of experimental apparatus with serial numbers

Measurement Abbreviation	Component Description	Component Serial #
T_{exh}	Thermocouple (Type K)	-
T_h	Thermocouple (Type K)	-
T_k	Thermocouple (Type K)	-
T_{wi}	Thermocouple (Type K)	-
T_{wo}	Thermocouple (Type T)	-
θ	RS rotation sensor	362 7276
P	HBM Pressure Transducer (type P3MA, 10 bar)	B14622
rpm	Hand held tachometer	-
-	HBM Amplifier	-
-	HP Data logger	34970A
-	Eagle Wave µDAQ *lite* Card	D100000942
T	HBM Torque transducer (Type T 4 A, 100 N.m)	G05445
-	Potter DC motor (110 V DC, 4 A, 0.2 Hp (149 W) part #: S202 333 1 1)	00300
-	Xytron DC power supply	GPC-3030E
V	Volt meter (150 V max)	L8Y1-194
A	Yokogawa Ampere meter (30 A max, type 2051, class 1.0)	-
-	136 ohm, 4 A transistor (providing DC load)	

Table 10: Placement of measurement equipment on HSE

Abbreviation	Description [unit]	Sensor Placement on HSE
T_{exh}	Exhaust gas temperature [^{0}C]	External to the hot-end finned section of the HSE. In the exhaust gas of the CCU
T_h	Hot-end gas temperature [^{0}C]	Inside the hot-end of the HSE between BDC of displacer piston and bottom of hot-end
T_k	Cold-end gas temperature [^{0}C]	Inside the cold-end of the HSE, fixed below the power piston (moving with the power piston)
T_{wi}	Inlet cooling water temperature [^{0}C]	Socket connected to inlet of cooling water supply pipe, at water jacket inlet

T_{wo}	Outlet cooling water temperature[°C]	Socket connected to outlet of cooling water supply pipe, at water jacket outlet
θ	Crank angle measurement [V]	On centre of HSE crank system
P	Internal engine pressure [V]	Below power piston (moving with the power piston)
rpm	Tachometer [rpm]	Hand held unit, measures DC and/or HSE rpm
T	Torque sensor [V]	Between DC motor and HSE output pulley
V	Volt meter [V]	Measures output voltage on DC motor armature
A	Ampere meter [A]	Measures output current of DC motor armature
-	DC motor	Connected to output pulley of HSE with fan belt. Used as DC generator

Note that the voltage and current measurement in Table 10 are used to obtain the engines output power. This measurement is only used to provide a reference or "double check" for the power determined using the torque transducer.

6.3 Test Procedure

Experimental testing was carried out as follows:

- Ensure general laboratory safety is met with special attention regarding easy access to fire extinguisher for emergencies
- Calibrations of the pressure and torque transducers (refer to Appendix I)
- Installation of the measurement equipment (Table 9 lists the equipment used while
- Table 10 indicates the placement/position of the equipment)
- Connection of measurement equipment to bridge amplifier and data logging hardware and software
- Start-up of CCU (refer to Section 6.2.2 for description of and operational settings of CCU)
- Wait for system (CCU and HSE) to reach steady state
- Log data
- Shut down CCU and data logging equipment

6.4 Quantification of HSE losses

The losses of the HSE were determined by running the engine at the same speed as the operating speed obtained during tests (refer to Table 2 for operating conditions of HSE as used for input to simulations). This is done by using the DC motor (previously used as a generator to measure output power of HSE) to turn the HSE at stand still (or non-operational) conditions i.e. with no thermal energy conversion in progress (no heat supplied to the engine). By doing so the following losses can be measured:

- Crank system frictional losses
- Fan belt and pulley system frictional losses

With the pistons disconnected from the crank system the frictional losses of the rotating components is obtained. Table 11 below indicates the results of the HSE losses test. Torque required to run the engine at the given operating frequency was used to calculate the power required to overcome the internal losses in the engine according to the $P = \omega . T$ relation, where ω [radians/s] is the operating frequency measured at the torque transducer and T [Nm] the measured torque.

Table 11: HSE losses test data

	Losses
rpm	72
Torque [Nm]	1.41
Power loss [W]	10.41

Inefficiencies of the DC motor, like windage, mechanical friction and copper losses do not have to be considered since the torque transducer is placed between the output shaft of the HSE and that of the DC motor. The system frictional losses are then added to the measured (by means of the DC generator) power output in order to obtain the total power developed by the Stirling cycle. This value is comparable to the predicted power output obtained from simulations; the section to follow compares the experimental and simulated results.

6.5 Comparison of Experimental and Analytical Results

Table 12 compares the power and efficiency of the HSE obtained from experimental tests to that obtained from simulations; refer to Appendix K for calculations regarding experimental results. Once again, in Table 12, the values stated in brackets for the results of the simple analysis includes the non-

ideal heat exchangers, pumping loss as well as non-ideal regeneration effects while the values not in brackets only include the effect of non-ideal heat exchangers.

Table 12: Experimental vs. simulation results

	Experimental	Simple	Adiabatic	Schmidt
Power [W] *	18	14.2 (14.0)	16.2	21.81
Efficiency [%] *	2.96	38.4 (3.51)	42.1	55.76

* Results for the Stirling cycle power and efficiency and not for the total engine thus excluding power required to overcome losses in the drive mechanism.

Keeping in mind that the temperatures (T_h and T_c) used as inputs for the simulation program (refer to Table 2) are the temperatures experimentally measured as the respective internal hot-end and cold-end gas temperatures. This is done because of the difficulty to accurately measure the wall temperature of the heat exchangers. The simulation is, however, developed as a design tool, and therefore these temperatures would be set as the hot and cold side or heat exchanger wall temperatures in practice, since the experimental gas temperatures will not be known beforehand. The Simple analysis specifically incorporates the effect of non-ideal heat exchangers in order to predict these gas temperatures when given the heat exchanger wall temperatures. Whereas for the adiabatic analysis, using the gas temperatures as inputs, instead of the wall temperatures, would give a more accurate prediction of the engines capabilities; due to the assumed adiabatic heater/expansion-space and cooler/compression-space. Once again during the design phase these gas temperatures are not known and therefore this is not possible. Note however, that for the predicted power this is the case for the results displayed in Table 12. Keep in mind that the three methods increase in complexity from Schmidt, adiabatic to the simple analysis as more realistic assumptions are made and more non-ideal effects are considered. The predicted results should thus also approach reality in that order (this effect can easily be seen in the PV diagram presented in Figure 33). Due to the fact that the internal gas temperatures are used as input values for the simple analysis, it under-predicts the power output of the engine.

It is, however, important to note that the very close correlation between the predicted results and experimental data is not the key success factor here. The mere fact that the predicted results is of the same order of magnitude as that of the actual engine is sufficient. This fact is backed by the well known engineering phrase: "*all models are wrong, but some are useful - W.E. Deming*". Walker (1980) also states that the real engine always rejects more heat and produces less power than that predicted by the analytical engine. He pointed out that practical experience accumulated over many years has made it possible for researchers to provide close and realistic predictions of the performance of Stirling engines; the Philips research group was one of the leaders in this aspect.

According to Reader (1983) it is clear from a thermodynamic analysis of the ideal Stirling cycle that the power output of Stirling engines is directly proportional to the mean cyclic pressure of the engine. He also states that in practice this is indeed the case as power output varies with mean cylinder pressure. This implies that an increase in the mean operating pressure of the engine would increase the power output of the engine. The HSE is however limited to operating at a mean engine pressure (1.14 bar – experimentally determined) only slightly higher than atmospheric due to the effect of the hydraulic seal between the internal engine pressure (just below the power piston) and the external atmospheric pressure (above power piston or external to engine). Should the internal engine pressure be increased the gas leakage will increase dramatically and an enormous supply reservoir (continuously supplying operating fluid in order to compensate for loss due to leakage) would be required. The use of hydraulic seals is therefore not recommended in future designs.

During experimental procedures the internal engine pressure is measured and logged continuously together with the crank angle. The experimental volume is determined as a function of the measured crank position and therefore depends on the accuracy of the crank position measurement. Should the setting up of the crank rotation sensor not be done correctly, the experimentally measured PV diagram will not be sensible. Due to the sensitivity of this setting it is not always possible to obtain results that are in phase with that of the simulations. In order to ensure a sensible experimental PV diagram the experimental pressure versus crank angle (theta) diagram had to be adjusted until it was in phase with that obtained from simulations (as shown in Figure 33). This was done by making slight adjustments in the phase of the experimental data and comparing it to the simulated results. With the pressure versus theta diagram of the simulation and experimental results in phase with each other, the experimental PV diagram could be compared to the simulated results (refer to Figure 33 for this comparison).

Kolin (2001) compared the PV diagrams for the ideal Stirling cycle of the alpha, beta and gamma type engines. He concluded that the beta type engine can be designed to have a PV diagram with almost the same surface area as the ideal PV diagram, thus having the highest possible engine power output of the three engine configurations. Since the Heinrici engine is known to be a simple, inefficient but reliable engine (Hargreaves, 1991), it is expected that this will not be the case; as can be seen in Figure 33.

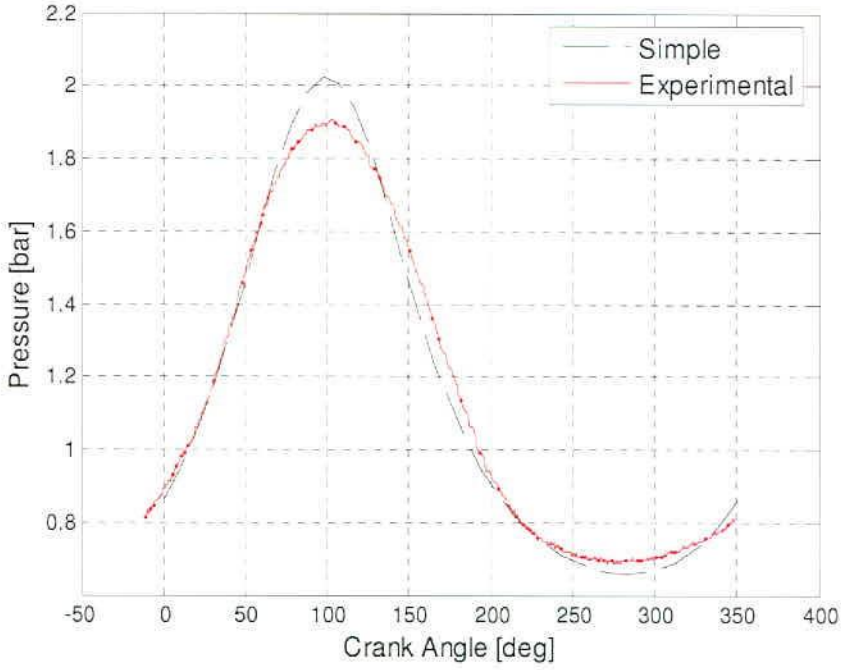

Figure 32: Pressure vs. Theta (Experimental)

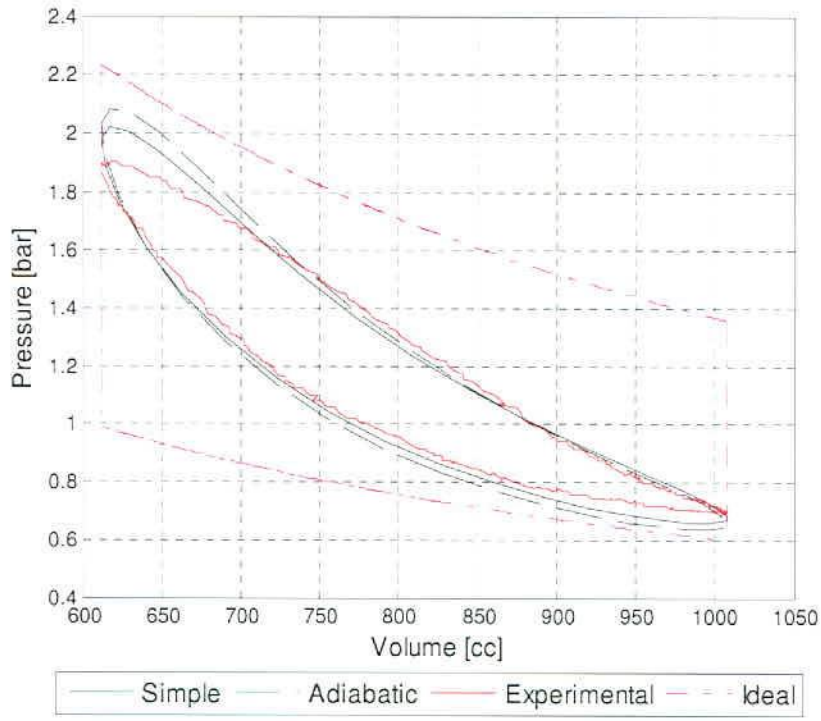

Figure 33: Pressure vs. Volume diagram (Experimental)

Note that the simple analysis is further away from the limits of the ideal PV diagram than that of the adiabatic analysis. As mentioned earlier, this is due to the fact that the adiabatic analysis is a less complex method i.e. it does not take into account the non-ideal effects present in the real engine. The simple analysis does consider some of these effects and therefore moves even further away from the ideal situation and similarly the real engine is even further removed from the ideal limits.

The simulated (simple analysis) pressure versus theta graph in Figure 32 predicts a higher peak pressure and a lower trough pressure than that which was found experimentally. This effect can also be seen in Figure 33 where the maximum pressure is higher (at minimum volume) than the experimentally measured value. Similarly, the lower pressure is lower (at maximum volume) than the experimental value. The lack of ability of the simulation to accurately predict the internal engine pressure can be prescribed to the incomplete incorporation of pumping and fluid friction effects. Shuttle heat transfer losses or periodic gas conduction effects (due to alternating heat transfer effects between cylinder walls and gas; cylinder walls also has in reality temperature gradients in the direction of flow and causes increase/decrease in temperatures) causes inaccurate temperature prediction and is complicated even more by the pressure variation within the engine this cause the incorrect evaluation of fluid properties. The latter may then lead to incorrect temperature and pressure calculations causing a minor "snow-ball effect". The interconnection of these two effects (temperature and pressure) complicates the theoretical approach even more (Hargreaves, 1991).

7. Project Conclusion

The program and methodology discussed in this document is based on work done by Berchowitz and Urieli (1984), which formed part of a course presented by the authors at the Ohio University, Athens Ohio. The literature is presented in Section 4 of this document, while Section 5 provides a discussion of the MATLAB implementation of the program in order to analyse the Heinrici Stirling engine used for experimental verification of simulated results. Experimental procedures and results are discussed in Section 6. The experimental and simulation results are compared in Section 6.5; it was found that the simulations predicted the output of the HSE accurately (refer to Table 12 for results) but it should be mentioned that the mere fact that the simulation results are of the same order of magnitude as that of the actual engine's output parameters, is sufficient proof that the simulations are trustworthy.

During experimental procedures the measurements (stipulated in Table 9 and Table 10) were logged and converted to presentable numeric results, these measurements were then used as inputs for the simulation program (refer to Table 1 for list of required inputs) discussed in Section 5. The measured internal hot and cold-end gas temperatures were used as respective source and sink temperature inputs instead of the actual internal hot and cold-end heat exchanger wall temperatures. This lead to the actual under-prediction of the engines output, refer to Table 12 for a comparison of experimental and simulated results. A reason for this under-prediction, specifically by the simple analysis (Sections 4.4 and 5.6) is attributed to the fact that the simple analysis considers the internal heat exchangers to be non-ideal i.e. the user defined input source and sink temperatures should be the actual wall temperatures of the internal heat exchangers, the simple analysis then calculates the actual internal gas temperatures. It therefore calculates an internal gas temperature lower (for the hot-end) and higher (for the cold-end) than the measured (or user defined input) values, which leads to a lower operating temperature difference and thus lower power output.

Assumptions made to simplify the theoretical modelling of the system causes inaccurate results when compared to experimental data (Section 6.5), however Figure 33, Figure 32 and Table 12 indicates that these assumptions still provide feasible answers. Incorporating shuttle heat transfer effects (amongst other losses) would create a more accurate model of the system but as Reader (1983) mentioned; years of combined experimental and theoretical experience is the only way to attain accurate models of the extremely complicated effects within Stirling engines. It is therefore recommended that this highly simplified model is applied to develop a model Stirling engine in order to do experimental tests which can then be used to improve the model and knowledge of the Stirling cycle.

Applying the five (5) volume methodology presented by Berchowitz and Urieli (1984) to the actual three (3) volume Heinrici engine seems unfeasible at first, however it should be noted the aim of the analysis

procedures presented in this document is not to simulate the relatively old and inefficient three (3) volume engine topologies but rather to synthesise and enable analysis during the Stirling engine design procedures of the more complex and efficient five (5) volume engine topologies. Due to availability problems and the extensive cost of purchasing modern Stirling engines, the five (5) volume methodology was applied to the available three (3) volume Heinrici engine in order to obtain experimental verification of the methodologies presented in this document.

Walker (1980) stipulated that Stirling engine designers and especially newcomers to the concept and application fields of the Stirling engine are often over optimistic with regards to the capabilities of these machines. However, in 1876 Rev. Dr. Robert Stirling wrote: "...*If Bessemer iron or steel had been known thirty five or forty years ago there is no doubt that the air engine would have been a great success...It remains for some skilled and ambitious mechanist in a future age to repeat it under more favourable circumstances and with complete success.*" (Walker, 1980). In a more recent document, Organ (1992) states that speeding up the development of Stirling cycle machines for commercial use depends on the improved insight to be gained of their complex inner workings. He mentions that acquiring such insight is certainly a stimulating and rewarding task, but eventually replacing certain conventional types of energy converters by Stirling machines working to the limits of their efficiency, quietness and freedom from pollution is an essential aspiration. Certainly the combined improvement in the quality and knowledge of modern engineering materials as well as simulation techniques provides the "favourable circumstances" referred to by Rev. Robert Stirling in 1876. As summarised in the literature review (Section 3.4) the application of Stirling cycle machines in the renewable energy sector has become a focal point for scientists throughout the world in the past decades. According to the above statements, the only deficiency preventing the Stirling cycle machine of today from reaching its full potential has to be the over-enthusiastic or even naive designer willing to persevere.

8. Recommendations

It is recommended for future work done on the analysis of Stirling engines, specifically beta type engines with configurations similar to that of the Heinrici engine, to incorporate the effect of varying cooler volume. Franken (2006) proposed a transient approach (instead of the crank-angle dependant method presented here) to investigate the dynamics of Stirling engines. This model developed by Franken (2006) was applied to simulate the relatively simple three (3) volume Heinrici engine, which enables easier incorporation of the instantaneous heat transfer and other fluid effects. Incorporating the varying cooler length in a time dependant method would be less complicated, however the method proposed by Franken (2006) requires much more simulation time than the method presented here. The approach presented in this document is base on a five (5) volume methodology and finds application in the synthesis and analysis procedures during Stirling engine design procedures. While the method of Franken (2006) enables the transient analysis of the complex dynamics within Stirling engines. It should however be mentioned that, as found in Section 5.6.2, within a certain range the effect of cooler length on obtained results is minimal. Attention should rather be given to incorporate more non-ideal effects like friction (mechanical and fluid), shuttle heat transfer as well as shuttle losses in operating fluid motion. Chapter 9 of the book "Stirling Engines" by Walker (1980) provides a discussion on some of these losses within the real Stirling engine.

In order to obtain the experimental PV diagram the pressure and corresponding crank position was measured, from the crank position the volume could be calculated as derived in Appendix C. The accuracy of the crank measurement thus plays an important role in the experimental results and is therefore recommended that for future testing that the measurement of the crank position should be done with a digital measurement device instead of the analogue device used during this project, thus eliminating the possible amplification and measurement errors. Correct installation of the measurement device also plays an important role in the accuracy of the experimental results.

8.1 Recommended future fields of study relevant to Stirling Technology

Van Heerden (2003) studied the application of a solar powered Stirling electricity generation unit, while solar powered Stirling refrigeration systems were studied by Koehler et al. (1997), as well as Kwon and Berchowitz (2003). The increased interest by companies and research groups (as mentioned by Onovwiona and Ugersal, 2004) over the past two (2) decades, specifically with regard to Stirling engine technology for use in the renewable energy sector, provides an indication of the increasing possibilities and relevance of this field of study. Developing an accurate and trustworthy method of analysing Stirling engines thus creates a firm foundation for further development and research at the University of

Stellenbosch. This documents presents such an analysis procedure that can be utilised for future design and manufacturing of Stirling engines.

One of the biggest advantages of Stirling engines is their ability to utilise any form of heat, from biodegradable products to fossil fuel and even solar energy. In the rural or off-grid parts of South Africa fires made from wood, cattle manure and domestic waste provides warm water, heating and energy for cooking. Developing small scale, low cost (only possible if large enough capital investments is obtained), reliable cogeneration units that can be powered by any form of heat source (like wood or cattle manure) could dramatically improve the lifestyle of people living in these areas. *Whispertech*, New Zealand, develops cogeneration units (called *WhisperGen* units) for remote applications. These Stirling powered units are gasoline fuelled and provide warm water, electricity and heating for yachts and off-grid sites (refer to *www.whispertech.co.nz* &/or *www.whispergen.com*). It is therefore possible to develop such domestic cogeneration units for use in the rural areas of South Africa (or anywhere in the world for that matter).

References

Berchowitz D, Urieli I. (1984), "Stirling Cycle Machine Analysis", Adam Hilger.

Çengel Y.A, Boles M.A. (2002)., "Thermodynamics – An Engineering Approach", 2nd Edition, McGraw-Hill, Inc. New York.

Cape Argus. Platinum Collection. "Motoring"., 10 February 2006

Hargreaves, C. M. (1991). "The Philips Stirling Engine". Elsevier, Amsterdam, Netherlands.

Hsu, S.T, Lin, F.Y, Chiou, J.S. (2002). "Heat-transfer Aspects of Stirling Power Generation using Incinerator Waste Energy". Department of Mechanical Engineering, National Cheng Kung University, Taiwan. Article on Renewable Energy. Accepted 11 January 2002.

Incropera, F. P, De Witt, D. P. (2002). "Fundamentals of Heat and Mass Transfer". 5th Edition. John Wiley & Sons. USA.

Janssen, M. Beks, P. (2002). "Measurement and Application of Performance Characteristics of a Free Piston Stirling Cooler". 9th International Refrigeration and Air Conditioning Conference, Perdue.

Koehler, J. Tegethoff, W.J. Westphalen, D. Sonnekalb, M. (1997). "Absorption Refrigeration System for Automobile Refrigeration Utilizing Exhaust Gases". Heat and Mass Transfer, Volume 32, page 333-340. © Springer-Verlag

Kolin. I. (2001). "Ideal Stirling Cycle in Alpha, Beta and Gamma Engines". University of Zagreb, Croatia. Proceedings of the 10th Stirling Engine Conference 24th – 26th September 2001. Osnabruck. Germany.

Kontragool. B, Wongwises. S. (2005). "Thermodynamic Investigation of a Stirling Engine Including Dead Volumes of Hot Space, Cold Space and Regenerator". Department of Mechanical Engineering, King Mongkut's University of Technology Thonburi, Bangkok, Thailand. *Renewable Energy 31, 2006.* Elsevier Ltd. Article accepted 22 March 2005.

Kontragool. B, Wongwises. S. (2004). "Investigation on Power Output of the Gamma-Configuration Low Temperature Differential Stirling Engines". Department of Mechanical Engineering, King Mongkut's University of Technology Thonburi, Bangkok, Thailand. *Renewable Energy 30, 2005.* Elsevier Ltd. Article accepted 10 June 2004.

Kröger, D. G. (1998). "Air Cooled Heat Exchangers and Cooling Towers", Department of Mechanical Engineering, University of Stellenbosch, South Africa.

Kwon, Y. Berchowitz, D.M. (2003). "Operational Characteristics of Stirling Machinery". International Congress of Refrigeration, Washington DC.

Lotun, D. (2001). "Design and Evaluation Through Simulation and Experimental Apparatus of a Small Scale Waste Heat Recovery System". Post Graduate M.Sc.Eng Thesis. University of Stellenbosch, South Africa. December 2001

Morrison, G. (1999). "Stirling Renewal". Associated Editor. American Society of Mechanical Engineering. Feature Article, May 1999

Onovwiona, H.I. Ugersal, V.I. (2004) "Residential Co-generation Systems: Review of the Current Technology". Renewable and Sustainable Energy Reviews, Article accepted 13 July 2004.

Organ, A. J. (1997). "The Regenerator and the Stirling Engine". J W Arrowsmith Ltd, Great Britain.

Organ, A. J. (1992). "Thermodynamics and Gas Dynamics of the Stilting Cycle Machine". Cambridge University Press. Cambridge, New York.

Pavoni, J. L. Heer jr, J. E. Hagerty, D. J. (1975). "Handbook of Solid Waste Disposal Materials and Energy Recovery". Litton Educational Publishing, Inc.

Pieterse, M.A. (2003). "Building and Testing of a Solar Thermal Stirling Engine Model". Final year undergraduate project. University of Stellenbosch, South Africa. October 2003

Reader, G. T, Hooper, C. (1983). "Stirling Engines", E. & F. N. Spon, London.

Redecker, H. H. (2004). "Bidirectional Converter for a Stirling Energy System". Post Graduate M.Sc.Eng Thesis. University of Stellenbosch, South Africa. December 2004

Reiter, S. (1983). "Industrial and Commercial Heat Recovery Systems". First Edition. Van Nostrand Reynold Company Inc.

Schmid, H. (2004). "Less Emissions through Waste Heat Recovery". Manager, Application Technology, Ship Power Wärtsilä Switzerland Ltd. Presentation at Green Ship Technology Conference, London, April 2004.

Twele, J. and Gasch, R. (2002). "Wind Power Plants - Fundamentals, Design, Construction and Operation". Solarpraxis, Berlin

Van Heerder, L. (2003). "Dish Stirling Applications for Rural Development". ESKOM special edition. Journal of Energy in South Africa, July 2003

Walker, G. (1980). "Stirling Engines". Oxford University Press, Oxford.

White, M. A. Colenbrander, K. Olan, R. W. Penswick, L. B. (1996). "Generators that won't wear out". South African Institute of Mechanical Engineering, February 1996 (page 92).

Wipplinger, K. P. M. (2004). "Utilising a High Pressure, Cross Flow, Stainless Steel Fintube Heat Exchanger for Direct Steam Generation from Recovered Waste Heat". MScEng Thesis, University of Stellenbosch, April.

Appendix A Summary of Equation Set for Schmidt Analysis: Literature

A summary of the equation set for the Schmidt analysis presented by Berchowitz and Urieli (1984) is done in this Appendix. The presented Schmidt analysis is for an alpha type Stirling engine with sinusoidal volume variation. A simplified configuration is shown in figure 5.1. Effective constant volume definitions like V_{clc}, V_{cle}, V_{swc}, V_{swe} as well as α are required for the equation set below and can be obtained from the sinusoidal volume variation definitions (refer to Appendix B for the derivation of the volume variations for the Heinrici engine considered in this document). The compression and expansion space volumes are obtained as follows:

$$\begin{aligned} V_c &= V_{clc} + V_{swc}.(1+\cos(\theta+\delta))/2 \\ V_e &= V_{cle} + V_{wse}.(1+\cos(\theta+\delta+\alpha))/2 \end{aligned} \tag{A.1}$$

Compression space, expansion space and total work:

$$\begin{aligned} W_c &= \pi.V_{swc}.p_{mean}.\sin(\beta).\left(\sqrt{1-b^2}-1\right)/b \\ W_e &= \pi.V_{swe}.p_{mean}.\sin(\beta-\alpha).\left(\sqrt{1-b^2}-1\right)/b \\ W &= W_c + W_e \end{aligned} \tag{A.2}$$

Cyclic efficiency (also Carnot efficiency)

$$\eta = W/Q_e = 1 - T_k/T_h \tag{A.3}$$

Where

$$\begin{aligned} \beta &= atn\left(\frac{V_{swe}.\sin(\alpha)/T_h}{V_{swe}.\cos(\alpha)/T_h + V_{swc}/T_k}\right) \\ c &= \frac{1}{2}\sqrt{\left(\frac{V_{swe}}{T_h}\right)^2 + 2\frac{V_{swe}}{T_h}.\frac{V_{swc}}{T_k}.\cos(\alpha) + \left(\frac{V_{swe}}{T_k}\right)^2} \\ s &= \left(\frac{V_{swe}}{2.T_k} + \frac{V_{clc}}{T_k} + \frac{V_k}{T_k} + \frac{V_r.\ln(T_h/T_k)}{(T_h-T_k)} + \frac{V_h}{T_h} + \frac{V_{swe}}{2.T_h} + \frac{V_{cle}}{T_e}\right) \\ b &= c/s \\ p_{mean} &= M.R\Big/\left(s.\sqrt{1-b^2}\right) \end{aligned} \tag{A.4}$$

With M being the total mass of gas in the engine while R is the gas constant of the particular working gas.

Appendix B Summary of Equation Set for Ideal Adiabatic Analysis: Literature

The equation set for the ideal adiabatic analysis presented by Berchowitz and Urieli (1984) is summarised in this Appendix. The presented Schmidt analysis is for an alpha type Stirling engine with sinusoidal volume variation. A simplified configuration is shown in Figure 3. The adiabatic equation set can be divided into several groups of equations, like:

Equations of pressure:

$$p = \frac{MR}{\left(V_c / T_c + V_k / T_k + V_r . \ln(T_h / T_k) / T_h - T_k + V_h / T_h + V_e / T_e\right)}$$
$$dp = \frac{-\gamma . p . \left(dV_c / T_{ck} + dV_e / T_{he}\right)}{\left(V_c / T_{ck} + \gamma . \left(V_k / T_k + V_r / T_r + V_h / Th\right) + V_e / T_{he}\right)} \qquad \text{(B.1)}$$

Equations for masses:

$$\begin{aligned} m_c &= p.V_c / (R.T_c) \\ m_k &= p.V_k / (R.T_k) \\ m_r &= p.V_r / (R.T_r) \\ m_h &= p.V_h / (R.T_h) \\ m_e &= p.V_e / (R.T_e) \end{aligned} \qquad \text{(B.2)}$$

Equations for change in mass or mass accumulation:

$$\begin{aligned} dm_c &= \left(p.dV_c + V_c.dp / \gamma\right) / R.T_{ck} \\ dm_k &= m_k.dp / p \\ dm_r &= m_r.dp / p \\ dm_h &= m_h.dp / p \\ dm_e &= \left(p.dV_e + V_e.dp / \gamma\right) / R.T_{he} \end{aligned} \qquad \text{(B.3)}$$

Equations for mass flow over cell interfaces:

$$\begin{aligned} m_{ck} &= -dm_c \\ m_{kr} &= m_{ck} - dm_k \\ m_{he} &= dm_e \\ m_{rh} &= m_{he} - dm_h \end{aligned} \qquad \text{(B.4)}$$

Equations for conditional temperatures (depending on direction of flow):

$$\begin{aligned} &if\ m_{ck} > 0 then T_{ck} = T_c\ else T_{ck} = T_k \\ &if\ m_{he} > 0 then T_{he} = T_h\ else T_{he} = T_e \end{aligned} \tag{B.5}$$

Equations for temperature change in working spaces:

$$\begin{aligned} dT_e &= T_e.(dp/p + dV_e/V_e - dm_e/m_e) \\ dT_c &= T_c.(dp/p + dV_c/V_c - dm_c/m_c) \end{aligned} \tag{B.6}$$

Equations for energy:

$$\begin{aligned} dQ_k &= c_v.V_k.dp/R - (c_p.T_{ck}.m_{ck} - c_p.T_{kr}.m_{kr}) \\ dQ_r &= c_v.V_r.dp/R - (c_p.T_{kr}.m_{kr} - c_p.T_{rh}.m_{rh}) \\ dQ_h &= c_v.V_h.dp/R - (c_p.T_{rh}.m_{rh} - c_p.T_{he}.m_{he}) \\ W &= W_e + W_c \\ dW &= dW_e + dW_c \\ dW_e &= p.dV_e \\ dW_c &= p.dV_c \end{aligned} \tag{B.7}$$

Thermal efficiency:

$$\eta = W/Q_h = (Q_h + Q_k)/Q_h \tag{B.8}$$

Appendix C Derivation of Volume Variation for Heinrici Stirling Engine

This Appendix includes a layout drawing of the Heinrici Stirling Engine (HSE) considered in this document for simulation as well as experimental purposes. Figure 34 shows a sectional view of the HSE indicating key connection points. These connection points are referred to during the derivation of the volume variation of the engine in this Appendix. Point O is the centre of the crank mechanism and is used as a reference point for displacements.

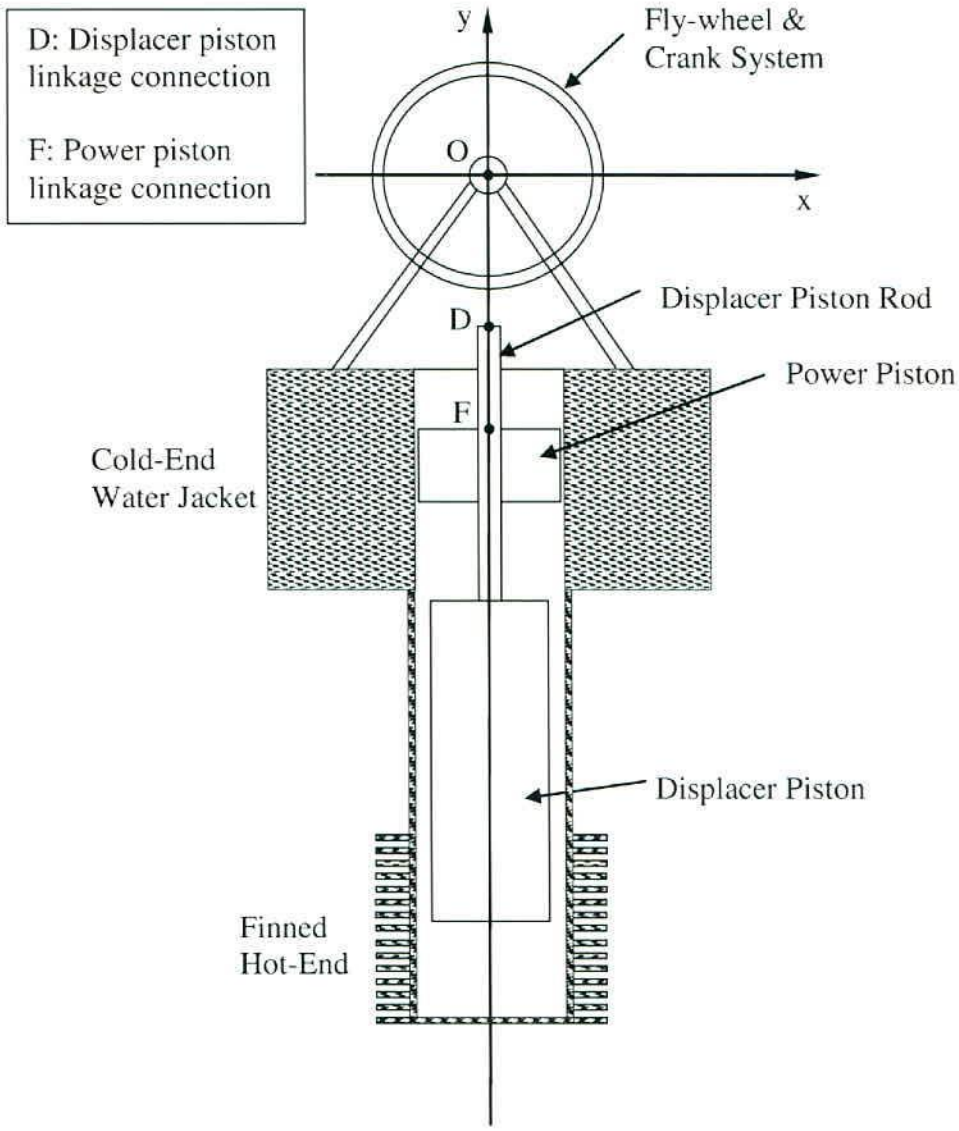

Figure 34: HSE Line Diagram

Figure 35 shows the power piston crank system layout. Once again point O is the centre of the crank mechanism. Point A is the connection point of the displacer piston's linkage system to the crank mechanism (illustrating relative movement of power and displacer pistons with respect to each other).

Point E is the power pistons linkage system connection point to the crank mechanism while point F is the connection point of the power pistons crank linkage system to the top of the power piston (see Figure 34).

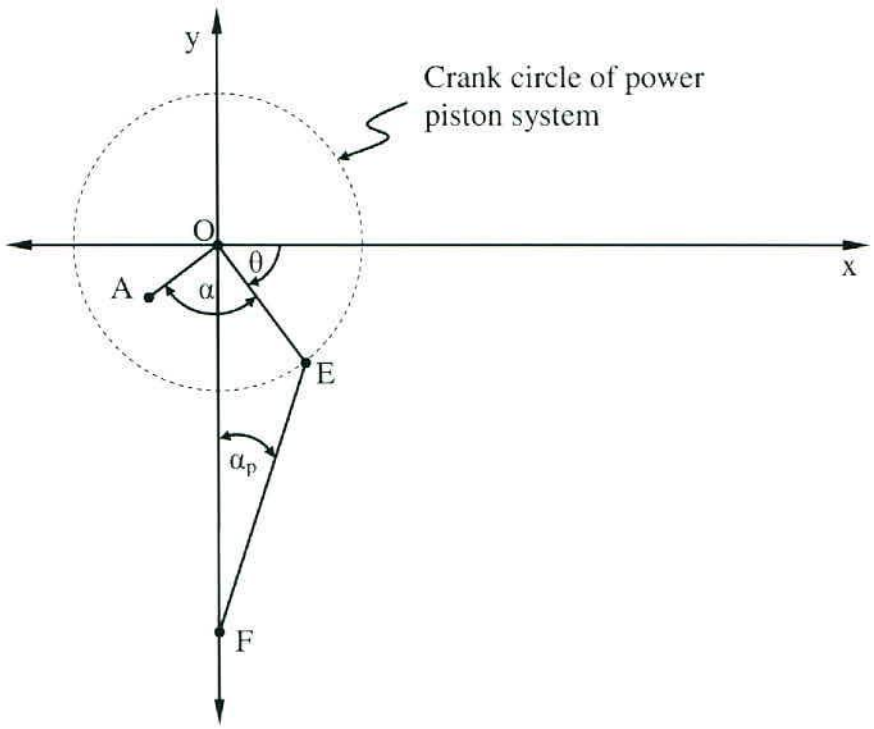

Figure 35: Power Piston Crank Linkage Layout of HSE

Angle α is the angle by which the displacer piston's crank arm leads the power piston's crank arm (90^0 for this engine), angle α_p is the absolute angle between power piston connection rod (or conrod) and the vertical y axis. Angle θ denotes the angle of rotation of the crank mechanism (or fly-wheel) and is measured relative to the positive x axis.

NOTE: For the derivation to follow linkage EF in Figure 35 will be referred to as L_{pc}, similarly linkage OE will be referred to as R_p.

NOTE: All points and linkages shown in Figure 35 and Figure 36 can only move with their relevant two (2) degrees of freedom within the illustrated Cartesian plane, unless stated otherwise.

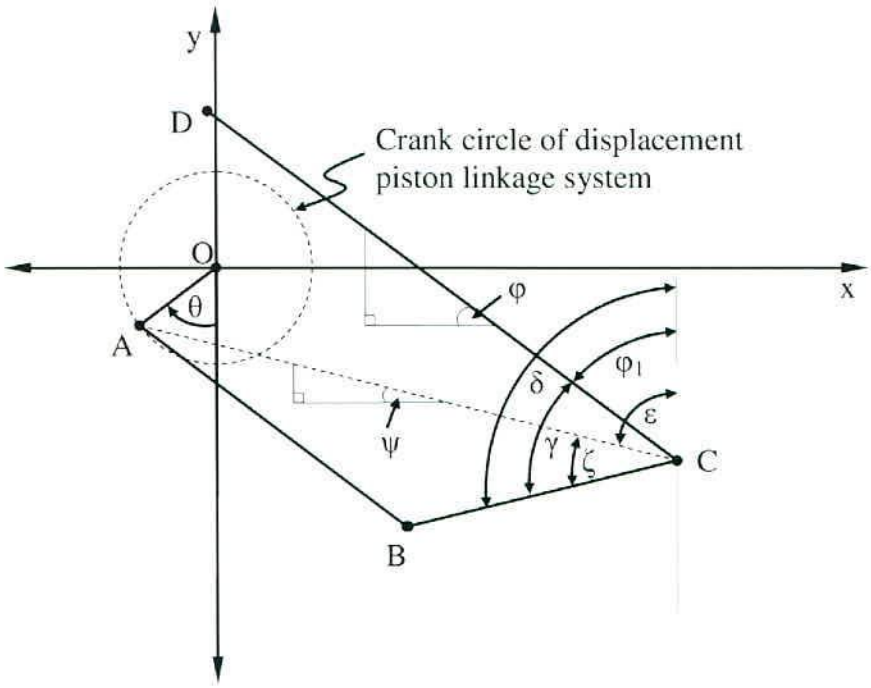

Figure 36: Displacer Piston Crank Linkage Layout of HSE

In Figure 36 point O is once again the centre of the crank mechanism and is used as a reference point (or intersection point of the x and y axis on the Cartesian plane). Point C is a fixed point with linkage BC and CD rigidly connected to each other and hinging at C. Angle γ is the fixed angle between linkages BC and CD.

For the derivations to follow in this Appendix the following linkages will be referred to as:

Table 13: HSE Linkage System Description

Linkage	**Henceforth referred to as:**
OA	R
AB	L_1
BC	L_2
CD	L3

Calculate X & Y Coordinates of point A as a function of θ with R = radius of displacement piston crank system :

$$x_A = -R \cdot \sin(\theta) \qquad y_A = -R \cdot \cos(\theta) \tag{C1-2}$$

Determine the gradient of line AC:

$$m = -\frac{y_A - y_C}{x_A - x_C} \tag{C3}$$

Determine angles:

$$\psi = \operatorname{atan}(m)$$

$$\varepsilon = \frac{\pi}{2} - \psi \tag{C4-5}$$

Length of line AC:

$$AC = \left[(x_A - x_C)^2 + (y_A - y_C)^2 \right]^{0.5} \tag{C6}$$

Determine angle ζ using law of cosines

$$\zeta = \operatorname{acos}\left(\frac{L_2^{\,2} + AC^2 - L_1^{\,2}}{2 \cdot L_2 \cdot AC} \right) \tag{C7}$$

$$\Delta = \varepsilon + \zeta$$

$$\phi_1 = \Delta - \gamma \tag{C8-10}$$

$$\phi = \frac{\pi}{2} - \phi_1$$

α_p is always: -90< α_p<90 thus cos(α_p) will always be positive

$$\alpha_p = \operatorname{asin}\left(\frac{R_p \cdot \cos(\theta)}{L_{pc}} \right) \tag{C11}$$

Determine Y-coordinate of displacer & power piston relative to crank centre with Hp = height/length of power piston and Ldrod = length of displacement piston rod (factor 28.5 is measured on power piston from bottom to connection point of PP conrod):

$$Y_p = -R_p \cdot \sin(\theta) - L_{pc} \cdot \cos(\alpha_p) - (H_p - 28.5) \qquad \text{(C12-13)}$$

$$Y_d = yC + L_3 \cdot \sin(\phi) - L_{drod}$$

Determine stroke of power & displacer pistons:

$$stroke_p = \max(Y_p) - \min(Y_p) \qquad \text{(C14-15)}$$

$$stroke_d = \max(Y_d) - \min(Y_d)$$

Determine coordinates of bottom of power & top & bottom of displacer piston

$$Y_{d.bot} = Y_d - H_d$$

$$Y_{d.top} = Y_d \qquad \text{(C16-18)}$$

$$Y_{p.bot} = Y_p$$

Calculate volume using above displacement definitions :

$minY_{clc}$ = minimum clearance between displacer & power piston

$minY_{cle}$ = minimum clearance between bottom of displacer piston and botom of hot-end sleeve

L_c = length/height of cold-end (water jacket height)

L_e = length/height of hot-end sleeve (finned hot-end & regenerator sections)

E_{top} = distance from crank centre (O) to top of engine (top of water jacket)

$$V_c = \frac{\pi \cdot \left(D_d^{\,2} - D_{dr}^{\,2} \right)}{4} \cdot \left(Y_{p.bot} - Y_{d.top} - \min Y_{clc} \right) \tag{C19}$$

$$V_e = \frac{\pi \cdot D_d^{\,2}}{4} \cdot \left(Y_{d.bot} + E_{top} + L_c + L_e - \min Y_{cle} \right) \tag{C20}$$

$$V_{swc} = \frac{\pi \cdot \left(D_c^{\,2} - D_{dr}^{\,2} \right)}{4} \cdot stroke_p \tag{C21}$$

$$V_{swe} = \frac{\pi \cdot D_d^{\,2}}{4} \cdot stroke_d \tag{C22}$$

$$V_{clc} = \frac{\pi \cdot \left(Dd^2 - Ddr^2 \right)}{4} \cdot \min Y_{clc} \tag{C23}$$

if $(D_e - D_d)/2 < \min Y_{cle}$

$$V_{cle} = \pi \cdot \frac{D_e^{\,2}}{4} \cdot \left[\min Y_{cle} - \frac{\left(D_e - D_d \right)}{2} \right] \tag{C24}$$

else

$$V_{cle} = \pi \cdot \frac{De^2}{4} \cdot \min Y_{cle}$$

Calculate volume derivatives by obtaining derivatives of piston displacements:

The volume derivatives are:

$$\frac{d}{d\theta}Vc = \frac{\pi\cdot\left(D_d{}^2 - D_{dr}{}^2\right)}{4}\cdot\left(\frac{d}{d\theta}Y_p - \frac{d}{d\theta}Y_d\right) \quad \text{(C25)}$$

$$\frac{d}{d\theta}Ve = \left[\frac{\pi\cdot\left(D_d\right)^2}{4}\right]\cdot\frac{d}{d\theta}Yd \quad \text{(C26)}$$

The Power pistons displacement derivatives :

$$\frac{d}{d\theta}Yp = -R_p\cdot\cos(\theta) + L_{pc}\cdot\sin\left(\alpha_p\right)\cdot\frac{d}{d\theta}\alpha_p \quad \text{(C27)}$$

With:

$$\frac{d}{d\theta}\alpha_p = \frac{d}{d\theta}\left(\operatorname{asin}\left(R_p\cdot\sin(\theta)\right)\right) \quad \text{(C28)}$$

$$\frac{d}{d\theta}\alpha_p = \frac{1}{\left[1-\left(\frac{R_p\cdot\cos(\theta)}{L_{pc}}\right)^2\right]^{0.5}}\cdot\frac{-R_p\cdot\sin(\theta)}{L_{pc}} \quad \text{(C29)}$$

The Displacer pistons displacement derivatives:

$$\frac{d}{d\theta}Y_d = L_3\cdot\cos(\phi)\cdot\frac{d}{d\theta}\phi \quad \text{(C30)}$$

With:

$$\frac{d}{d\theta}\phi = -\frac{d}{d\theta}\phi_1$$

$$\frac{d}{d\theta}\phi_1 = \frac{d}{d\theta}\Delta \quad \text{(C31-34)}$$

$$\frac{d}{d\theta}\Delta = \frac{d}{d\theta}\varepsilon + \frac{d}{d\theta}\zeta$$

$$\frac{d}{d\theta}\varepsilon = -\frac{d}{d\theta}\psi$$

$$\frac{d}{d\theta}\zeta = \frac{1}{\left[1-\left(\frac{L_2^{\,2}+AC^2-L_1^{\,2}}{2\cdot L_2\cdot AC}\right)^2\right]}\cdot\frac{d}{d\theta}\left(\frac{L_2^{\,2}+AC^2-L_1^{\,2}}{2\cdot L_2\cdot AC}\right) \qquad \text{(C35-38)}$$

Thus:

$$\frac{d}{d\theta}\zeta = \frac{-1}{\left[1-\left(\frac{L_2^{\,2}+AC^2-L_1^{\,2}}{2\cdot L_2\cdot AC}\right)^2\right]^{0.5}}\cdot\left[\frac{2\cdot AC\cdot\frac{d}{d\theta}AC\cdot\left(2\cdot L_2\cdot AC\right)-\left(L_2^{\,2}+AC^2-L_1^{\,2}\right)\cdot 2\cdot L_2}{\left(2\cdot L_2\cdot AC\right)^2}\right]$$

$$\frac{d}{d\theta}AC = 0.5\cdot\left[(xA-xC)^2+(yA-yC)^2\right]^{-0.5}\cdot\left[\frac{d}{d\theta}\left[(xA-xC)^2\right]+\frac{d}{d\theta}\left[(yA-yC)^2\right]\right]$$

Thus:

$$\frac{d}{d\theta}AC = 0.5\cdot\left[(xA-xC)^2+(yA-yC)^2\right]^{-0.5}\cdot\left[2\cdot(xA-xC)\frac{d}{d\theta}xA+2\cdot(yA-yC)\frac{d}{d\theta}yA\right]$$

$$\frac{d}{d\theta}\psi = \frac{1}{1+m^2}\cdot\left(\frac{d}{d\theta}m\right) \qquad \text{(C39)}$$

$$\frac{d}{d\theta}m = \frac{\frac{d}{d\theta}yA\cdot(xC-xA)-(yC-yA)\cdot\left(\frac{d}{d\theta}xA\right)}{(xC-xA)^2} \qquad \text{(C40)}$$

Finally:

$$\frac{d}{d\theta}xA = -R\cdot\cos(\theta) \qquad \text{(C41)}$$

$$\frac{d}{d\theta}yA = R\cdot\sin(\theta) \qquad \text{(C42)}$$

Appendix D SEA Program Layout (MATLAB)

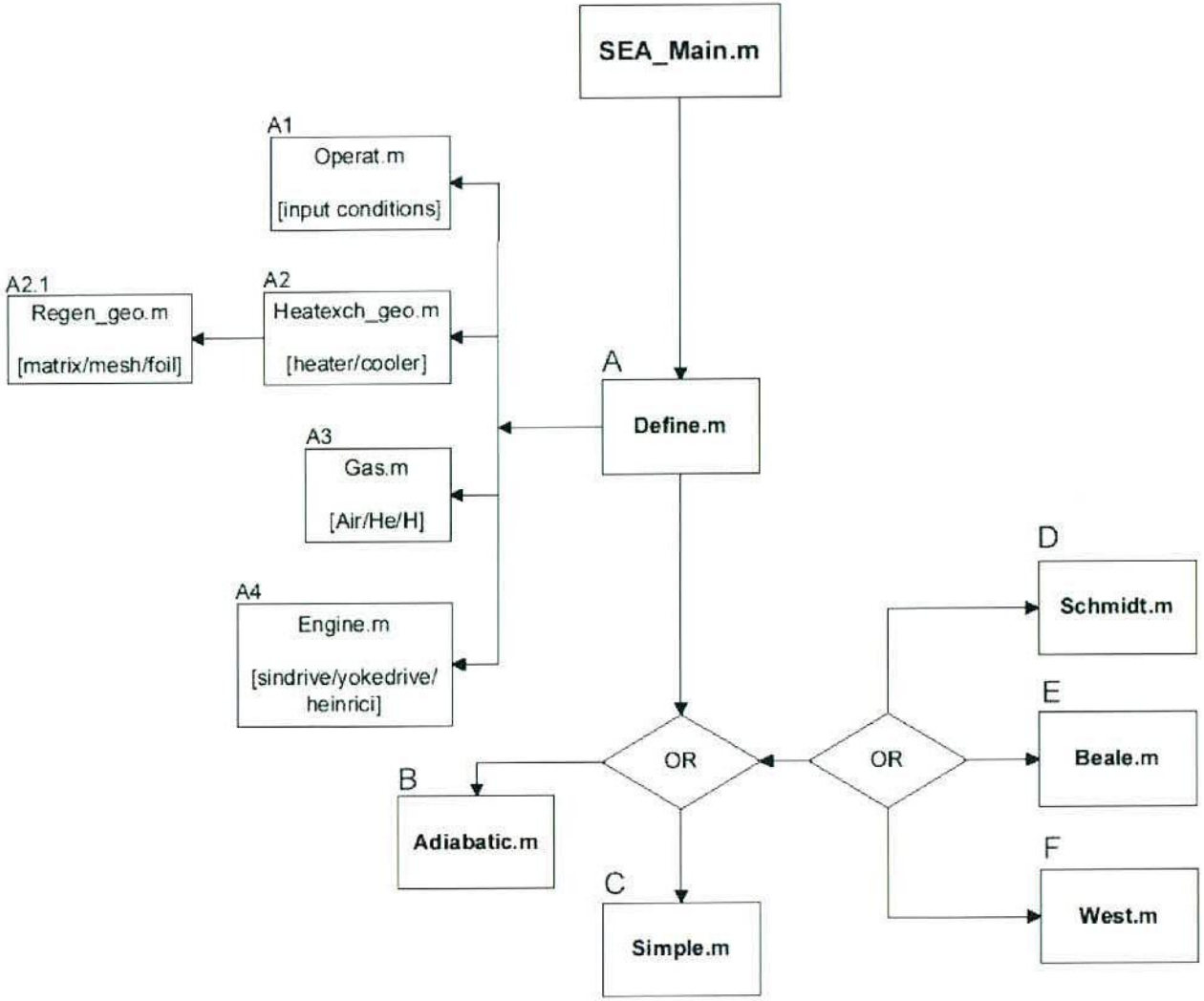

Figure 37: SEA MATLAB program layout

Appendix E Flow Diagram of Ideal Adiabatic Simulation (MATLAB)

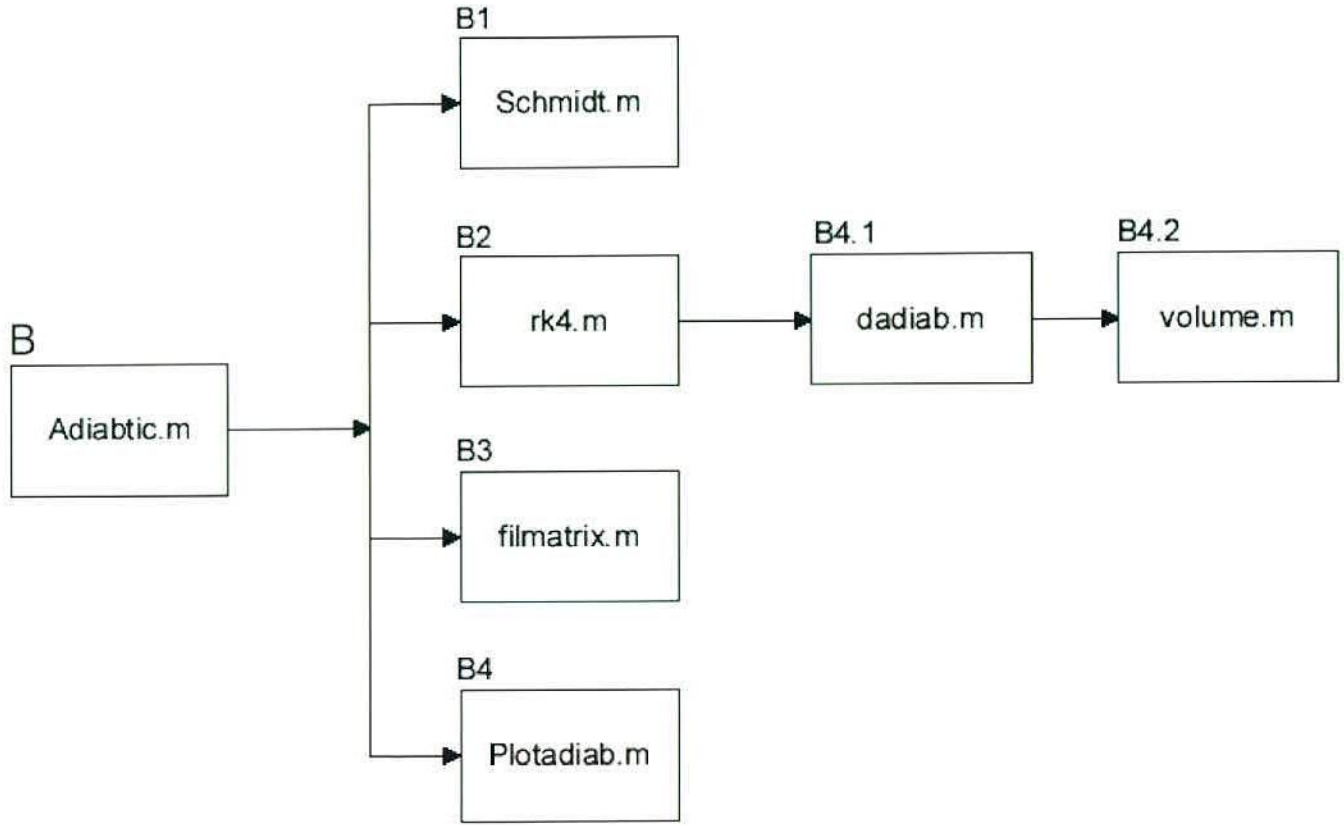

Figure 38: Adiabatic MATLAB program layout

Appendix F Flow Diagram of Simple Analysis (MATLAB)

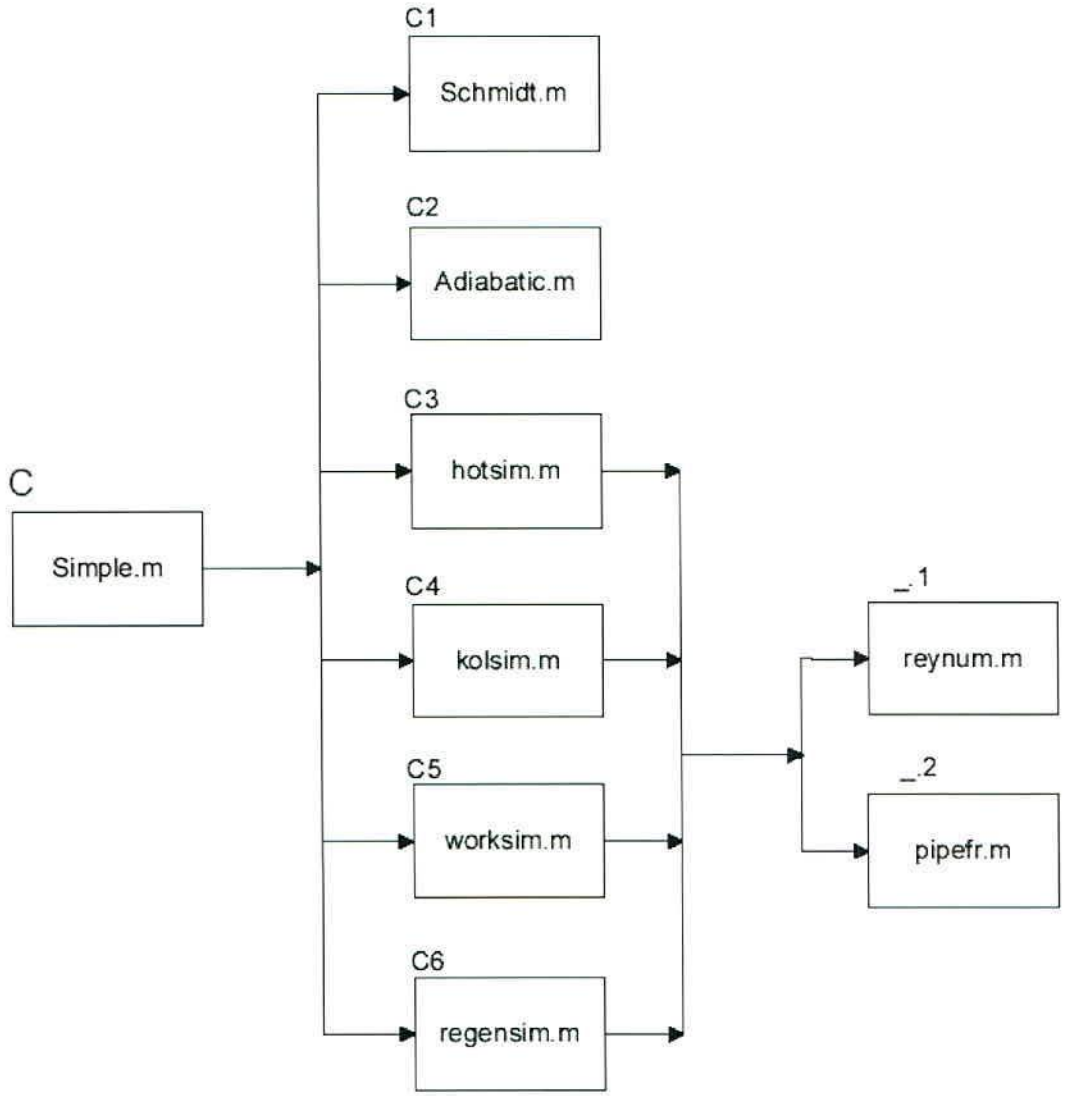

Figure 39: Simple MATLAB program layout

Appendix G Photographs and Discussions on Heinrici Stirling Engine

A discussion of the Heinrici Stirling engine (HSE) used for experimental verification of simulations is presented in Section 6.2.1 of this document. Pictures and descriptions of the HSE are presented in this appendix in order to create a better understanding of the engine.

Figure 40: Heinrici Motor

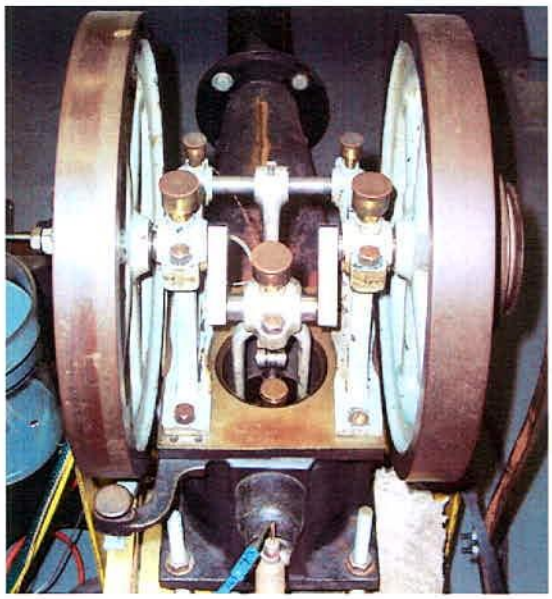

Figure 41 : HSE crank mechanism and water jacket

Figure 40 shows the name of the engine as indicated on the side of the water jacket body of the engine. Figure 41 shows the crank and fly-wheel of the HSE in the position as installed during experimental testing. Note the exhaust gas line of the CCU in the background as well as the thermocouple placement (blue cable at bottom of picture) to measure the outlet cooling water temperature.

Figure 42: Flywheel and crank unit

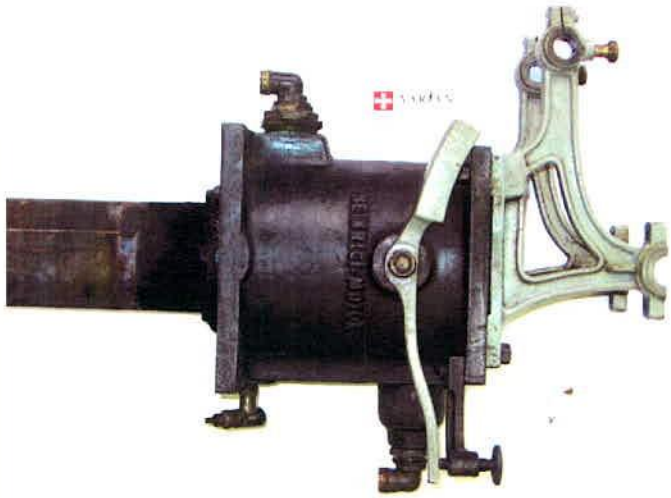

Figure 43: HSE water jacket

Figure 42 shows the fly-wheel crank unit of the HSE separated from the engine. Figure 43 shows a side view of the water jacket of the HSE with the hot-end sleeve (cylinder on left hand side of water jacket) as well as the fly-wheel connection frame (right hand side of water jacket). Cooling water inlet is shown at the top of the water jacket while the cooling water outlet is shown at the bottom of the water jacket.

Figure 44: HSE piston assembly

Figure 44 shows the piston assembly of the HSE. The power piston is the smaller of the two pistons and is shown on the left hand side of the bigger displacement piston. Note the displacement pistons rod passing through the centre of the power piston. Also note the oil groove in the power piston; this provides an oil film on the sides of the piston that forms the hydraulic seal.

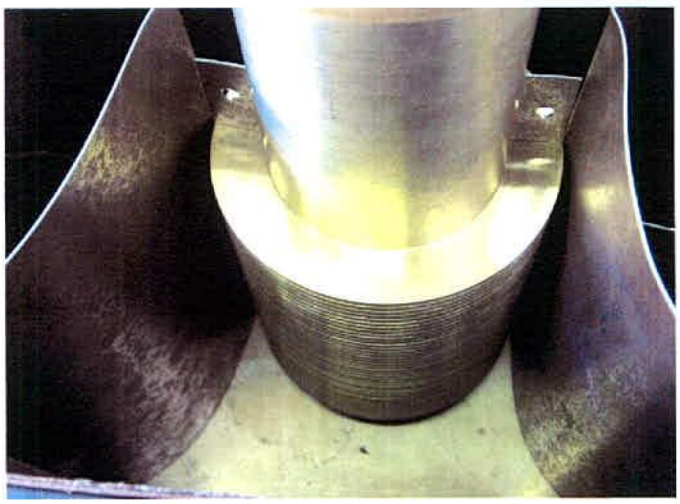

Figure 45: Exhaust gas guide vanes at hot-end

Figure 46: Bottom view of finned hot-end

Figure 45 shows the installation of the finned hot-end in the exhaust system of the CCU. Guide vanes are shown on the left and right hand side of the finned hot-end. Figure 46 shows a bottom view of the finned hot-end of the HSE. Fins were machined in a yellow brass hollow tube thus eliminating the contact heat transfer resistance between fins and tube. Note the position of the thermocouple connector at the bottom of the figure. This thermocouple measures the internal hot-end gas temperature (T_h).

Appendix H Layout Drawing of Finned Hot-End of HSE

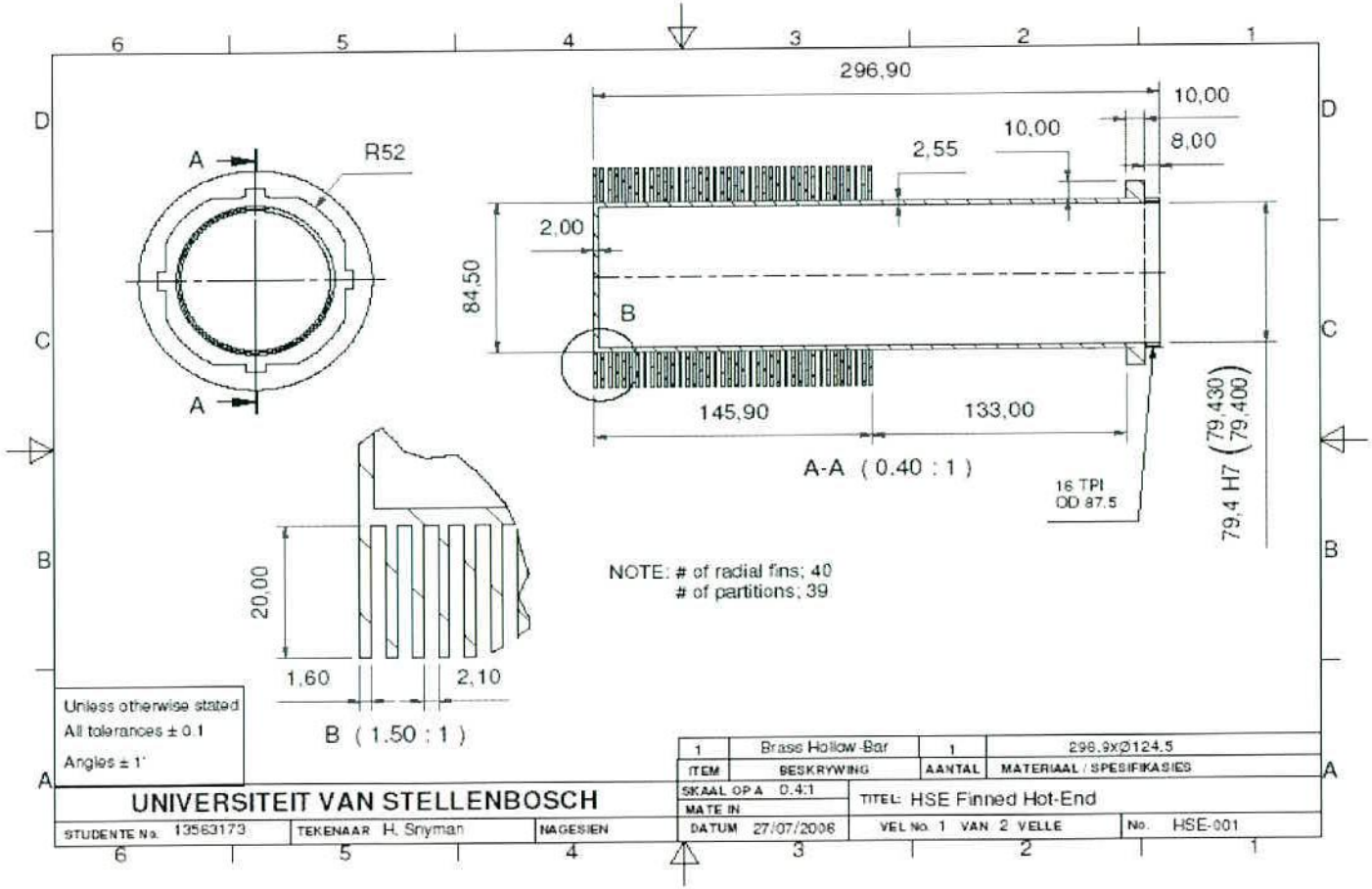

Figure 47: Layout drawing of finned hot-end heat exchanger

Appendix I Calibration of Pressure & Torque Transducers

Figure 48 below shows the calibration curve (pressure versus voltage) for the HBM pressure transducer used to measure internal engine pressure. Refer to Table 9 for the serial number of the transducers. A pressure pump and gauge was used to apply pressure to the transducer, the voltage output signal was then recorded (after amplification) and logged against measured gauge pressure.

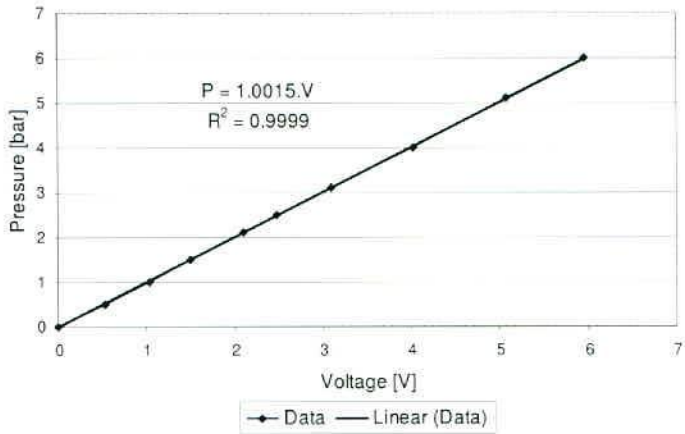

Figure 48: Pressure transducer calibration curve

By suspending a weight at a fixed torque arm to the shaft of the torque transducer, the voltage output of the transducer was logged (after amplification) against torque (or applied weight). Figure 49 indicates the calibration curve of the torque transducer. Refer to Table 9 for the serial number of the transducer.

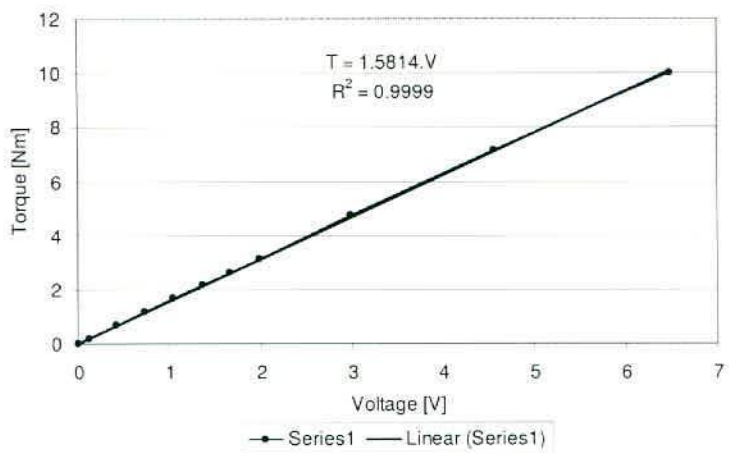

Figure 49: Torque transducer calibration curve

Appendix J *Finned Heat Exchanger & Experimental Efficiency Calculations*

Calculation of finned hot-end heat transfer for HSE

Note: Refer to Incropera and De Witt (2002) unless sated otherwise

Properties of Exhaust Gases

$T_{exh} = (527 + 273)\cdot K$ $T_{exh} = 800K$ Exhaust gas temperature

Assume hot-end wall (metal) temperature to be the average temperature between external exhaust gas and internal hot-end gas temperature

$$T_{wh} = \left(\frac{527 + 448}{2} + 273\right)\cdot K \qquad T_{wh} = 760.5K \qquad (J1)$$

$P_{exh} = 101325Pa$ Assumed pressure of exhaust gasses

$rho_{exh} = 0.696\frac{kg}{m^3}$ Refer to Lotun (2001)

Use exhaust gas mass flow rate as measured for CCU (Air + propane mass flow rate)

$$m_{exh} = (78.5 + 5)\cdot\frac{kg}{hr} \qquad m_{exh} = 0.0232\frac{kg}{s} \qquad (J2)$$

Dimensions of Heinrici hot-end (refer to Appendix H)

Inner and outer dia of SE hot-end:

$D_i = 79.4mm$ $D_o = 0.0845m$ (J3)

Inner radius of SE hot-end:

$$r_i = \frac{D_i}{2} \qquad r_i = 0.0397m \qquad (J4)$$

radius to root of fin

$$r_1 = \frac{D_o}{2} \qquad r_1 = 0.0423m \qquad (J5)$$

Height of hot-end extending into exhaust chamber/gases or finned height:

$H = 0.1459\text{m}$

Frontal area of exhaust chamber in flow direction of exhaust gases:

$$A_{exh} = 0.298\text{m} \cdot 0.251\cdot\text{m} \qquad A_{exh} = 0.0748\text{m}^2 \tag{J6}$$

Heat Transfer calculation

film temperature to evaluate properties of gas

$$T_f = \frac{(T_{exh} + T_{wh})}{2} \qquad T_f = 780.25\text{K} \tag{J7}$$

Specific heat of exhaust gas:
(Taken to be the same as air, from Kröger (1998), equation A.1.2)

$$kk = 0.0007083814\frac{J}{kg\cdot K^3}\cdot T_f^{\,2} - 2.70520910^{-7}\cdot\frac{J}{kg\cdot K^4}\cdot T_f^{\,3}$$

$$cp_{exh} = 1045.356\frac{J}{kg\cdot K} - 0.3161783\frac{J}{kg\cdot K^2}\cdot T_f + kk \tag{J8}$$

$$cp_{exh} = 1101.4137\frac{J}{kg\cdot K}$$

Thermal conductivity of exhaust gas:
(Taken to be the same as air, from Kröger (1998), equation A.1.4)

$$rr = -4.62793710^{-8}\cdot\frac{W}{m\cdot K^3}\cdot T_f^{\,2} + 1.25050310^{-11}\cdot\frac{W}{m\cdot K^4}\cdot T_f^{\,3}$$

$$k_{exh} = -0.0004937787\frac{W}{m\cdot K} + 1.01808710^{-4}\cdot\frac{W}{m\cdot K^2}\cdot T_f + rr \qquad (J9)$$

$$k_{exh} = 0.0567\frac{W}{m\cdot K}$$

Dynamic viscosity of exhaust gas (Taken to be the same as air, from Kröger (1998), equation A.1.3):

$$tt = -3.13195610^{-11}\cdot\frac{kg}{m\cdot s\cdot K^2}\cdot T_f^{\,2} + 8.1503810^{-15}\cdot\frac{kg}{m\cdot s\cdot K^3}\cdot T_f^{\,3}$$

$$\mu_{exh} = 2.28798310^{-6}\cdot\frac{kg}{m\cdot s} + 6.25979310^{-8}\cdot\frac{kg}{m\cdot s\cdot K}\cdot T_f + tt \qquad (J10)$$

$$\mu_{exh} = 0.00003593\frac{kg}{m\,s}$$

Prantl number of exhaust gas:

$$Pr_{exh} = \frac{\mu_{exh}\cdot cp_{exh}}{k_{exh}} \qquad Pr_{exh} = 0.6979 \qquad (J11)$$

Reynolds number of exhaust gas:

$$Re = \frac{m_{exh}\cdot D_o}{A_{exh}\cdot\mu_{exh}} \qquad Re = 729.1877 \qquad (J12)$$

To satisfy the Churchill-Bernstein correlation for a cylinder in cross flow in order to calculate Nu the Pr > 0.2 for all Re.
(refer to Incropera and De Witt (2002), equation 7.57)

$$Nu = 0.3 + \frac{0.62 \cdot Re^{\frac{1}{2}} \cdot Pr_{exh}^{\frac{1}{3}}}{\left[1 + \left(\frac{0.4}{Pr_{exh}}\right)^{0.6666}\right]^{0.25}} \cdot \left[1 + \left(\frac{Re}{282000}\right)^{0.625}\right]^{0.8} \qquad \text{(J13)}$$

$Nu = 13.5761$ Nusselts number

Convective heat transfer coefficient between exhaust gas & SE finned heat exchanger:

$$h = \frac{Nu \cdot k_{exh}}{D_o} \qquad h = 9.1109 \frac{W}{K \cdot m^2} \qquad \text{(J14)}$$

Dimensions of fins

$N = 40$ Number of fins

$t = 0.0016m$ thickness of fins

space between fins:

$$S = \frac{(H - N \cdot t)}{N - 1} \qquad S = 0.0021m \qquad \text{(J15)}$$

$L = 20 \cdot mm$ radial length of fins

$r_2 = L + r_1$ radius to tip of fin

$d_r = 2 \cdot r_1$ diameter for Kröger' s (1998) equation for fin efficiency (in equation 3.3.12)

$d_f = 2 \cdot r_2$ diameter for Kröger' s (1998) equation for fin efficiency (in equation 3.3.12)

Fin Calculations as from Table 3.5 and equations 3.99-101 (Incropera and De Witt (2002))

Corrected radius to tip of fin:

$$r_{2c} = r_2 + \frac{t}{2} \tag{J16}$$

fin surface area:

$$A_f = 2 \cdot \pi \cdot \left[(r_{2c})^2 - r_1^{\,2} \right] \tag{J17}$$

prime/base area (excluding fin base area):

$$A_b = 2 \cdot \pi \cdot r_1 \cdot (H - N \cdot t) \tag{J18}$$

total HE surface area:

$$A_t = N \cdot A_f + A_b$$

variable in table 3.5 (not mass!):

$$m1 = \left(\frac{2 \cdot h}{k_{exh} \cdot t} \right)^{0.5} \cdot m \qquad m1 = 448.1398 \tag{J19}$$

variable in table 3.5:

$$C_2 = \frac{2 \cdot r_1}{m \cdot \left[(r_{2c})^2 - r_1^{\,2} \right]} \tag{J20}$$

Fin efficiency according to Kröger (1998) eq 3.3.12-13

$$\phi = \left(\frac{d_f}{d_r} - 1 \right) \cdot \left(1 + 0.35 \cdot \ln \left(\frac{d_f}{d_r} \right) \right) \tag{J21}$$

$$ww = \frac{m1 \cdot d_r \cdot \phi}{2} \cdot \left(\frac{1}{m} \right) \qquad \text{remove units for equation (J22)}$$

Fin efficiency:

$$\eta_{fin} = \frac{\tanh(ww)}{ww} \qquad \eta_{fin} = 0.0982 \qquad \text{(J22)}$$

Overall surface efficiency of the fin array
(Incropera and De Witt (2002), equation 3.102):

$$\eta_o = 1 - \frac{N \cdot A_f}{A_t} \cdot \left(1 - \eta_{fin}\right) \qquad \eta_o = 0.1325 \qquad \text{(J23)}$$

Total rate of heat transfer by convection for fin and unfinned (prime) surface is
(Incropera and De Witt (2002), equation 3.101):

Overall finned heat transfer:

$$q_t = h \cdot A_t \cdot \eta_o \cdot \left(T_{exh} - T_{wh}\right) \qquad q_t = 27.2871W \qquad \text{(J24)}$$

This is the total rate of heat transfer by convection for the fins and prime area

fin perimeter (from figure 3.16 Incropera, 2002):

$$P = 2 \cdot \pi \cdot \left(r_2 \cdot 2\right) \qquad P = 0.7823m \qquad \text{(J25)}$$

tip area fig 3.16

$$Ac = 2 \cdot \pi \cdot r_2 \cdot t \qquad Ac = 0.0006m^2 \qquad \text{(J26)}$$

should be > 2 to justify the use of fins (Incropera, 2002):

$$\varepsilon_{fin} = \left(\frac{k_{exh} \cdot P}{h \cdot Ac}\right)^{\frac{1}{2}} \qquad \varepsilon_{fin} = 2.7893 \qquad \text{(J27)}$$

Appendix K Calculations for Experimental Results

Calculate the effective heat energy that is available at the hot-end of the Stirling cycle i.e. heat energy in hot-end wall and Experimental Stirling cycle efficiency.

Available exhaust gas energy according to Lotun (2001):

$$Q_{avl} = 4600\,W$$

Use overall surface efficiency of fin array (η_o) from equation (J23) to calculate available hot-end heat energy:

$$Q_{hot} = \eta_o \cdot Q_{avl} \qquad Q_{hot} = 609.5403W \qquad \text{(K1)}$$

Angular rotation of DC generator (@ Torque transducer)

$$\omega_{DC} = \frac{2 \cdot \pi \cdot 66}{60} \text{ rad/s} \qquad \omega_{DC} = 6.9115 \text{ rad/s} \qquad \text{(K2)}$$

Experimentaly measured operational torque (@ steady-state conditions):

$$T_{out} = 1.105 \text{ N.m} \qquad \text{(K3)}$$

Experimentally determined system frictional losses:

$$P_{loss} = 10.4 \text{ W} \qquad \text{(K4)}$$

Experimentally measured work produced by the Stirling cycle (Experimental HSE power output)

$$W_{HSE} = \left(P_{loss} + \omega_{DC} \cdot T_{out}\right) \cdot W \qquad W_{HSE} = 18.0372W \qquad \text{(K5)}$$

Experimentally determined efficiency of the Stirling cycle (not complete engine)

$$\eta_{exp} = \frac{W_{HSE}}{Q_{hot}} \qquad \eta_{exp} = 0.0296 \qquad \text{(K6)}$$

Appendix L D-90 Ross Yoke Operating Conditions and Engine Dimensions

Table 14: Operating conditions for D-90 Ross-yoke engine

Description/Variable	Value	Units
Cooler Temperature (T_k)	300	K
Heater Temperature (T_h)	923	K
Mean Operating Pressure (p_{mean})	2	bar
Operating Frequency (*rpm*)	3000	rpm
Air Gas Constant (R)	287	J/kg.K
Gamma (γ)	1.4	-
Dynamic Viscosity (μ)	17.08e-6	kg.m/s
Sutherland Constant (T_{suth})	112	K
Expansion Space Swept Volume (V_e)	61	cm^3
Expansion Space Clearance Volume (V_{cle})	10	cm^3
Compression Space Swept Volume (V_c)	61	cm^3
Compression Space Clearance Volume (V_{clc})	8	cm^3
Total Mass of Gas	0.253	gram

Table 15: Heat exchanger volumes for D-90 Ross-yoke engine

Description	Value	Units
Heater		
Void volume	28.4	cm^3
Free flow area	0.08	cm^2
Wetted area	7.52	cm^2
Hydraulic diameter	1.51	mm
Heater length	3.79	cm
Cooler		
Void volume	33.02	cm^3
Free flow area	0.07	cm^2
Wetted area	14.41	cm^2
Hydraulic diameter	0.92	mm
Cooler length	4.8	cm
Regenerator		
Porosity	0.708	-
Void volume	35.97	cm^3
Total wetted area	0.4274	m^2
Hydraulic diameter	0.337	mm
Regenerator wall thermal conductance	0.09795	W/K

Foil thickness	0.07	mm
Foil length	6.075	m

Table 16: D-90 Ross-yoke drive engine dimensions

Description	**Variable**	**Value**	**Units**
Yoke length	b1	35.4	mm
Yoke height	b2	35.4	mm
Crank radius	-	8.5	mm
Compression piston diameter	-	55.9	mm
Expansion piston diameter	-	55.9	mm
y_{min}	-	22	mm
y_{max}	-	4.7	mm
alpha	-	95.6	0